

Investigation and Optimization of the Effects of Application of Ultrasonic Sound Frequencies during Turning Operation of Steel on Machinability Responses

By
Mohammad Shariful Islam Chowdhury (111601)

SUPERVISED BY
Prof. Dr. Md. Anayet Ullah Patwari

A thesis submitted to the Department of Mechanical & Chemical Engineering (MCE) in partial fulfilment of the requirement for the degree of

MASTER OF SCIENCE IN MECHANICAL ENGINEERING

بِسْمِ اللَّهِ الرَّحْمَنِ الرَّحِيمِ



Department of Mechanical & Chemical Engineering (MCE)

ISLAMIC UNIVERSITY OF TECHNOLOGY (IUT)

August, 2014

CERTIFICATE OF APPROVAL

The thesis titled “*Investigation and Optimization of the Effects of Application of Ultrasonic Sound Frequencies During Turning Operation of Steel on Machinability Responses*” submitted by Mohammad Shariful Islam Chowdhury bearing Student No. 111601 of Academic Year 2011-2012 has been found as satisfactory and accepted as partial fulfillment of the requirement for the degree of Master of Science in Mechanical Engineering on 7th August, 2014.

BOARD OF EXAMINERS

1. **Dr. Md. Anayet Ullah Patwari**

Professor
Department of Mechanical and Chemical Engineering
Islamic University of Technology (IUT)
Board Bazar, Gazipur
Dhaka, Bangladesh.

Chairman
(Supervisor)

2. **Dr. Md. Abdur Razzaq Akhanda**

Professor and Head
Department of Mechanical and Chemical Engineering
Islamic University of Technology (IUT)
Board Bazar, Gazipur
Dhaka, Bangladesh.

Member
(Ex-Officio)

3. **Dr. Md. Nurul Absar Chowdhury**

Professor
Department of Mechanical and Chemical Engineering
Islamic University of Technology (IUT)
Board Bazar, Gazipur
Dhaka, Bangladesh.

Member

4. **Prof. Dr. Mohammed Alauddin**

Vice Chancellor
Dhaka University of Engineering and Technology (DUET)
Board Bazar, Gazipur
Dhaka, Bangladesh.

Member
(External)

CANDIDATE'S DECLARATION

It is hereby declared that this thesis or any part of it has not been submitted elsewhere for the award of any degree or diploma.

Signature of the Candidate

Mohammad Shariful Islam Chowdhury

Student No.-111601

Session 2011-2012

Department of Mechanical and Chemical Engineering (MCE)

Islamic University of Technology (IUT), OIC

Board Bazar, Gazipur

Dhaka, Bangladesh.

Signature of the Supervisor

Dr. Md. Anayet Ullah Patwari

Professor

Department of Mechanical & Chemical Engineering (MCE)

Islamic University of Technology (IUT), OIC

Board Bazar, Gazipur

Dhaka, Bangladesh.

DEDICATION

This thesis is dedicated to my beloved parents, wife and all my well wishers helping me to accomplish this work.

TABLE OF CONTENTS

Recommendation of the Board of Examiners	
Candidate's Declaration	
Dedication	
Table of Contents	
List of Tables	
List of Figures	
List of Abbreviations of Technical Symbols and Terms	
Acknowledgement	
Abstract	

PAGE NUMBER

CHAPTER 1: INTRODUCTION	1-29
1.1 General Background Information	2
1.2 Turning Operation	2
1.2.1 Cutting Tool Geometry.....	3
1.3 Inserts	6
1.4 Tool Wear	7
1.4.1 Types of Tool Wear.....	9
1.4.2 Effects of tool wear on technological performance measures.....	12
1.4.3 Tool life.....	13
1.5 Surface Roughness	14
1.5.1 Surface Finish in Machining.....	14
1.5.2 Factors Influencing Surface Roughness in Turning.....	16
1.5.3 Roughness Parameters.....	17
1.5.4 Bearing area curve and amplitude distribution curve.....	19
1.6 Material Removal Rate (MRR)	20
1.7 Chip Morphology	21

1.7.1	Types of Chips.....	21
1.8	Ultrasound.....	24
1.9	Problem Statement.....	25
1.10	Research Philosophy.....	26
1.11	Research Methodology.....	26
1.12	Research Objectives of the Study.....	27
1.13	Significance and Benefits of the Research.....	28
1.14	Thesis Organization.....	28
 CHAPTER 2: LITERATURE REVIEW		 30-48
2.1	Contemporary Research.....	31
2.2	Summary of Literature Review.....	46
2.3	Scope of Current Research.....	47
 CHAPTER 3: EXPERIMENTAL DETAILS		 64-76
3.1	Introduction.....	50
3.2	Experimental Procedure.....	50
3.3	Process Variables and their Values.....	52
3.4	Equipments and Apparatus Used.....	53
	3.4.1 Centre Lathe.....	53
	3.4.2 Surface Profilometer or Surface Roughness Tester.....	55
	3.4.3 Optical Microscope.....	56
	3.4.4 Thermometer.....	57
	3.4.5 Oscilloscope.....	58
	3.4.6 Ultrasound Frequency Generator Device.....	59
	3.4.7 Accelerometer.....	66
	3.4.8 Cutting Tool.....	68
	3.4.6 Work piece.....	68
3.5	Measurement Technique.....	70
	3.5.1 Measurement of Surface Roughness.....	70

3.5.2 Measurement of Tool Wear.....	72
3.5.3 Observation of Chip Behavior.....	73
3.5.4 Measurement of Temperature.....	74
3.5.5 Measurement of Vibration.....	75
CHAPTER 4: RESULTS, ANALYSIS AND DISCUSSIONS	77-100
4.1 Introduction.....	78
4.2 Effect of Ultrasound Frequency on Surface Roughness.....	78
4.3 Effect of Ultrasound Frequency on Tool Wear.....	85
4.4 Effect of Ultrasound Frequency on Vibration of Tool Holder and Cutting Tool.....	89
4.5 Effect of Ultrasound Frequency on Cutting Temperature.....	90
4.6 Effect of Ultrasound Frequency on Chip Behavior.....	91
4.7 Effect of Orientation of the Application of Ultrasound Frequency.....	94
4.8 Effect of Input Power Variation.....	97
CHAPTER 5: CONCLUSIONS AND RECOMMENDATIONS	101-104
5.1 Conclusions.....	102
5.2 Recommendations.....	103
BIBLIOGRAPHY	105-110
APPENDIX A: DATA TABLES	111-114
APPENDIX B: PICOSCOPE GRAPHS	115-118

LIST OF TABLES

<u>LIST</u>	<u>PAGE NUMBER</u>
CHAPTER 1	
Table 1.1: Recommended wear land size for different tool material and operations....	11
Table 1.2: Tool life measurement.....	13
CHAPTER 3	
Table 3.1: Process variables and their values.....	52
Table 3.2: Specifications of the surface profilometer used in this research.....	55
Table 3.3: Specifications of Metallurgical Microscope MMB2300.....	56
Table 3.4: Specifications of Digital Thermometer Model 305.....	57
Table 3.5: Specifications of PC oscilloscope PicoScope 3204.....	59
Table 3.6: Input and output data of ultrasound frequency measured for calibration purposes.....	64
Table 3.7: Work piece material and dimensions.....	69
Table 3.8: Chemical composition of the mild steel used in the experimentation.....	69
CHAPTER 4	
Table 4.1: Material removal rate at different depth of cuts and spindle speeds.....	84
Table 4.2: Images of surfaces at 1 mm depth of cut, 530 RPM spindle speed and different ultrasound frequencies.....	85
Table 4.3: Tool wear values at depth of cut of 1 mm and spindle speed of 530 RPM...	86
Table 4.4: Images of tool wear for normal machining and machining with 60 kHz ultrasound frequency taken by optical microscope at depth of cut of 1 mm and spindle speed of 530 RPM.....	87
Table 4.5: Cutting Temperature measured at depth of cut of 1 mm and spindle speed of 530 RPM for without ultrasound and with ultrasound frequency of 60 kHz.....	91
Table 4.6: Chip collected in each cutting environment showed different continuity....	92
Table 4.7: Images of chips for normal machining and machining with 60 kHz ultrasound frequency taken by optical microscope at depth of cut of 1 mm and spindle speed of 530 RPM.....	93
Table 4.8: Surface roughness data measured at depth of cut of 1 mm and spindle speed of 530 RPM for horizontal and vertical orientation.....	95

Table 4.9: Images of surfaces at 1 mm depth of cut, 530 RPM spindle speed and different ultrasound frequencies for horizontal and vertical orientation.....	96
Table 4.10: Surface Roughness data at 1 mm depth of cut, 530 RPM spindle speed and 60 kHz ultrasound frequency for different input voltages.....	97
Table 4.11: Images of surfaces at 1 mm depth of cut, 530 RPM spindle speed and 60 kHz ultrasound frequency for different input voltages.....	98

APPENDIX A: DATA TABLES

Table A1: Surface Roughness data at 0.5 mm depth of cut, 360 RPM spindle speed and different ultrasound frequencies.....	111
Table A2: Surface Roughness data at 0.5 mm depth of cut, 530 RPM spindle speed and different ultrasound frequencies.....	111
Table A3: Surface Roughness data at 1 mm depth of cut, 360 RPM spindle speed and different ultrasound frequencies.....	112
Table A4: Surface Roughness data at 1 mm depth of cut, 530 RPM spindle speed and different ultrasound frequencies.....	112
Table A5: Comparison of Surface Roughness data at 0.5 mm depth of cut and different ultrasound frequencies for different spindle speeds.....	113
Table A6: Comparison of Surface Roughness data at 1 mm depth of cut and different ultrasound frequencies for different spindle speeds.....	113
Table A7: Comparison of Surface Roughness data at 360 RPM spindle speed and different ultrasound frequencies for different depth of cuts.....	114
Table A8: Comparison of Surface Roughness data at 530 RPM spindle speed and different ultrasound frequencies for different depth of cuts.....	114

LIST OF FIGURES

<u>LIST</u>	<u>PAGE NUMBER</u>
CHAPTER 1	
Figure 1.1: Turning Operation.....	3
Figure 1.2: Geometry of a single point cutting tool.....	3
Figure 1.3: Tool holder with an insert.....	5
Figure 1.4: Inserts of different shapes.....	6
Figure 1.5: Different modes of wear.....	8
Figure 1.6: Tool wear phenomenon.....	8
Figure 1.7: Flank wear.....	10
Figure 1.8: Parameters used to measure flank wear.....	10
Figure 1.9: Typical stages of flank wear.....	11
Figure 1.10: Idealized model of surface roughness.....	15
Figure 1.11: Roughness parameter R_a and R_q	18
Figure 1.12: Roughness parameter R_z and R_{max}	18
Figure 1.13: Sketches depicting surfaces with negative and positive skew. The roughness trace is on the left, the amplitude distribution curve is in the middle, and the bearing area curve (Abbott-Firestone curve) is on the right.....	19
Figure 1.14: Schematic illustration of the basic turning operation, showing depth of cut, d ; feed, f ; and spindle rotational speed, N , in rev/min.....	20
Figure 1.15: Mass of continuous chips.....	22
Figure 1.16: Basic types of chips produced in metal cutting and their micrographs: (a) continuous chip with narrow, straight primary shear zone; (b) secondary shear zone at the tool-chip interface; (c) continuous chip with built-up edge; (d) segmented or non-homogeneous chip; and (e) discontinuous chip.....	23
Figure 1.17: (a) The spectrum of sound; (b) The spectrum of medical ultrasound.....	24

CHAPTER 3

Figure 3.1: Flow sequence of experimentation.....	51
Figure 3.2: Schematic of the experimental setup.....	52
Figure 3.3: Photograph of labelled centre lathe used in this research.....	53
Figure 3.4: Specifications of the centre lathe used in this research.....	54
Figure 3.5: Photograph of Mitutoyo SURFTEST SJ-210 Surface Profilometer.....	55
Figure 3.6: Photograph of labelled Metallurgical Microscope MMB2300.....	56
Figure 3.7: Photograph of Model 305 Digital Thermometer.....	57
Figure 3.8: Photograph of PicoScope 3204.....	58
Figure 3.9: Photograph of labelled ultrasound generator device developed specifically for this research.....	60
Figure 3.10: Functional block diagram of AD9850.....	61
Figure 3.11: Circuit diagram of the signal generator.....	61
Figure 3.12: Piezo Driver.....	62
Figure 3.13: Circuit diagram of the Piezo Driver.....	62
Figure 3.14: Complete circuit diagram of the ultrasound generator device.....	63
Figure 3.15: Photograph of the setup for calibrating the ultrasound generator device...	64
Figure 3.16: Ultrasound wave generated at 60 kHz obtained with a picoscope from the left-sided ultrasound emitter for calibration purposes.....	65
Figure 3.17: Ultrasound wave generated at 60 kHz obtained with a picoscope from the right-sided ultrasound emitter for calibration purposes.....	65
Figure 3.18: Photograph of three-Axis MEMS MPU-6050 Accelerometer.....	66
Figure 3.19: Typical operating circuit of MPU-6050 Accelerometer.....	67
Figure 3.20: Block diagram of MPU-6050 Accelerometer.....	67
Figure 3.21: Photograph of insert with dimensions.....	68
Figure 3.22: Photograph of Mild Steel work piece.....	68
Figure 3.23: Photograph of the setup of the SURFTEST SJ-210 for measuring surface roughness.....	71
Figure 3.24: Surface roughness result sample measured by SURFTEST SJ-210.....	71
Figure 3.25: Tool wear measured with scopetek.....	72

Figure 3.26: Samples of mounted chips.....	74
Figure 3.27: Instruments used for chip analysis (a) Polishing wheel (b) Optical microscope....	74
Figure 3.28: Photograph of arrangement for measuring cutting temperature a) thermocouple b) thermocouple hot end attached with insert tip.....	75
Figure 3.29: Photograph of the setup of the accelerometer for measuring the vibration of the tool holder and the cutting tool.....	76

CHAPTER 4

Figure 4.1: Surface Roughness (R_a) readings at 0.5 mm depth of cut, 360 RPM spindle speed and different ultrasound frequencies.....	79
Figure 4.2: Surface Roughness (R_a) readings at 0.5 mm depth of cut, 530 RPM spindle speed and different ultrasound frequencies.....	79
Figure 4.3: Surface Roughness (R_a) readings at 1mm depth of cut, 360 RPM spindle speed and different ultrasound frequencies.....	80
Figure 4.4: Surface Roughness (R_a) readings at 1mm depth of cut, 530 RPM spindle speed and different ultrasound frequencies.....	80
Figure 4.5: Comparison of Surface Roughness data at 0.5 mm depth of cut and different ultrasound frequencies for different spindle speeds.....	81
Figure 4.6: Comparison of Surface Roughness data at 1 mm depth of cut and different ultrasound frequencies for different spindle speeds.....	81
Figure 4.7: Comparison of Surface Roughness data at 360 RPM spindle speed and different ultrasound frequencies for different depth of cuts.....	82
Figure 4.8: Comparison of Surface Roughness data at 530 RPM spindle speed and different ultrasound frequencies for different depth of cuts.....	82
Figure 4.9: Surface roughness result measured by SURFTEST SJ-210 at a depth of cut of 1 mm, spindle speed of 530 RPM and ultrasound frequency of 60 kHz.....	84
Figure 4.10: Comparison of tool wear at depth of cut of 1 mm and spindle speed of 530 RPM for cutting without ultrasound and with ultrasound frequency of 60 kHz.....	88
Figure 4.11: Tool holder vibration during non cutting condition at 530 RPM.....	89
Figure 4.12: Tool holder vibration during cutting without ultrasound at a depth of cut of 1 mm and spindle speed of 530 RPM.....	89
Figure 4.13: Tool holder vibration during cutting with 60 kHz ultrasound frequency at a depth of cut of 1 mm and spindle speed of 530 RPM.....	90
Figure 4.14: Comparison of cutting temperature at depth of cut of 1 mm and spindle speed of 530 RPM for cutting without ultrasound and with ultrasound frequency of 60 kHz.....	91
Figure 4.15: Schematic of chip showing sectioning for viewing side cross sectional view.....	93
Figure 4.16: Experimental setup for (a) Horizontal orientation (b) Vertical orientation	94
Figure 4.17: Comparison of surface roughness at depth of cut of 1 mm and spindle speed of 530 RPM for horizontal and vertical orientation.....	95
Figure 4.18: Effect of input voltage of the ultrasound wave generator on surface roughness.....	98

Figure 4.19: Ultrasound wave generated at input voltage of 6V.....	99
Figure 4.20: Ultrasound wave generated at input voltage of 9V.....	99
Figure 4.21: Ultrasound wave generated at input voltage of 12V.....	100

APPENDIX B: PICOSCOPE GRAPHS

Figure A1: Ultrasound wave generated at 20 kHz obtained with a picoscope from the left-sided ultrasound emitter for calibration purposes.....	115
Figure A2: Ultrasound wave generated at 30 kHz obtained with a picoscope from the left-sided ultrasound emitter for calibration purposes.....	115
Figure A3: Ultrasound wave generated at 40 kHz obtained with a picoscope from the left-sided ultrasound emitter for calibration purposes.....	116
Figure A4: Ultrasound wave generated at 50 kHz obtained with a picoscope from the left-sided ultrasound emitter for calibration purposes.....	116
Figure A5: Ultrasound wave generated at 20 kHz obtained with a picoscope from the right-sided ultrasound emitter for calibration purposes.....	117
Figure A6: Ultrasound wave generated at 30 kHz obtained with a picoscope from the right-sided ultrasound emitter for calibration purposes.....	117
Figure A7: Ultrasound wave generated at 40 kHz obtained with a picoscope from the right-sided ultrasound emitter for calibration purposes.....	118
Figure A8: Ultrasound wave generated at 50 kHz obtained with a picoscope from the right-sided ultrasound emitter for calibration purposes.....	118

LIST OF ABBREVIATIONS OF TECHNICAL SYMBOLS AND TERMS

MRR	Material Removal Rate
TWR	Tool Wear Rate
BUE	Build-Up Edge
RPM	Revolution Per Minute
ADC	Amplitude Distribution Curve
BAC	Bearing Area Curve
DOC	Depth of Cut

ACKNOWLEDGEMENT

The author expresses gratefulness to the almighty Allah for his blessings, which enabled him to complete this thesis successfully.

The author expresses gratitude to his supervisor Dr. Md. Anayet Ullah Patwari, Professor, Department of Mechanical and Chemical Engineering (MCE), Islamic University of Technology (IUT), for his continuous guidance, helpful suggestions and supervision at all stages of this thesis work. Deepest gratitude to Dr. Ahsan Habib, Assistant, Professor, Department of Mechanical and Chemical Engineering (MCE), Islamic University of Technology (IUT), for his inputs throughout the research.

Special thanks to the B. Sc. in Engineering (Mechanical) students: Afzal Hossain Neelav, Sharafat Latif Sezan and TM Moniruzzaman Sunny of Islamic University of Technology (IUT), who helped the author with various research and analysis work. Also, the author expresses sincere thanks to Md. Shakhawat Hossain, Senior Operator (CAM lab), Md. Matiar Rahman, Senior Operator (Machine shop), Md. Rajaul Karim, Operator (Machine shop), for their useful suggestion and cooperation which made it easier for me to carry out my experiments.

The author expresses his thanks to IUT authority for financial assistance to conduct the research and granting permission for using the lab facilities of the university. Special thanks to all the Faculty and Staff members of the Mechanical and Chemical Engineering Department (MCE), Islamic University of Technology (IUT) for their support and cooperation.

Finally, the author is indebted to his parents and wife for providing the mental support in pursuing the Masters degree and research work and without whose support none of this would have been.

Although I have given my best effort to complete this thesis paper, I seek excuses if there is any mistake found in this report.

Author

ABSTRACT

Turning is one of the most common and popular process in industry for manufacturing metallic products. The two single most important output parameters that define the product quality are surface roughness and tool wear. So it is of primary concern to reduce tool wear and surface roughness of the product in any machining process. Different studies have been carried out to determine the tool wear and surface roughness of the product and their subsequent improvements. Different techniques have been adopted to replace the traditional turning process in an attempt to minimize the tool wear and the surface roughness of the finished product.

In this research, a new novel technique has been proposed and adopted with an aim to reduce tool wear and surface roughness of the product. External ultrasonic sound waves were applied during the turning process of mild steel in an attempt to reduce the cutting tool vibration thereby leading to improvements in both surface quality and tool life. Detailed experimentations were carried out to study the effect of external ultrasonic sound wave on tool life of inserts, surface roughness and cutting tool vibration. Experiments were carried out under different ultrasonic frequencies to determine the effective frequency range which optimizes the above parameters to the best degree possible. The goal was to achieve improved machinability and analyze the extent of improvement obtained in the above mentioned machinability factors and the interrelation among them by the application of ultrasonic sound wave. The experimental results showed improvements in all the above machinability factors. In addition to these, the effect of orientation of the application of the ultrasonic sound waves and the amplitude of the waves were studied in detail. Cutting tool vibration and chip morphology were also studied to support the theory suggested.

CHAPTER 1

Introduction

1.1 General Background Information

Tool wear adversely affects productivity, dimensional accuracy, as well as product quality in most machining processes. Because of tool wear the surface finish of the product also deteriorates. Surface roughness represents the dimensional accuracy of the finished product and is one of the most important quality requirements of the finished product. So it is of primary concern to reduce tool wear and surface roughness of the product in any machining process. Different studies have been carried out to determine the tool wear and surface roughness of the product and their subsequent improvements. This study investigates the effect of the application of the ultrasound in turning operation. This study also investigates the material removal rate and chip morphology in addition to the surface roughness and tool wear to have a comprehensive view of the effect of ultrasound in machining operation. Experiments were carried out with different ultrasonic frequencies to determine the effective frequency range which optimizes the above parameters to the best degree possible. Finally this study aims to establish the advantages of the application of the ultrasound in machining process over normal machining and proposes the most suitable cutting environment in different cutting conditions.

1.2 Turning Operation

Turning is a form of machining, a material removal process, which is used to create rotational parts by cutting away unwanted material. Turning is used to produce rotational, typically axi-symmetric, parts that have many features, such as holes, grooves, threads, tapers, various diameter steps, and even contoured surfaces. It is one of the most common and popular process in industry for manufacturing metallic products. Due to global competitiveness, there is an increasing demand for product quality, reduction in cutting tool vibration leading to surface quality, high material removal rate (MRR) leading to higher productivity, longer life and stability of the cutting tool. Dimensional accuracy, tool wear and surface quality are the key factors

that must be controlled to ensure product quality, higher productivity, better performance and service life of engineering component.

In its basic form, it can be defined as the machining of an external surface:

1. With the work piece rotating.
2. With a single-point cutting tool, and
3. With the cutting tool feeding parallel to the axis of the work piece and at a distance that will remove the outer surface of the work.

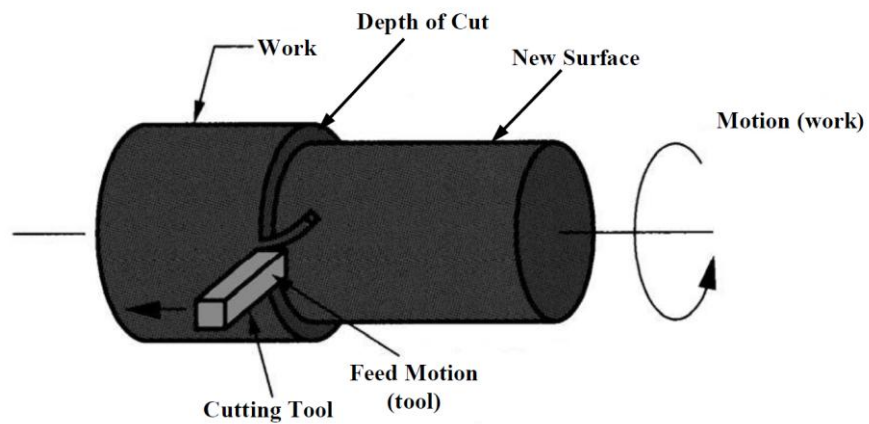


Figure 1.1: Turning Operation

1.2.1 Cutting Tool Geometry

For cutting tools, geometry depends mainly on the properties of the tool material and the work material. The standard terminology is shown in the following figure.

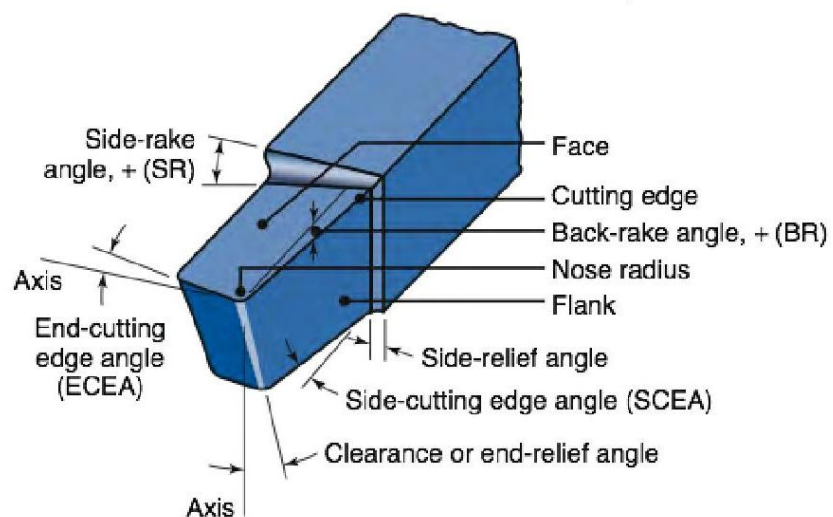


Figure 1.2: Geometry of a single point cutting tool

Flank:

A flat surface of a single-point tool that is adjacent to the face of the tool. During turning, the side flank faces the direction that the tool is fed into the work piece, and the end flank passes over the newly machined surface.

Face:

The flat surface of a single point tool through which, the work piece rotates during turning operation. On a typical turning setup, the face of the tool is positioned upwards.

Back rake angle:

If viewed from the side facing the end of the work piece, it is the angle formed by the face of the tool and a line parallel to the floor. A positive back rake angle tilts the tool face back, and a negative angle tilts it forward and up.

Side rake angle:

If viewed behind the tool down the length of the tool holder, it is the angle formed by the face of the tool and the centerline of the work piece. A positive side rake angle tilts the tool face down toward the floor, and a negative angle tilts the face up and toward the work piece.

Side cutting edge angle:

If viewed from above looking down on the cutting tool, it is the angle formed by the side flank of the tool and a line perpendicular to the work piece centerline. A positive side cutting edge angle moves the side flank into the cut, and a negative angle moves the side flank out of the cut.

End cutting edge angle:

If viewed from above looking down on the cutting tool, it is the angle formed by the end flank of the tool and a line parallel to the work piece centerline. Increasing the end cutting edge angle tilts the far end of the cutting edge away from the work piece.

Side relief angle:

If viewed behind the tool down the length of the tool holder, it is the angle formed by the side flank of the tool and a vertical line down to the floor. Increasing the side relief angle tilts the side flank away from the work piece.

End relief angle:

If viewed from the side facing the end of the work piece, it is the angle formed by the end flank of the tool and a vertical line down to the floor. Increasing the end relief angle tilts the end flank away from the work piece.

Nose radius:

It is the rounded tip on the cutting edge of a single point tool. A zero degree nose radius creates a sharp point of the cutting tool.

Side cutting edge angle:

It is commonly known as lead angle. If a tool holder is built with dimensions that shift the angle of an insert, the lead angle takes this change into consideration.

The back rake angle affects the ability of the tool to shear the work material and form the chip. It can be positive or negative. Positive rake angles reduce the cutting forces resulting in smaller deflections of the work piece, tool holder, and machine. If the back rake angle is too large, the strength of the tool is reduced as well as its capacity to conduct heat. In machining hard work materials, the back rake angle must be small, even negative for carbide and diamond tools. The higher the hardness, the smaller will be the back rake angle. For high-speed steels, back rake angle is normally chosen in the positive range.

The following figure shows tool holder with a square shaped insert.



Figure 1.3: Tool holder with an insert

1.3 Inserts

A tipped tool generally refers to any cutting tool where the cutting edge consists of a separate piece of material either brazed, welded or clamped on to a separate body. Common materials for tips include tungsten carbide, polycrystalline diamond, and cubic boron nitride. The advantage of tipped tools is only a small insert of the cutting material is needed to provide the cutting ability. The small size makes manufacturing of the insert easier than making a solid tool of the same material. This also reduces cost because the tool holder can be made of a less-expensive and tougher material. In some situations a tipped tool is better than its solid counterpart because it combines the toughness of the tool holder with the hardness of the insert. Cutting tool inserts are replaceable attachments for cutting tools that typically contain the actual cutting edge. It has multiple cutting edges. Once a cutting edge is excessively worn, it can be indexed to another edge without disturbing the overall geometry of the tool (effective diameter, tool length offset, etc.), or the insert can be replaced. This saves time in manufacturing by allowing fresh cutting edges to be presented periodically without the need for tool grinding and setup changes.

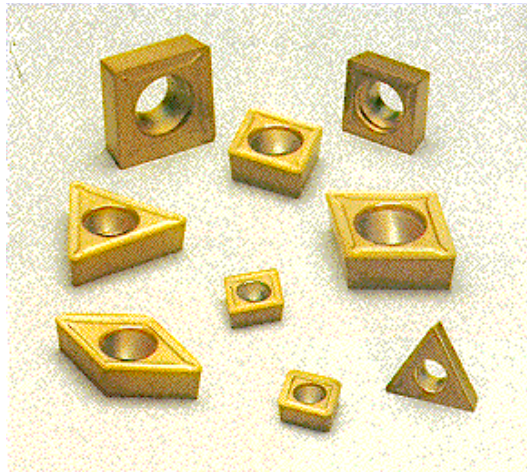


Figure 1.4: Inserts of different shapes

Cutting Tool Material:

Cutting tool materials include:

- ❖ High speed steels (HSS)
- ❖ Cast Cobalt alloys
- ❖ Carbides

Coatings:

Coatings are frequently applied to carbide tool tips to improve tool life or to enable higher cutting speeds. Coated tips typically have lives 10 times greater than uncoated tips. Common coating materials include titanium nitride, titanium carbide and aluminum oxide, usually 2 - 15 μm thick.

1.4 Tool Wear

Tool wear is the change of shape of the tool from its original shape, during cutting, resulting from the gradual loss of tool material or deformation. Tool wear in machining is defined as the amount of volume loss of tool material on the contact surface due to the interactions between the tool and work piece. Specifically, tool wear is described by wear rate (volume loss per unit area per unit time) and is strongly determined by temperature, stresses, and relative sliding velocity generated at the contact interface. Tool wear leads to tool failure. According to many authors, the failure of cutting tool occurs as premature tool failure (*i.e.*, tool breakage) and progressive tool wear.

According to the ISO standard 3685:1993, there are multiple types of wear. Most important of the wear types are flank wear and crater wear. Flank wear is present in all situations and it is the best known type of wear. It can be found on the major flank of the tool. Crater wear appears on the face of the tool as a crater. Crater wear is the most commonly found wear on the face of the tool. Flank wear is most commonly used for wear monitoring. Generally, wear of cutting tools depends on tool material and

geometry, work piece materials, cutting parameters (cutting speed, feed rate and depth of cut), cutting fluids and machine-tool characteristics.

The wear process itself changes under the influence of different conditions. However, three main factors contributing to the wear are known: adhesion, abrasion and diffusion. Adhesion occurs when the work material, that the tool is cutting, welds onto the tool. This happens because of the friction between the tool and work material, which generates heat. When these welds are broken, small pieces of the tool are lost. Abrasion is mechanical wear resulting from the cutting action, where the tool grinds itself on to the work material. Diffusion wear occurs on a narrow reaction zone between the tool and work material. In diffusion wear the atoms from the tool move to the work material. This usually accelerates the other two wear processes as the tool material is weakened.

During operation, one or more of the following wear modes may occur:

- ❖ Flank
- ❖ Notch
- ❖ Crater
- ❖ Edge rounding
- ❖ Edge chipping
- ❖ Edge cracking
- ❖ Catastrophic failure

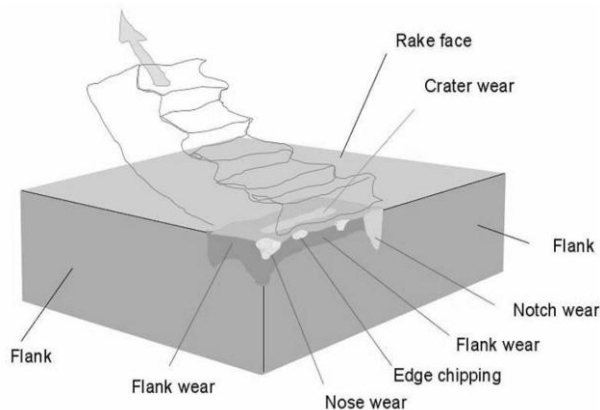


Figure 1.5: Different modes of wear

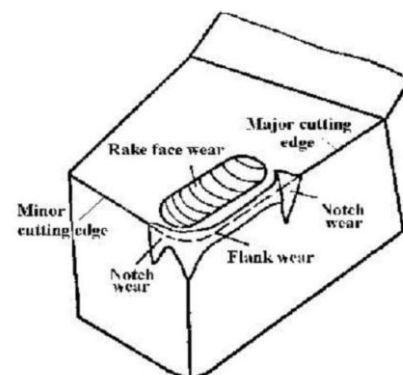


Figure 1.6: Tool wear phenomenon

During machining, cutting tools remove material from the component to achieve the required shape, dimension and surface roughness (finish). However, wear occurs during the cutting action, and it will ultimately result in the failure of the cutting tool. When the tool wear reaches a certain extent, the tool or active edge has to be replaced to guarantee the desired cutting action.

1.4.1 Types of Tool Wear

There are different types of tool wear that occurs based on different cutting conditions as well as tool geometry. The different types are listed below:

- Crater wear
- Flank wear (Clearance surface)
- Notch wear
- Chipping wear
- Spalling wear
- Attrition wear
- Abrasive wear
- Flaking wear
- Fracture wear
- Built up edge
- Thermal cracking
- Plastic deformation
- Ultimate failure

Most important of the wear types is flank wear. Flank wear is present in all situations and it is the best known type of wear. Flank wear is most commonly used for wear monitoring.

Flank wear (Clearance surface):

Wear on the flank (relief) face is called Flank wear. It occurs on the tool flank as a result of friction between the machine surface of the work piece and the tool flank. Flank wear appears in the form of so-called *wear land*. Wear land formation is not

always uniform along the major and minor cutting edges of the tool. Flank wear most commonly results from abrasive wear of the cutting edge against the machined surface. Flank wear can be monitored in production by examining the tool or by tracking the change in size of the tool or machined part.

Cutting forces increase significantly with flank wear. If the amount of flank wear exceeds some critical value, the excessive cutting force may cause tool failure.

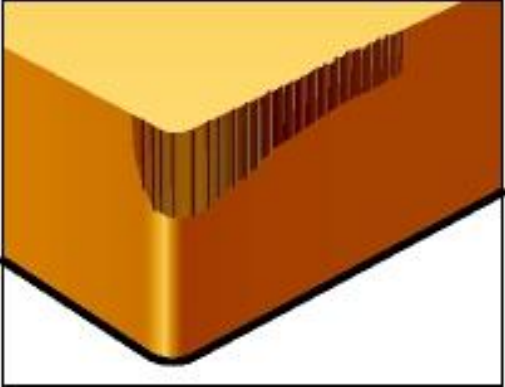


Figure 1.7: Flank wear

Flank wear can be measured by using the average and maximum wear land size VB and VB_{max} .

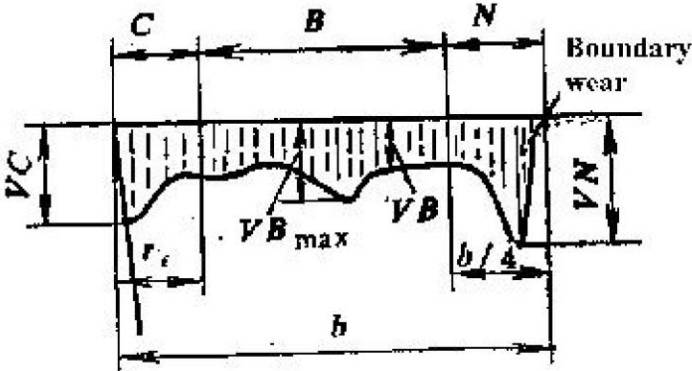


Figure 1.8: Parameters used to measure flank wear

The figure below shows the typical stages of flank wear. After the rapid initial (or preliminary) wear (cutting edge rounding), the micro-roughness is improved, in this region the wear size is proportional to the cutting time. During this stage the wear rate is relatively constant. When the wear size increases to a critical value, the surface roughness of the machined surface decreases, cutting force and temperature increase

rapidly, and the wear rate increases. Then the tool loses its cutting ability. In practice, this region of wear should be avoided.

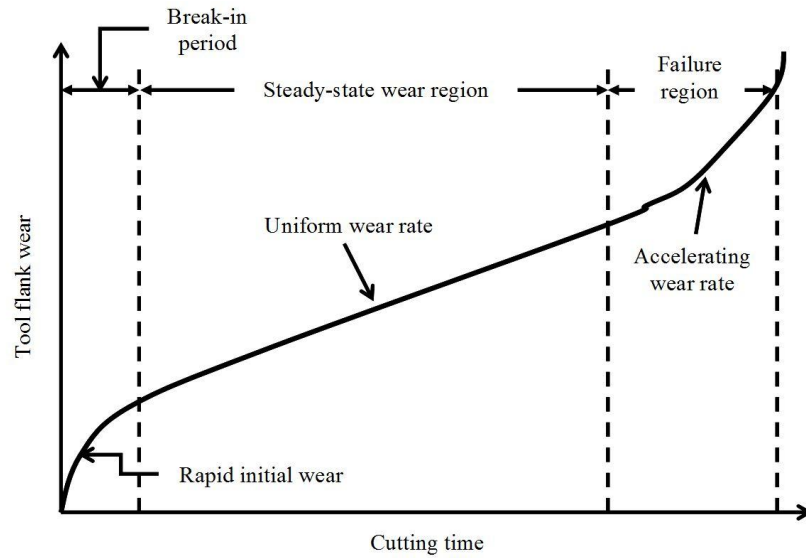


Figure 1.9: Typical stages of flank wear

Table 1.1 below shows the recommended wear land size for different operations and tool material.

Table 1.1: Recommended wear land size for different tool material and operations

Wear (in)	Tool Material	Remarks
0.030 (0.76 mm)	Carbide	Roughing passes
0.010-0.015 (0.25-0.38 mm)	Carbide	Finishing passes
0.060 or total destruction(1.25 mm)	H.S.S.	Roughing passes
0.010-0.015 (0.25-0.38 mm)	H.S.S.	Finishing passes
0.010-0.015 (0.25-0.38 mm)	Cemented oxides	Roughing and finishing passes

1.4.2 Effects of tool wear on technological performance measures

Consequences of tool wear:

1. Increase the cutting force;
2. Increase the surface roughness;
3. Decrease the dimensional accuracy;
4. Increase the temperature;
5. Vibration;
6. Lower the production efficiency, component quality;
7. Increase the cost.

Influence on cutting forces:

Crater wear, flank wear (or wear-land formation) and chipping of the cutting edge affect the performance of the cutting tool in various ways. The cutting forces are normally increased by wear of the tool. Crater wear may, however, under certain circumstances, reduce forces by effectively increasing the rake angle of the tool. Clearance-face (flank or wear-land) wear and chipping almost invariably increase the cutting forces due to increased rubbing forces.

Surface finish (roughness):

The surface finish produced in a machining operation usually deteriorates as the tool wear occurs. This is particularly true for a tool worn by chipping and generally the case for a tool with flank-land wear; although there are circumstances in which a wear land may polish the work piece and produces a good finish.

Dimensional accuracy:

Flank wear influences the plan geometry of a tool; this may affect the dimensions of the component produced in a machine with set cutting tool position or it may influence the shape of the components produced in an operation utilizing a form tool.

Vibration or chatter:

Vibration or chatter is another aspect of the cutting process which may be influenced by tool wear. A wear land increases the tendency of a tool to dynamic instability. A cutting operation which is quite free of vibration when the tool is sharp may be subjected to an unacceptable chatter mode when the tool wears.

1.4.3 Tool life

Tool wear is a time dependent process. As cutting proceeds, the amount of tool wear increases gradually. But tool wear must not be allowed to go beyond a certain limit in order to avoid tool failure.

There is no single universally accepted definition of tool life. The life needs to be specified with regard to the process aims. The most important wear type from the process point of view is the flank wear; therefore a common way of quantifying the end of a tool life is to put a limit on the maximum acceptable flank wear, VB or VB_{max} . Typical figures are shown in table 1.2.

Table 1.2: Tool life measurement

Tool Materials	Maximum Acceptable Flank Wear
HSS tools, roughing	1.5 mm
HSS tools, finishing	0.75 mm
Carbide tools	0.7 mm
Ceramic tools	0.6 mm

Parameters, which affect the rate of tool wear, are

- *cutting conditions* (cutting speed V , feed f , depth of cut d)
- *cutting tool geometry* (tool orthogonal rake angle)
- *properties of work material*

From these parameters, cutting speed is the most important one. As cutting speed is increased, wear rate increases, so the same wear criterion is reached in less time, i.e., tool life decreases with cutting speed.

Mathematically the tool life can be expressed in the following equation (the Taylor equation):

$$V_c T^n = C$$

Here, V_c is cutting speed, T is the tool life and n , C are constants.

The constants n and C may be found for specific work piece and tool material and feed, f , either by experiment or from published data.

An expanded version of Taylor equation can be formulated to include the effect of feed and depth of cut with further development of tool materials it was found that the cutting feed and the depth of cut are also significant. The expanded Taylor formula is:

$$V_c T^n f^a d^b = C$$

Where d is the depth of cut (mm) and f is the feed (mm/rev). The exponents a and b are to be determined experimentally for each combination of the cutting conditions.

1.5 Surface Roughness

1.5.1 Surface Finish in Machining

The resultant roughness produced by a machining process can be thought of as the combination of two independent quantities:

- a. Ideal roughness, and
- b. Natural roughness.

Ideal roughness:

Ideal surface roughness is a function of feed and geometry of the tool. It represents the best possible finish which can be obtained for a given tool shape and feed. It can be achieved only if the built-up-edge, chatter and inaccuracies in the

machine tool movements are eliminated completely. For a sharp tool without nose radius, the maximum height of unevenness is given by:

$$R_{max} = \frac{f}{\cot \phi + \cot \beta}$$

Here f is feed rate, ϕ is major cutting edge angle and β is the minor cutting edge angle.

The surface roughness value is given by, $R_a = R_{max}/4$

Idealized model of surface roughness has been clearly shown in figure below:

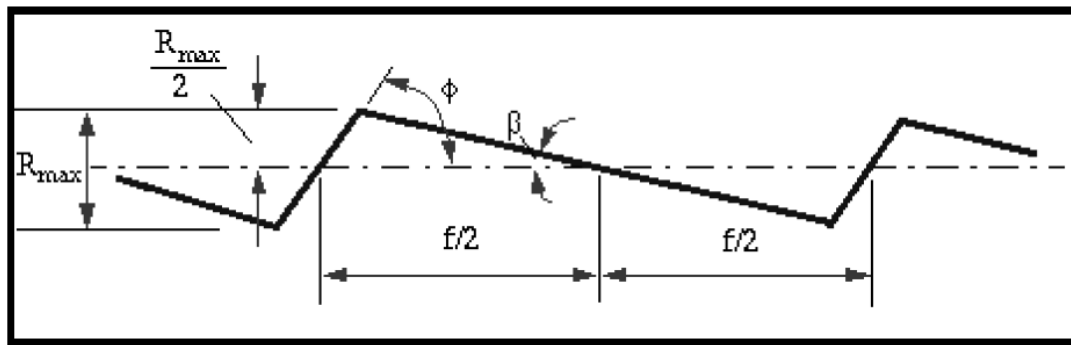


Figure 1.10: Idealized model of surface roughness

Practical cutting tools are usually provided with a rounded corner. It can be shown that the roughness value is closely related to the feed and corner radius by the following expression:

$$R_a = \frac{0.0321 f^2}{r}, \text{ where } r \text{ is the corner radius.}$$

Natural roughness:

In practice, it is not usually possible to achieve conditions such as those described above, and normally the natural surface roughness forms a large proportion of the actual roughness. One of the main factors contributing to natural roughness is the occurrence of a built-up edge and vibration of the machine tool. Thus, larger the built up edge, the rougher would be the surface produced, and factors tending to reduce chip-tool friction and to eliminate or reduce the built-up edge would give improved surface finish.

1.5.2 Factors Influencing Surface Roughness in Turning

Generally, it is found that the factors influencing surface roughness in turning are:

(i) Depth of cut:

Increasing the depth of cut increases the cutting resistance and the amplitude of vibrations. As a result, cutting temperature also rises. Therefore, it is expected that surface quality will deteriorate.

(ii) Feed:

Experiments show that as feed rate increases surface roughness also increases due to the increase in cutting force and vibration.

(iii) Cutting speed:

It is found that an increase of cutting speed generally improves surface quality.

(iv) Engagement of the cutting tool:

This factor acts in the same way as the depth of cut.

(v) Cutting tool wears:

The irregularities of the cutting edge due to wear are reproduced on the machined surface. Apart from that, as tool wear increases, other dynamic phenomena such as excessive vibrations will occur, thus further deteriorating surface quality.

(vi) Use of cutting fluid:

The cutting fluid is generally advantageous in regard to surface roughness because it affects the cutting process in three different ways. Firstly, it absorbs the heat that is generated during cutting by cooling mainly the tool point and the work surface. In addition to this, the cutting fluid is able to reduce the friction between the rake face and the chip as well as between the flank and the machined surface. Lastly, the washing action of the cutting fluid is considerable, as it consists in removing chip fragments and wear particles. Therefore, the quality of a surface machined with the presence of cutting fluid is expected to be better than that obtained from dry cutting.

(vii) **Three components of the cutting force:**

It should be noted that force values cannot be set a priori, but are related to other factors of the experiment as well as to factors possibly not included in the experiment, i.e. force is not an input factor and is used as an indicator of the dynamic characteristics of the work piece—cutting tool—machine system.

1.5.3 Roughness Parameters

There are many different roughness parameters in use, but R_a is the most common. Other common parameters include R_q , R_z , R_{max} etc. Some parameters are used only in certain industries or within certain countries. Each of the roughness parameters is calculated using a formula for describing the surface. R_q is more sensitive to the highest peak and valley dimensions of surface roughness. R_{max} measure is most useful when the polishing a particular piece of rough work-piece is involved. It gives the best idea for how much material needs to be removed in order to obtain mirror finish. R_a , being easier to calculate than R_q and are therefore more widely used in scientific measurements and research.

Since these parameters reduce all of the information in a profile to a single number, great care must be taken in applying and interpreting them. Small changes in how the raw profile data is filtered, how the mean line is calculated, and the physics of the measurement can greatly affect the calculated parameter.

Mean Roughness:

The **Mean Roughness (*Roughness Average* R_a)** is the arithmetic average of the absolute values of the roughness profile ordinates. R_a is one of the most effective surface roughness measures commonly adopted in general engineering practice. It gives a good general description of the height variations in the surface. The units of R_a are micrometers or microinches.

$$R_a = \frac{1}{n} \sum_{i=1}^n |Z_i|$$

The **Root Mean Square (RMS) roughness (R_q)** is the root mean square average of the roughness profile ordinates.

$$R_q = \sqrt{\frac{1}{n} \sum_{i=1}^n Z_i^2}$$

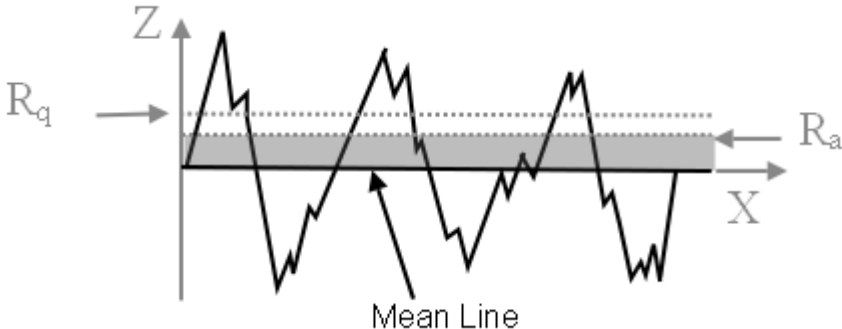


Figure 1.11: Roughness parameter R_a and R_q

Roughness Depth:

The **Single Roughness Depth (R_{zi})** is the vertical distance between the highest peak and the deepest valley within a sampling length.

The **Mean Roughness Depth (R_z)** is the arithmetic mean value of the single roughness depths of consecutive sampling lengths. The units of R_z are micrometers or microinches.

The **Maximum Roughness Depth (R_{max})** is the largest single roughness depth within the evaluation length.

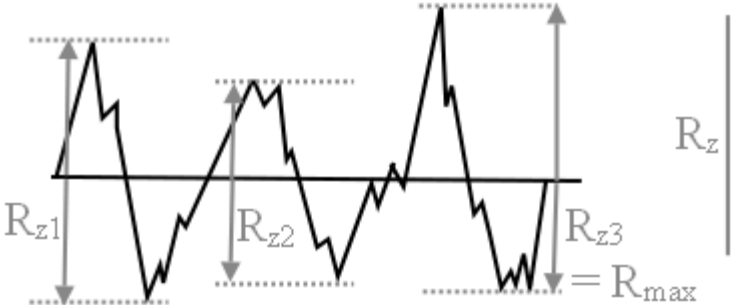


Figure 1.12: Roughness parameter R_z and R_{max}

1.5.4 Bearing area curve and amplitude distribution

curve

The amplitude distribution curve (ADC), also known as amplitude distribution function (ADF), is a probability function that gives the probability that a profile of the surface has a certain height, z , at any position x . Ordinarily the ADC is computed for the roughness profile, although the texture or even primary profiles might be used in specialized applications.

The Abbott-Firestone curve or bearing area curve (BAC) describes the surface texture of an object. The curve could be found from a profile trace by drawing lines parallel to the datum and measuring the fraction of the line which lies within the profile [1].

It is related to the ADC. It is the corresponding cumulative probability distribution and sees much greater use in surface finish. Mathematically it is the cumulative probability density function of the surface profile's height and can be calculated by integrating the profile trace [2].

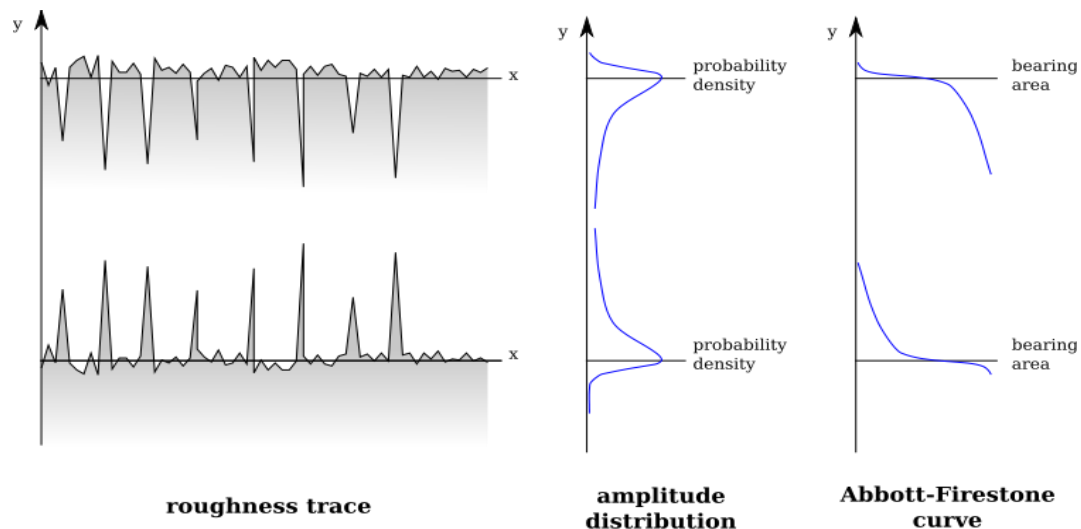


Figure 1.13: Sketches depicting surfaces with negative and positive skew. The roughness trace is on the left, the amplitude distribution curve is in the middle, and the bearing area curve (Abbott-Firestone curve) is on the right.

1.6 Material Removal Rate (MRR)

The material-removal rate (MRR) in turning is the volume of material removed per unit time, with the units of mm^3/min [3].

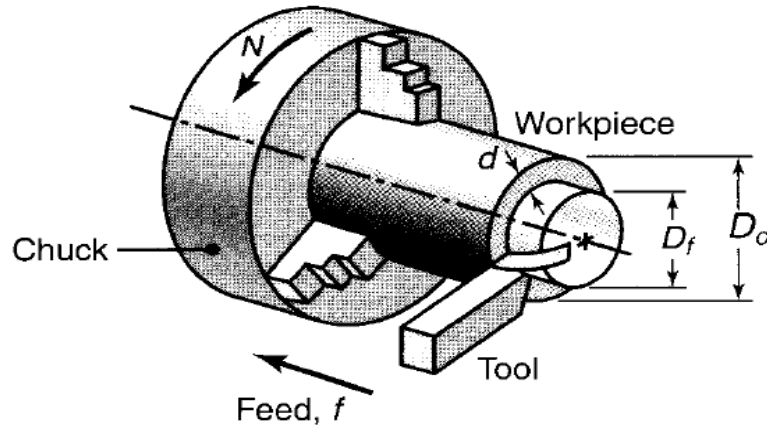


Figure 1.14: Schematic illustration of the basic turning operation, showing depth of cut, d ; feed, f ; and spindle rotational speed, N , in rev/min.

For each revolution of the work piece, a ring-shaped layer of material is removed which has a cross-sectional area that equals the product of the distance the tool travels in one revolution (feed, f) and the depth of cut, d . The volume of this ring is the product of the cross-sectional area (f)(d) and the average circumference of the ring, πD_{avg} , where

$$D_{avg} = \frac{D_o + D_f}{2}$$

For light cuts on large-diameter work pieces, the average diameter may be replaced by D_o .

The cutting speed is the surface speed of the work piece at the tool tip. The rotational speed of the work piece is N , and the material removal rate per revolution is $(\pi)(D_{avg})(d)(f)$. Since there are N revolutions per minute, the removal rate is

$$MRR = \pi D_{avg} dfN$$

The dimensional accuracy of this equation can be checked by substituting dimensions into the right-hand side. For instance, $(\text{mm})(\text{mm})(\text{mm}/\text{rev})(\text{rev}/\text{min}) =$

mm³/min, which indicates volume rate of removal. The above equation can also be written as

$$MRR = dfV$$

where V is the cutting speed and MRR has the same unit of mm³/min.

The cutting time, t, for a work piece of length, l, can be calculated by noting that the tool travels at a feed rate of $fN = (\text{mm/rev})(\text{rev/min}) = \text{mm/min}$. Since the distance traveled is l mm, the cutting time is

$$t = \frac{l}{fN}$$

1.7 Chip Morphology

Metal cutting is a chip forming process. Different types of chips are formed during machining. The nature of chip formation process depends on the material being machined and the cutting conditions at the time. These conditions may involve the tool, the rate of cutting, the type or condition of the machine and the use or absence of a cutting lubricant. The formation of all types of chips involves a shearing of the work material in the region of a plane extending from the tool edge to the position where the upper surface of the chip leaves the work surface. A very large amount of strain takes place in this region in a very short interval of time, and not all metals and alloys can withstand this strain without fracture. The types of chips produced significantly influence the surface finish of the work piece and the overall cutting operation.

1.7.1 Types of Chips

The types of chips are divided as following four types:

1. Continuous Chips:

Usually, continuous chips are formed with ductile materials at high cutting speeds and high rake angles. Although they generally produce good surface finish, continuous chips are not always desirable, particularly in the CNC manufacturing widely used today. Continuous chips tend to become tangled around the tool holder, the fixturing, and the work piece, as well as chip-disposal system, and the operation has to

be stopped to clear away the chips. This problem can be alleviated with chip breakers and by changing machining parameters, such as cutting speed, feed, and cutting fluids.



Figure 1.15: Mass of continuous chips

2. Built-up Edge Chips:

A built-up edge (BUE), consisting of layers of material from the work piece that are gradually deposited on the tool, may form at the tip of the tool during cutting. The layers build-up and welded to the tool face under the heavy pressure and heat generated at the tip of the tool face. As it becomes larger, the BUE becomes unstable and eventually breaks up. Part of the BUE material is carried away by the tools side of the chip, the rest is deposited randomly on the work piece surface. The process of BUE formation and destruction is repeated continuously during cutting operation unless measures are taken to eliminate it.

3. Serrated Chips:

Serrated chips are semi-continuous chips with zones of low and high shear strain. Metals with low thermal conductivity and strength that decrease sharply with temperature, such as titanium, exhibit this behavior. The chips have a saw tooth like appearance. It is also known as segmented or non-homogeneous chips.

4. Discontinuous Chips:

Discontinuous chips consist of segments that may be firmly or loosely attached to each other and results from brittle work piece material, work piece materials that

contain hard inclusion and impurities, very low or very high cutting speeds, large depth of cuts, low rake angles, lack of an effective cutting fluid.

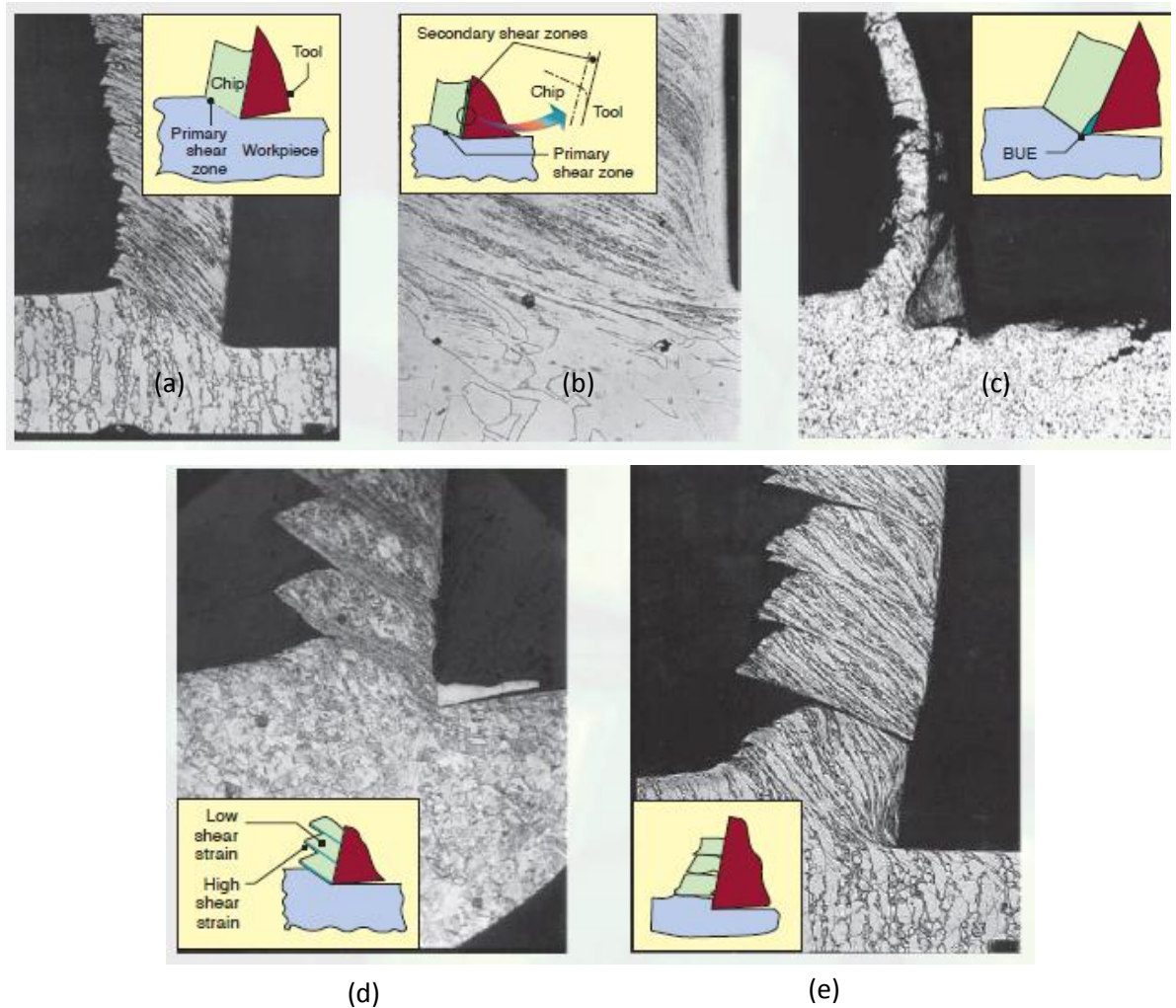


Figure 1.16: Basic types of chips produced in metal cutting and their micrographs: (a) continuous chip with narrow, straight primary shear zone; (b) secondary shear zone at the tool-chip interface; (c) continuous chip with built-up edge; (d) segmented or non-homogeneous chip; and (e) discontinuous chip. [3]

1.8 Ultrasound

Ultrasound is defined as “the vibrations of the same physical nature as sound but with frequencies above the range of human hearing”. Ultrasound is thus not separated from ‘normal’ (audible) sound based on differences in physical properties, only the fact that humans cannot hear it. Although this limit varies from person to person, it is approximately 20 kilohertz (20,000 hertz) in healthy, young adults. Ultrasound devices operate with frequencies from 20 kHz up to several gigahertz’s.

Ultrasound is used in many different fields. Ultrasonic devices are used to detect objects and measure distances. Ultrasonic imaging (sonography) is used in both veterinary medicine and human medicine. In the nondestructive testing of products and structures, ultrasound is used to detect invisible flaws. Industrially, ultrasound is used for cleaning and for mixing, and to accelerate chemical processes. Organisms such as bats and porpoises use ultrasound for locating prey and obstacles.

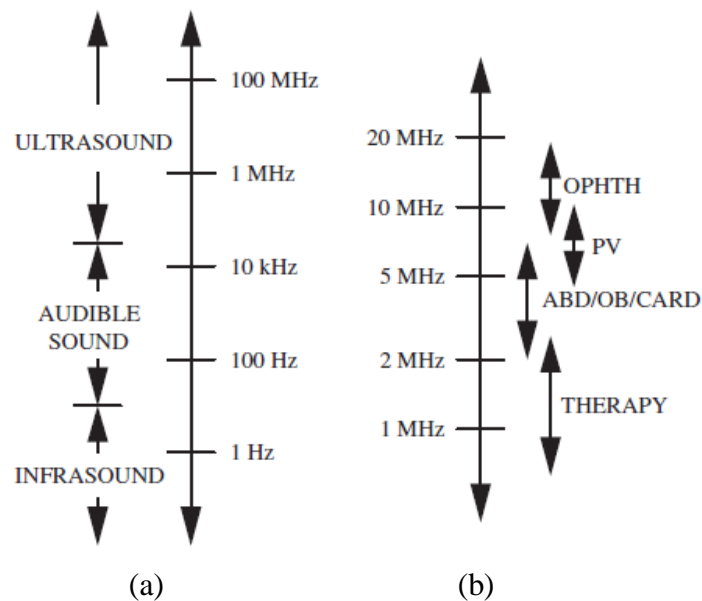


Figure 1.17: (a) The spectrum of sound; (b) The spectrum of medical ultrasound

1.9 Problem Statement

Tool wear and Surface Roughness are inevitable consequences of machining processes. Several techniques have been adopted to optimize and minimize both tool wear and surface roughness. But almost all of them requires an expensive setup or requires modification of the conventional machines (e.g. Tool post modification)

This research develops and applies a new technique of introducing external ultrasonic sound wave during turning operation with specific aims to improve the machining responses such as tool wear and surface roughness. The technique is cost effective and easy to introduce. These errors and failures in machinability results because of vibration phenomena during machining which in turn is due to the instability of the system formed by machine tool structure and metal cutting process. Hence to better relate the results of this research, cutting tool vibration were also measured.

In this research, experiments were carried out under different ultrasonic frequencies to determine the effective frequency range which optimizes the above parameters to the best degree possible. The goal was to achieve improved machinability and analyze the extent of improvement obtained in the above mentioned machinability factors and the interrelation among them by the application of ultrasonic sound wave. The measurements of tool wear were carried out by optical microscope and surface roughness by surface roughness tester. Chip morphology and temperature of the tool inserts were also studied and their effects were analyzed. Improvements in tool life and surface finish were observed during the application of ultrasonic sound waves in turning operation of mild steel. An obvious change in the chip behavior was also present. These observations give a clear indication of the possibility of the application of ultrasonic sound waves in metal cutting processes to improve tool life and reduce surface roughness.

1.10 Research Philosophy

The surface roughness and tool wear incurred during turning operation depends on a combination of machining parameters. Different techniques have been used in an attempt to minimize tool wear and surface roughness. In this research, a novel technique has been used and studied extensively to obtain minimum tool wear and surface roughness. External ultrasound has been applied to the machining process and the effect of external ultrasonic sound wave on tool life of inserts, surface roughness, material removal rate and cutting tool vibration have been studied. Detailed experiments were carried out under different machining conditions and combination of machining parameters. The results were analyzed to obtain relationship between the machinability improvement and interrelation between different machinability factors. Optimized conditions of ultrasonic sound waves for surface roughness, tool wear, etc were obtained and studied in detail.

1.11 Research Methodology

The steps of research methodology are discussed below:

- a) An ultrasound emitting device will be developed which will apply ultrasonic sound waves on the cutting tool insert from both sides. The sound waves will be applied with two piezo device controlled by piezo driver. Signal generators will be used in the device to generate ultrasound frequency within a range of 1 kHz-60 kHz. Experiments will be carried out with five frequencies in this range. The signals will be controlled using microcontroller. LCD controller and display will be used which will display the values of the frequency used in each experiment for flexibility of control.
- b) The experimental study will be conducted on a precision lathe (GATE PINACHO- Model-180) under dry cutting conditions. The insert used will be coated tungsten carbide insert. In the experiments depth of cut and spindle speed will be varied to study their effects. Different ultrasonic frequency will be applied during the cutting operation and their effects on different machining

parameters will be observed. Control experiment without sound wave will also be carried out for comparison.

- c) Tool wear will be measured using optical microscope.
- d) Surface roughness will be measured by surface roughness tester.
- e) The effect of ultrasonic sound wave during turning process will also be investigated by studying generated surface profile, tool investigation, and chip morphology for both with and without ultrasonic sound wave.
- f) Temperature of the tool insert will be measured using digital thermocouple and its effect will be analyzed for both with ultrasonic and without ultrasonic wave.
- g) Different samples of chip will be collected and mounted to observe chip behaviour for further analysis.
- h) Orientation of the application of the ultrasonic sound wave will be changed (i.e. horizontal and vertical) and the effect will be analyzed.
- i) Input power to the ultrasonic sound wave generator will be varied which in turn varies the amplitude of the ultrasound waves and its effect will be analyzed.

1.12 Research Objectives of the Study

There are a number of objectives of this research. They are:

- a) To develop a method and design a device for applying ultrasonic sound waves during turning operation of mild steel.
- b) To find out the effect of ultrasonic sound waves on machinability factors (surface roughness, tool wear, chip morphology, temperature, and cutting tool vibration) by using different frequencies of ultrasonic sound wave.
- c) To compare the machining responses by ultrasonic sound waves with normal machining.
- d) To find out the optimum ultrasonic frequency for cutting operation.
- e) To find out the effect of power variation and orientation of the application of ultrasonic sound wave.

- f) To establish a comprehensive method for improvement of machinability factors during turning operation of steel.

1.13 Significance and Benefits of the Research

The research will have significant benefits in terms of industrial applications and cost savings. Surface roughness and tool wear, as previously mentioned, are a source of a lot of expensive machinery failure or their poor performance. Hence improvements in these machining outputs are of utmost importance. In this research, the effect of ultrasonic sound wave on tool life, surface roughness, chip behaviour and cutting tool vibration will be studied and optimized. Preliminary experiments showed improvements in both tool wear and surface roughness with the application of ultrasonic sound waves. Detailed experiments will be carried out within a range of ultrasonic frequencies to determine the most effective frequency range of operation. Correlation between machining parameters and machining outputs like surface roughness and tool wear will also be determined and the relative dominance of the machining parameters can be found. This research therefore will develop and apply a new technique of introducing external ultrasonic sound wave during turning operation with specific aims to improve the machining outputs.

1.14 Thesis Organization

This thesis is arranged in five chapters. All the details about the study with general information and research background are described in those chapters. A brief summary of each of the chapters are as follows:

The First Chapter is the introduction. It contains general description of the process and theory related with the study. The parameters necessary for the study with formulas are described. It also contains general information about insert, surface roughness, tool wear and chip morphology along with problem statement, methodology, objective and benefits of the study.

In Chapter Two the background of the current study along with the research of contemporary scientists in related fields is described. It gives an idea about the potential of the current project and relates it with the work of others.

Chapter Three is titled as experimental details. In this section the detailed description of each of the equipment used in the study is provided with specification and pictures. The techniques used in the study for measurement of tool wear, surface roughness and chip behavior are also described in this section.

The Fourth Chapter is the results and discussions. This chapter contains the graphs generated based on the experimental data and comparative analysis among different experimental conditions.

Chapter Five is the conclusions and recommendations where the decisions derived from the study are elaborately stated along with the scope of future work on this current study.

CHAPTER 2

Literature Review

There has been significant amount of research on turning operations and improvements of machinability parameters during turning operations. Some of the important research topics and results are discussed in the following sections. The discussion however is in no way comprehensive as there is a huge volume of research literature in the field.

2.1 Contemporary Research

The followings are a summary of the researches done on surface roughness, tool wear, material removal rates and chip morphology:

Silberschmidt et al. [4] studied surface roughness improvement with a technique called ultrasonic assisted turning. Ultrasonically assisted machining is a hybrid technique based on superimposition of ultrasonic vibration on a movement of a cutting tool. The paper presents the results of analysis of the effect of ultrasonically assisted turning (UAT) on surface roughness (using a broad range of parameters) for a broad range of metals and alloys – from copper, aluminium and stainless steel to Ni- and Ti-based alloys. The results show noticeable improvements in surface roughness of all the studied alloys, with its inherent decrease in cutting forces being the main reason for this. This was observed for all the combinations of cutting parameters used, and in all the materials.

Mahdy et al. [5] investigated the effect of different machining parameters on stainless steel and brass alloys, during both ultrasonic assisted turning and conventional turning, and evaluated improvements of cutting forces, surface roughness, surface integrity, and machining accuracy. The results show that the tangential and radial components of the cutting force in case of UAT are lower than those in CT for both studied materials: stainless steel and brass. The average surface roughness in case of UAT is also lower than that in case of CT in both materials.

Muhammad et al. [6] studied the effect of ultrasonic assisted machining on titanium alloy namely Ti-6Al-2Sn-4Zr-6Mo. A 3D thermo-mechanically coupled finite element model for UAT and CT of Ti-6246 was developed. The model was used to

undertake a parametric study of the UAT of Ti-6246. The results showed substantial reduction in the cutting forces in the processing of Ti-alloy. The developed model was validated by experimental results.

Rimkevičienė et al. [7] conducted experiments and simulations of ultrasonically assisted turning tool. They analyzed the adequacy of a model and frequency response characteristics were measured and numerically estimated. The model showed good adequacy.

Maurotto et al. [8] investigated enhanced ultrasonically assisted turning of a β -titanium alloy. Comparisons were made between ultrasonic assisted turning and conventional turning. Different combinations of cutting parameters were used. Results show that average cutting forces are reduced in excess of 70% for depths of cut up to 0.5 and that surface quality improves substantially in UAT.

Patil et al. [9] studied the effect of ultrasonic vibrations on machining of Ti6Al4V through modeling and simulation. The simulation shows that UAT reduces the stress level on cutting tool, significant reduction in cutting forces and cutting temperature during machining as compared to that of in continuous turning (CT). The experimental analysis of UAT process shows that the surface roughness in UAT is lower than in CT.

Sahoo et al. [10] studied the turning on hardened AISI 4340 steel (47 ± 1 HRC) using coated carbide inserts (TiN/TiCN/Al₂O₃/ZrCN) under dry environment. The aim was to assess the tool life of inserts and evolution of flank wear with successive machining time. It was found that the gradual growth of flank wear for multilayer coated insert indicates steady machining without any premature tool failure by chipping or fracturing. Abrasion is found to be the dominant wear mechanisms in hard turning.

Das et al. [11] investigated the optimization method of the cutting parameters namely cutting speed, depth of cut and feed in dry turning of AISI D2 steel to achieve minimum tool wear and low work piece surface temperature. The experimental layout was based on Taguchi's L9 orthogonal array technique. Analysis of variance was performed to determine the relationship between cutting parameters and response

variables. The result showed that depth of cut and cutting speed are the most influential parameters for tool wear.

Zhou et al. [12] investigated a new tool life criterion based on a pattern-recognition technique and neural network and wavelet techniques in raw turning. The experimental results showed that it was applicable to tool condition monitoring in a wide range of cutting conditions.

Braghini et al. [13] studied tool wear behavior of Polycrystalline Cubic Boron Nitride (PCBN) and cemented carbide tool in end milling of hardened steels. They discovered that the minimal wear mechanism was a combination of adhesion and abrasion and found that wear occurred predominantly on the flank face.

Chien and Tsai [14] developed a model for predicting flank wear in tools followed by an optimization model for determining optimal cutting conditions in machining 17-4PH stainless steel. The back-propagation neural network (BPN) and genetic algorithm (GA) were used to construct the predictive model and optimization model respectively.

Ghani et al. [15] investigated the performance of TiN coated carbide inserts in semi-finish and finish end milling of hardened tool steel at high cutting speeds. They compared the performance of the TiAlN inserts under room temperature condition with the effectiveness of the same tool material under preheated room temperature conditions. Tool wear was found to be one of the factors for the variation of performance.

Özel and Karpat [16] utilized the neural network model in comparison with regression model to predict surface roughness and tool flank wear. The data set from measured surface roughness and tool flank wear were used to train the neural network models. It was found that predictive neural network models were capable of better predictions for surface roughness and tool flank wear within the range in between which they were trained.

Kumar et al. [17] investigated the wear mechanism of alumina based ceramic tools in the machining of hardened stainless steel and discovered that flank wear affected tool life at lower speed.

Amin et al. [18] proposed a predictive model for the estimation of tool life under different cutting conditions in end milling of tool steel using TiAlN (Titanium Aluminum Nitride).

Mahmoud and Abdel Karim [19] investigated turning operation using High-Speed Steel (HSS) cutting tool with 45° approach angles. This tool showed longer tool life and could perform cutting operation at higher speed than traditional tool with 90° approach angle. The study finally determined optimal cutting speed for high production rate and minimum cost, better tool life, lower production time and operation costs.

In their study on tool flank wear, Takeyama and Murata [20] argued that the amount of tool flank wear is given by the sum of the wear due to abrasion and temperature sensitive diffusion. They considered abrasion to be proportional to the cutting distance and independent of tool temperature. The wear rate could be represented by Arrhenius type equation and diffusion was considered to be temperature dependant. Tool temperature, tool life and tool wear rate results were obtained when machining steel and cast iron using P10 grade WC tools. It was shown that the experimental results for temperatures above 800°C could be represented well by equations which are an indication that wear of tested tools was dominated by diffusion.

Al-Ahmari [21] developed empirical models for surface roughness, tool life and cutting force for turning operation. The process parameters used to develop the machinability model were speed, feed, depth of cut and nose radius. The methods used for developing the models were Response Surface Methodology (RSM) and neural networks (NN).

Hastings and Oxley [22] and Trent and Wright [23] considered abrasion and oxidation of WC tools as the wear mechanisms. They pointed out that, when machining steel work materials, these mechanisms are unlikely to be dominant under the conditions normally used in practice (i.e. at relatively high cutting speeds). This is due to (i) the insufficient amount of abrasives present in the work material, (ii) insufficient hardness of abrasives to abrade WC and (iii) inability to detect any significant signs of abrasive wear in extensive metallurgical studies. However, there are certain conditions under which abrasive wear of WC tools have been observed.

Natarajan et al. [24] presented an on-line tool wear monitoring technique in turning operation. Spindle speed, cutting force, spindle-motor power, feed, depth of cut and temperature were selected as the input parameters for the monitoring technique. Two methods of Hidden Markov Model (HMM) such as the Bar-graph Method and the Multiple Modeling Methods were used to find out the extent of tool wear. To increase the reliability of the output a decision fusion centre algorithm (DFCA) was used which combined the outputs of the individual methods to make a global decision about the wear status of the tool. Finally, all the proposed methods were combined in a DFCA to determine the wear status of the tool during the turning operations.

Ozel et al. [25] studied surface finish and tool flank wear of finished turning of AISI D2 steels (60 HRC) using ceramic wiper (multi-radii) design inserts. Multiple linear regression models and neural network models were developed for predicting surface roughness and tool flank wear. Neural network based predictions of surface roughness and tool flank wear were compared with a non-training experimental data and the results showed that the proposed neural network models were efficient to predict tool wear and surface roughness patterns for a range of cutting conditions. The study concluded that best tool life was obtained in lowest feed rate and lowest cutting speed combination.

Wang and Lan [26] used Orthogonal Array of Taguchi method coupled with grey relational analysis for optimizing surface roughness, tool wear and material removal rate in precision turning on an ECOCA-3807 CNC Lathe. They considered four parameters viz. speed, cutting depth, feed rate, tool nose run off etc. The MINITAB software was used to analyze the mean effect of Signal-to-Noise (S/N) ratio to achieve the multi-objective features. This study not only proposed an optimization approaches using Orthogonal Array and grey relational analysis but also developed a satisfactory technique for improving the multiple machining performances in precision CNC turning with profound insight.

Fnides et al. [27] investigated the influences of cutting parameters: feed rate, cutting speed, depth of cut and flank wear on cutting forces as well as on surface roughness in machining of slide-lathing grade X38CrMoV5-1 steel treated at 50 HRC

by a mixed ceramic tool (insert CC650). The authors found that tangential cutting force was very sensitive to the variation of cutting depth and surface roughness was very sensitive to the variation of feed rate. It was also found that flank wear had a great influence on the evolution of cutting force components and on the criteria of surface roughness.

Biswas et al. [28] studied that on-line flank wear directly influenced the power consumption, quality of the surface finish, tool life, productivity etc. The authors developed a Neuro-Fuzzy model for prediction of the tool wear. Experimental data were obtained from the orthogonal machining of aluminium with high-speed steel tool for various rake angles, feed and velocity along with other machining parameters. Ratio between cutting force and tangential forces was collected. These were used to predict the tool wear. The final parameters of the model were obtained by tuning the crude values obtained from mountain clustering method by using back-propagation learning algorithm and finally the present Neuro-Fuzzy system which predicted the flank wear with reasonable accuracy and proved it to be an effective tool in estimating flank wears on-line.

Fu and Hope [29] applied a unique fuzzy neural hybrid pattern recognition system to establish an intelligent tool condition monitoring system. The investigation concluded that when coupled with the advanced pattern recognition methodology, the established intelligent tool condition monitoring system had the advantages of being suitable for different machining conditions, robust to noise and tolerant to faults.

Wang et al. [30] studied Hybrid Neural Network-based modeling approach integrated with an analytical tool wear model and an artificial neural network that was used to predict CBN tool flank wear in turning of hardened 52100 bearing steel. Experimental results showed that the proposed Hybrid Neural Network excelled the general neural network-based modeling approach and the analytical tool wear model approach.

Kitagawa et al. [31] assumed that, under practical conditions, wear of WC tools was due to adhesion, that wear should increase with the normal stress on the tool flank and that wear rate could be represented by a relation. Major drawbacks of the study

were there since reliable experimental results or an analytical method to determine normal stress is not yet available. Another drawback is that the predicted results indicate elastic contact at flank/work interface in spite of experimental evidence of plastic contact reported by Trent and Wright [23].

Iwata et al. [32] showed that adhesion between WC and steel (hence adhesive wear rate) becomes maximum around 600°C and thereafter falls off rapidly with further increase in temperature.

Lin et al. [33] adopted an abdicative network to construct a prediction model for surface roughness and cutting force. The input process parameters for the model were cutting speed, feed rate and depth of cut. Regression analysis was also adopted as a second prediction model. Both models were compared and it was found that abdicative network was more accurate than regression analysis.

Feng and Wang [34] developed an empirical model by considering working parameters: work piece hardness (material), feed, cutting tool point angle, depth of cut, spindle speed, and cutting time to investigate the prediction of surface roughness in finish turning operation. Data mining techniques, nonlinear regression analysis with logarithmic data transformation were employed for developing the empirical model.

Suresh et al. [35] machined mild steel by TiN-coated tungsten carbide (CNMG) cutting tools and developed a surface roughness prediction model using Response Surface Methodology (RSM). Genetic Algorithms (GA) was used to optimize the objective function and compared with RSM results. It was observed that GA program provided minimum and maximum values of surface roughness and their respective optimal machining conditions.

Lee and Chen [36] developed an on-line surface recognition system based on artificial neural networks (OSRR-ANN) using a sensing technique to monitor the effect of vibration produced by the motions of the cutting tool and work piece during the cutting process. The authors employed tri-axial accelerometer for determining the direction of vibration that significantly affected surface roughness and then analyzed the data by a statistical method and compared prediction accuracy of both the ANN and SMR.

Choudhury and Bartarya [37] focused on design of experiments and neural network for prediction of tool wear. The input parameters were cutting speed, feed and depth of cut. Flank wear, surface finish and cutting zone temperature were selected as outputs. Empirical relation between different responses and input variables and also the neural network (NN) program helped in predictions for all the three response variables. Comparisons were made to determine which method was best for the prediction.

Kirby et al. [38] developed a prediction model for surface roughness in turning operation. The regression model was developed by a single cutting parameter and vibrations along three axes were chosen for in-process surface roughness prediction system. A strong linear relationship among the parameters (feed rate and vibration measured in three axes) and the response (surface roughness) was found by using multiple regression and Analysis of Variance (ANOVA). The authors demonstrated that spindle speed and depth of cut might not necessarily have to be fixed for an effective surface roughness prediction model.

Eze et al. [39] investigated experimentally the relationship between induced vibration and surface roughness in turning of 41Cr4 Alloy steel using Response Surface Methodology. The process parameters considered were depth of cut, cutting speed, feed rate, tool nose radius, tool overhang and work piece overhang. The results showed that induced vibration has a significant effect on surface roughness of work piece which is proportional to cutting tool acceleration.

Kumar et al. [40] analyzed the optimum cutting conditions to get lowest surface roughness in facing by regression analysis. Investigation were done to observe the effects of cutting parameters like spindle speed, feed and depth of cut on surface finish on EN-8. A multiple regression analysis (RA) using analysis of variance was conducted to determine the performance of experimental measurements. Correlation between cutting speed, feed rate and depth of cut were obtained. It was seen that the effect of feed rate is greater than the effect of cutting speed and that the relationship between feed rate and surface roughness is proportional.

Basha et al. [41] studied the effect of process parameter in CNC turning operation to predict surface roughness. The research aimed to predict the surface

roughness on aluminium 6061, by optimizing the input parameters such as spindle speed, feed rate and depth of cut by using coated carbide tool. A second order mathematical model is developed using regression technique and optimization is carried out using Box- Behnken of response surface methodology. It was found that change in feed rate has a significant effect on surface roughness at higher spindle speed but has no significant effect on surface roughness at lower spindle speed.

Raghuandan et al. [42] adopted a Regression Analysis to construct a prediction model for surface roughness for CNC turning of EN19 with carbide insert. The process parameters taken were cutting speed, feed, depth of cut, Nose Radius and Speed. Regression analysis is done considering Non-Linear model. Most significant interactions were found between work materials, feed and cutting speeds. It was observed that the increase in cutting speed tends to improve the average surface roughness and that feed rate is the most critical parameter when finish is the criterion.

Rodrigues et al. [43] studied the effect of speed, feed and depth of cut on surface roughness and cutting force in turning mild steel using high speed steel cutting tool. Experiments were conducted on a precision centre lathe and the influence of cutting parameters was studied using analysis of variance (ANOVA) based on adjusted approach. Linear regression equation of cutting force has revealed that feed, depth of cut, and the interaction of feed and depth of cut significantly influenced the variance. In case of surface roughness, the influencing factors were found to be feed and the interaction of speed and feed.

Kohli and Dixit [44] proposed a neural-network-based methodology with the acceleration of the radial vibration of the tool holder as feedback. The back-propagation algorithm was used for training the network model in order to predict surface roughness in turning process. The methodology was validated for dry and wet turning of steel using high speed steel and carbide tool. It was observed that the proposed methodology was able to make accurate prediction of surface roughness by utilizing small sized training and testing datasets.

Pal and Chakraborty [45] studied the development of a back propagation neural network model for prediction of surface roughness in turning operation and used mild

steel work-pieces with high speed steel as the cutting tool for performing a large number of experiments. The authors used speed, feed, depth of cut and the cutting forces as inputs to the neural network model for prediction of the surface roughness. It was found that predicted surface roughness was very close to the experimental value.

Singh and Kumar [46] studied the optimization of feed force through setting of optimal value of process parameters namely speed, feed and depth of cut in turning of EN24 steel with TiC coated tungsten carbide inserts. The authors used Taguchi's parameter design approach and concluded that the effect of depth of cut and feed were more as compare to speed in variation of feed force.

Ahmed [47] developed the methodology required for obtaining optimal process parameters for prediction of surface roughness in Al turning. For development of empirical model nonlinear regression analysis with logarithmic data transformation was applied. The developed model showed satisfactory results with minor errors. The study concluded that low feed rate gave reduced surface roughness and also that high speed could produce high surface quality within the experimental domain.

Abhuri and Dixit [48] utilized fuzzy set theory and neural networks to develop a knowledge-based system for the prediction of surface roughness in turning process. The authors developed rule for predicting the surface roughness for given process variables as well as for the prediction of process variables for a given surface roughness.

Zhong et al. [49] predicted the surface roughness in turning processes using networks with seven inputs namely tool insert grade, work piece material, tool nose radius, rake angle, depth of cut, spindle rate, and feed rate.

Kumanan et al. [50] proposed the methodology for prediction of machining forces using multi-layered perception trained by genetic algorithm (GA). The data obtained from experimental results of a turning process were used to train the proposed artificial neural networks (ANNs) with three inputs to get machining forces as output. The optimal ANN weights were obtained using GA search. This function-replacing hybrid made of GA and ANN was found computationally efficient as well as accurate to predict the machining forces for the input machining conditions.

Doniavi et al. [51] used response surface methodology (RSM) in order to develop empirical model for the prediction of surface roughness by deciding the optimum cutting condition in turning. The authors showed that the feed rate influenced surface roughness remarkably. With increase in feed rate surface roughness was found to be increased. With increase in cutting speed, the surface roughness decreased. The analysis of variance showed that the influence of feed and speed were more in surface roughness than depth of cut.

Kassab and Khoshnaw [52] used cutting speed, depth of cut, feed rate and tool overhanging as the process parameters to determine the correlation between surface roughness and cutting tool vibration for turning operation. Experiments were carried out on lathe using dry turning (no cutting fluid) operation of medium carbon steel with different level of aforesaid process parameters. The authors developed good correlation between the cutting tool vibration and surface roughness for controlling the surface finish of the work pieces during mass production. The study concluded that the surface roughness of work piece was affected more by cutting tool acceleration and that acceleration increased with overhang of cutting tool. Surface roughness was found to be increased with increase in feed rate.

Thamizhmanii et al. [53] applied Taguchi method for finding out the optimal value of surface roughness under optimum cutting condition in turning SCM 440 alloy steel. Experiments were conducted and results were analyzed with the help of ANOVA (Analysis of Variance) method. The causes of poor surface finish as detected were machine tool vibrations. The authors concluded that the results obtained by this method would be useful to other researches for similar type of study on tool vibrations, cutting forces etc. The work concluded that depth of cut was the only significant factor which contributed to the surface roughness.

Srikanth and Kamala [54] evaluated optimal values of cutting parameters by using a Real Coded Genetic Algorithm (RCGA) and explained various issues of RCGA and its advantages over the existing approach of Binary Coded Genetic Algorithm (BCGA). They concluded that RCGA was reliable and accurate for solving the cutting parameter optimization and construct optimization problem with multiple decision

variables which were cutting speed, feed, depth of cut and nose radius. The authors highlighted that faster solution can be obtained with RCGA with relatively high rate of success, with selected machining conditions thereby providing overall improvement of the product quality by reduction in production cost, reduction in production time and flexibility in machining parameter selection.

Arif et al. [55] used standard deviation of Grey level as an indicator of surface roughness. They used grey scale binary images of machined parts with known Ra values. From the set of Ra values they were able to device a linear regression model concerning the relation of Standard Deviation of the image pixels' brightness and the samples' known roughness. The correlation coefficient was 0.98. They were then able to predict the surface roughness of some sample machined plates with known Ra to an accuracy of 95 %. They concluded that with the aid of even more precise photographic processes, such as Optical Microscope, SEM, Laser Contouring, and AFM, the digital image processing technique could be made more reliable.

Patwari et al. [56] used MATLAB 2008 to develop a cheap and reliable surface roughness measurement and topological contour generation using digital image processing. They applied their unique technique for analyzing surface roughness in shaped and horizontally milled plates.

Sahoo et al. [57] studied the optimization of machining parameters combinations emphasizing on fractal characteristics of surface profile generated in CNC turning operation. The authors used L27 Taguchi Orthogonal Array design with machining parameters: speed, feed and depth of cut on three different work piece materials viz. aluminum, mild steel and brass. It was concluded that feed rate was more significant in influencing surface finish in all three materials. It was observed that in case of mild steel and aluminum, feed showed some influences while in case of brass, depth of cut was noticed to impose some influences on surface finish. The factorial interaction was responsible for controlling the fractal dimensions of surface profile produced in CNC turning.

Reddy et al. [58] adopted surface roughness prediction model for machining of aluminium alloys by CNC turning by multiple regression model and artificial neural

network. The authors used the percentage deviation and average percentage deviation for judging the efficiency and ability of the model in predicting surface roughness. Experimental results showed that the artificial neural network was efficient compared to multiple regression models for the prediction of surface roughness.

Wannas [59] carried out experiments for hard turning of graphitic cast iron for the prediction of tool wear by using radial basis function neural network (RBFNN) model. The RBFNN had speed, feed and depth of cut as inputs and state variable node as the output. The error was less from neural network model than the regression model.

Lan et al. [60] considered four cutting parameters: speed, feed, depth of cut, and nose runoff varied in three levels for predicting the surface roughness of CNC turned product.

Thamma [61] constructed the regression model to find out the optimal combination of process parameters in turning operation for Aluminium 6061 work pieces. The study showed that cutting speed, feed rate, and nose radius had a major impact on surface roughness. Smoother surfaces could be produced when machined with a higher cutting speed, smaller feed rate, and smaller nose radius.

Shetty et al. [62] discussed the use of Taguchi and response surface methodologies for minimizing the surface roughness in turning of discontinuously reinforced aluminum composites (DRACs) having aluminum alloy 6061 as the matrix and containing 15 vol.% of silicon carbide particles of mean diameter 25 μ m under pressured steam jet approach. The measured results were then collected and analyzed with the help of the commercial software package MINITAB15. The experiments were conducted using Taguchi's experimental design technique. The matrix of test conditions included cutting speeds of 45, 73 and 101 m/min, feed rates of 0.11, 0.18 and 0.25 mm/rev and steam pressure 4, 7, 10 bar while the depth of cut was kept constant at 0.5 mm. The effect of cutting parameters on surface roughness was evaluated and the optimum cutting condition for minimizing the surface roughness was also determined. A second order model was established between the cutting parameters and surface roughness using response surface methodology. The experimental results revealed that the most significant machining parameter for surface roughness was steam pressure

followed by feed. The predicted values and measured values were fairly close, which indicated that the developed model could be effectively used to predict the surface roughness in the machining of DRACs.

Meenu Sahu and Komesh Sahu [63] researched on an optimization method to achieve minimum tool wear, low work piece surface temperature and maximum material removal rate (MRR) in dry turning of AISI D2 steel. The input cutting parameters included cutting speed, depth of cut and feed. The experimental layout was based on the Taguchi's L9 (34) Orthogonal array technique and analysis of variance (ANOVA). The results showed that t depth of cut and cutting speed are the most important parameter influencing the tool wear. Optimal range of tool wear, work piece surface temperature and MRR values were predicted through the experiments. Relationship between factors and the performance measures were also developed by using multiple regression analysis.

Tian-Syung Lan [64] used fuzzy Taguchi deduction to optimize material removal rate for CNC turning. In this study, four parameters (cutting depth, feed rate, speed, tool nose runoff) with three levels (low, medium, high) were considered to optimize the MRR in finish turning based on L9(34) orthogonal array. Through this study a general deduction optimization scheme using orthogonal array was proposed.

Shivakoti et al. [65] applied Genetic Algorithm (GA) for optimizing machining parameters (namely cutting speed, feed rate and spindle speed) to obtain maximum material removal rate during turning operation of mild steel using conventional lathe machines. Through the experiments it has been found that material removal rate increases with the increase of feed rate. However, at low spindle speed of rotation, the material removal rate is high compared to high spindle speed of rotation. A regression equation for material removal rate (MRR) was also developed using statistical Minitab software and it was validated through comparative results of MRR achieved during experimentation.

Hakif Zeqiri et al. [66] researched on the influence of tool geometry on chip morphology. A statistical method with five factors was used for data processing. The

result of the experiments showed that tool geometry affected the chip morphology significantly. Results showed that cutting speed was the most important factor.

Mohammad Sima et al. [67] investigated the influence of material constitutive models and elastic –viscoplastic finite element formulation on serrated chip formation of titanium alloy. Here finite element simulations were validated with experimental results at two different rake angles, three different under formed chip thickness values and two different cutting speeds. The results showed that material flow stress and finite element formulation greatly affects not only chip formation mechanism but also forces and temperatures.

L. Deshayes et al. [68] characterized the chip morphology of serrated-chip and discussed the physical phenomena accompanying the serrated-chip formation according to finite element modeling (FEM) simulations. The experimental study was based on metallographic analysis of chip morphology and hardness measurements. Finally, the FEM results were compared with the hardness measurements.

Mason D. Morehead et al. [69] researched on saw-toothed chips formed in hard machining. Through experimentation they studied the effect of tool wear and cutting conditions on the saw-toothed chip morphology in machining of 52100 hardened bearing steel. It was found in the experiments that the chip dimensional values and segmentation frequency were affected by tool wear and cutting conditions while the chip segmentation angles were approximately constant under different tool wear and cutting conditions.

Patwari et al. [70] had previously used digital image processing techniques, on grey scale sample profile pictures, to study a different machining phenomenon, chatter formation. They used Visual Basic to determine the primary and secondary serrated teeth of machined chips. This was used to correlate chip serration frequency to chattering.

Chen et al. [71] studied the deformation mechanism of serrated chip formation process and its chip morphology of chips produced during precision turning process of the hardened steel GCr15 by the methods such as numerical simulation of two-dimensional finite element analysis of turning, chip cross-sectional microscopic analysis

and other methods. The results show that the reason of hardened GCr15 steel forming serrated chip is periodic adiabatic shear fracture, and the research provides a theoretical reference application of hard turning technology.

Mhamdi et al. [72] studied the mechanism of chip formation in order to be able to obtain the optimal cutting conditions in turning of hardened AISI D2 steel. Hard turning tests were carried out for this steel at different cutting conditions. The chips obtained were examined under a microscope. The observation showed that the chip formation is influenced by cutting conditions. The chips contained a white layer, and this layer was examined under scanning electronic microscope (SEM) to study its variation depending on cutting parameters which showed that cutting forces decrease with the increase of cutting speed.

Shankar et al. [73] studied in detail the chip formation and chip morphology in Turning of Ti-6Al-4V Alloy in order to attain high efficiency in metal cutting by high pressure cooling using neat oil & water soluble oil.

Salem et al. [74] investigated the chip formation of hardened AISI D2 steel to obtain the optimal cutting conditions and to observe the different chip formation mechanisms. Results showed that there are relationships between the chip geometry, cutting conditions and the different micrographs under different metallurgical states.

2.2 Summary of Literature Review

Literature shows that a considerable amount of work has been carried out by previous investigators for modeling, simulation and parametric optimization of surface properties of the product in turning operation. Issues related to surface roughness of the product, tool life, tool wear, cutting forces have been addressed and relationships between different process parameters like feed, depth of cut, cutting speed etc. and machining output parameters have been developed. Several techniques have also been developed to reduce the machining responses like surface roughness and tool wear than that could have been obtained with conventional turning. One such technique which showed great promise is ultrasonic assisted turning (UAT).

So, the authors of this research in lieu of the search for a better, optimized and cost-effective technique developed and investigated a new technique of application of ultrasonic sound waves externally. Here the ultrasound air waves interacted with the machining vibrations externally. A wide range of several cutting conditions have been used in the experiment to study the effect.

2.3 Scope of Current Research

Literature depicts that a considerable amount of work has been carried out by many researchers for reducing tool wear and improving surface quality by several techniques. Ultrasonically assisted turning has been one of the techniques which showed great promise. Ultrasonic Assisted Turning (UAT) is a process of turning a work piece with the help of high-frequency low-amplitude vibrations. However, this technique requires the conventional tool post setup of a lathe machine to be replaced with a new setup with sonotrode and other accessories required for UAT. The vibration direction in relation to the tool movements has a great effect on the surface produced. This direction could be either in lateral feed direction or in the longitudinal feed direction. The first moves the tool intermittently in a hammer-wise movement in relation to the work piece's rotating surface; this movement results in an instantaneous increase in the radial force component. The second direction is linked to the tool movement in a direction parallel to the work piece's rotating axis; this movement results in an instantaneous increase in the axial force component each time the vibratory movement brings tool closer. A sonotrode is usually used for applying the ultrasound frequency. A sonotrode usually consists of a stack of piezoelectric transducers attached to a tapering metal rod. The tool insert is connected to the end of the rod which is the assembly applied to the working material. An alternating current oscillating at ultrasonic frequency is applied by a separate power supply unit to the piezoelectric transducers. The current causes them to expand and contract. The frequency of the current is chosen to be the resonant frequency of the tool, so the entire sonotrode acts as a half-wavelength resonator, vibrating lengthwise with standing waves at its resonant

frequency. The standard frequencies used with ultrasonic sonotrodes range from 20 kHz to 70 kHz. The amplitude of the vibration is small, about 13 to 130 micrometres.

However, the present study investigates a new technique of application of ultrasonic sound waves. Instead of superimposing the ultrasound on the tool movement, ultrasonic sound waves have been applied into the turning cutting process externally. The ultrasound waves were sent from two piezo's from both sides of the cutting tool insert during the machining process. Hence, here the ultrasound air waves interacted with the machining vibrations externally. A wide range of several cutting conditions have been used in the experiment to study the effect.

The study can lead to the following outcomes:

- a) An effective cutting process with the application of ultrasonic sound waves for turning operation of mild steel.
- b) Determination of the optimum ultrasonic frequency for cutting operation.
- c) Reduction of tool wears during turning leading to lower production cost.
- d) Improvement of surface roughness resulting in higher product quality.
- e) Reduction of cutting tool vibration leading to better surface quality.
- f) Better understanding of chip morphology in different cutting conditions.
- g) Better understanding of the effect of temperature for both with ultrasonic and without ultrasonic wave.
- h) Better understanding of the effect of the orientation of the application of ultrasonic sound waves.
- i) Better understanding of the effect of the input power variation of the ultrasonic sound wave generator which results in amplitude variation of the ultrasonic sound waves.

CHAPTER 3

Experimental Details

3.1 Introduction

The primary idea behind the research endeavor was to study the effect of the application of external ultrasonic sound waves on surface roughness and tool wear in turning process. Different frequencies of ultrasound signals were applied to study the effect on the process with variations in machining parameters like depth of cut, spindle speed etc. Comparison with normal machining was also one to establish the degree of improvement. Finally, optimized range of ultrasonic frequency was identified.

3.2 Experimental Procedure and Design

The following sequence of experimentation was followed in this research:

- ❖ One particular lathe is selected for carrying out the whole research to ensure that no disparities occur because of lathe machine.
- ❖ Checking and preparing the centre lathe before starting operation.
- ❖ Cutting mild steel bars of similar composition, desired length and diameter by power saw.
- ❖ Performing facing and centre drilling of job piece for fixing it in between chuck and tail stock.
- ❖ Performing straight turning operation on specimens in various cutting environments involving various combinations of process control parameters like: spindle speed, depth of cut and ultrasonic frequency.
- ❖ Determining surface roughness using surface roughness tester.
- ❖ Analysis of surface roughness data to determine the optimum ultrasound frequency.
- ❖ Repeating experiments with the optimum ultrasound frequency to study the effect of tool wear.
- ❖ Measuring tool flank wear using microscope and digital image processing technique.
- ❖ Collecting chip and calculating chip serration frequency.

- ❖ Repeating experiments with the optimum ultrasound frequency to determine the best orientation of the application of ultrasound (i.e. horizontal or vertical).
- ❖ Repeating experiments with the optimum ultrasound frequency to study the effect of input power variations.
- ❖ Final analysis and comparison of collected data

The flowchart below shows the experimentation sequence that will be followed in this research.

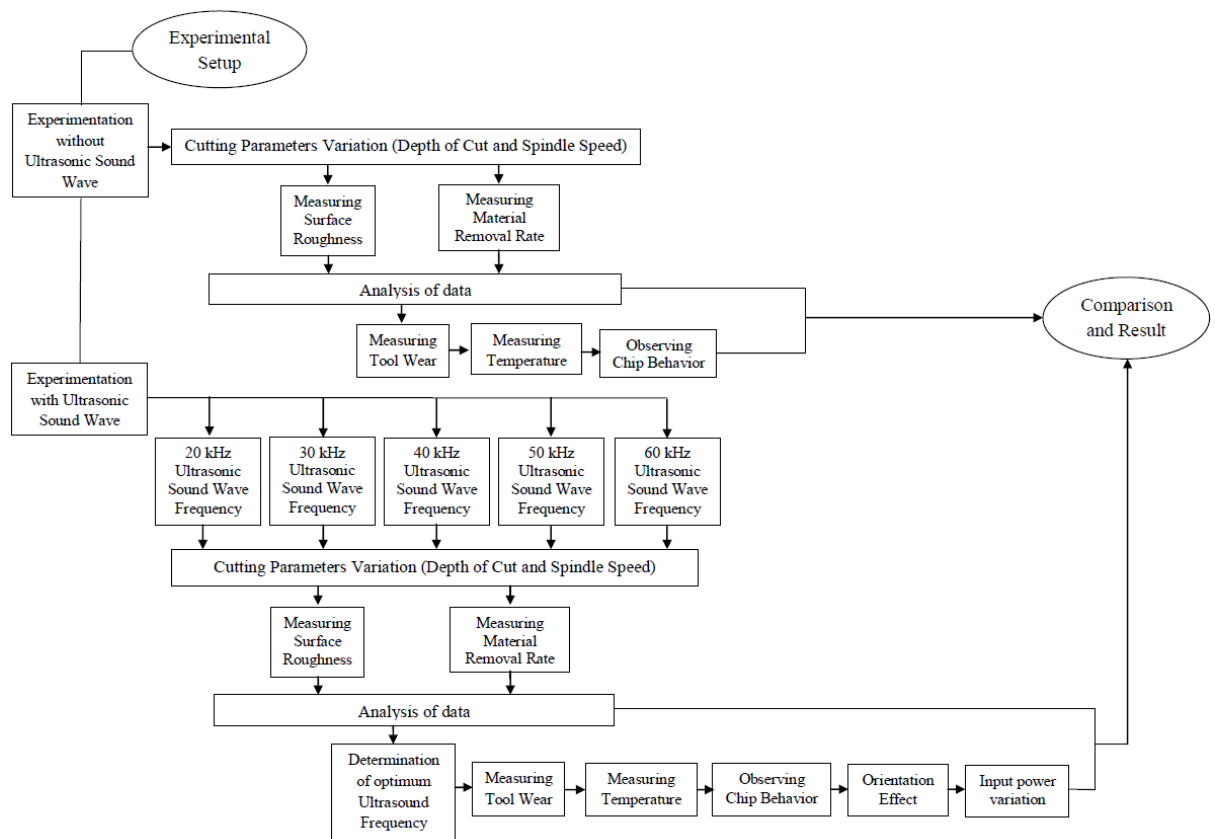


Figure 3.1: Flow sequence of experimentation

The figure below shows a schematic of the experimental setup used in this research.

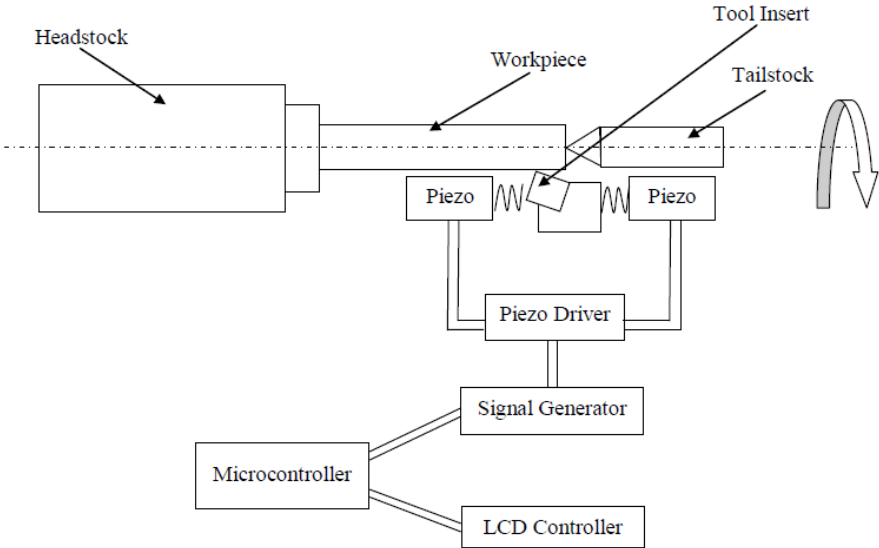


Figure 3.2: Schematic of the experimental setup

3.3 Process Variables and their Values

In the present experimental study, spindle speed, feed rate and depth of cut have been considered as process variables. Feed was kept constant for all the experimentation. The process variables with their units (and notations) are listed in Table 3.1.

Table 3.1: Process variables and their values

Process Variables		
Spindle Speed (RPM)	Depth of cut (d) (mm)	Ultrasound Frequency (kHz)
360	0.5, 1	20, 30, 40, 50, 60
530	0.5, 1	20, 30, 40, 50, 60

3.4 Equipments and Apparatus Used

3.4.1 Centre Lathe

For performing the experiments, centre lathe in the IUT machining laboratory will be utilized. The centre lathe model details are shown below:

Manufactured by: GATE INC. (United Kingdom)
Model: L-1/180

The figure below shows a labeled figure of the centre lathe used in this research.

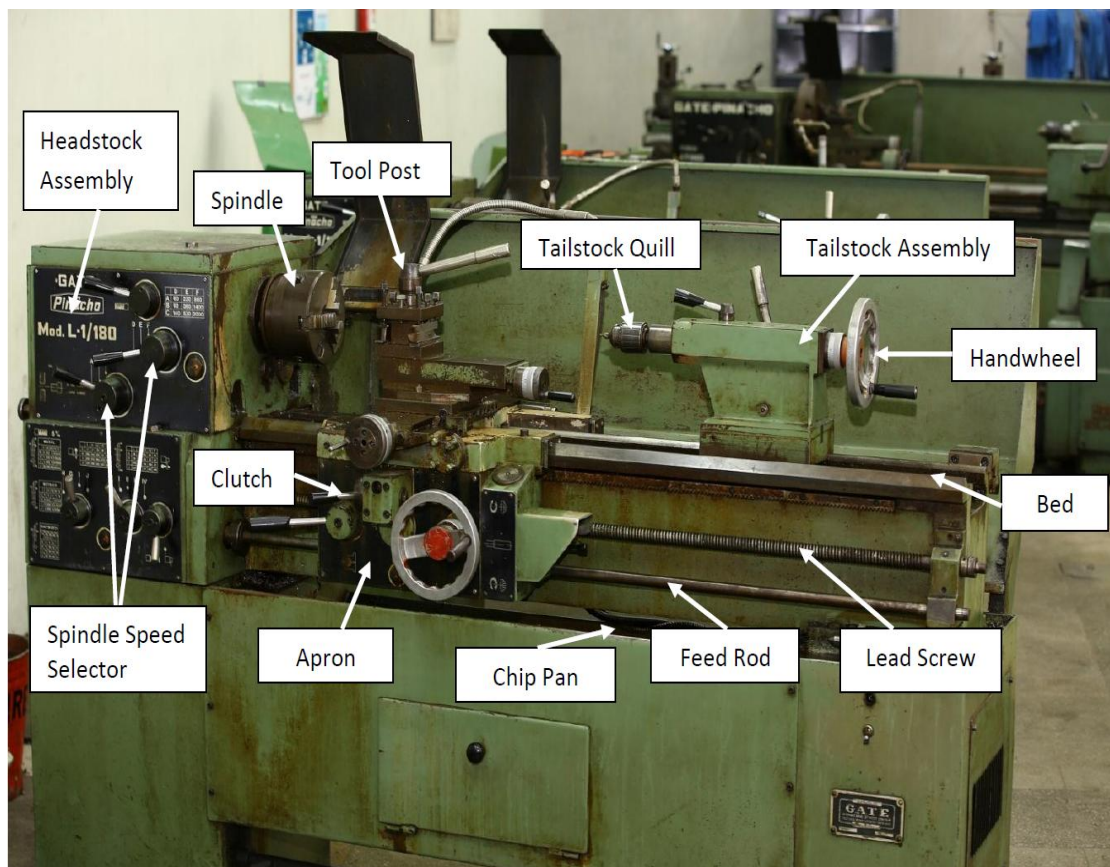


Figure 3.3: Photograph of labelled centre lathe used in this research

The specifications of the lathe machine used in this study are given in the figure below.

CAPACITY	SP/200	
	mm	inches
center height	200	7 7/8"
center distance	750-1000	30"-40"
swing over bed	400	15 3/8"
swing over gap	560	22"
swing over carriage	375	14 3/4"
swing over cross slide	245	9 5/8"
bed width	250	10"
gap length in front of face plate	120	4 3/4"
HEAD STOCK		
main spindle bore	42	1 5/8"
main spindle nose	DIN 55027-5	cam lock no 5
main spindle morse taper	4	4
9 speed range	60-2000	60-2000
THREAD AND FEED BOX		
44 longitudinal feeds	0,05-0.75	0.0018-0,026"
44 cross feeds	0,025-0,375	0,0005-0,0076"
44 metric threads	0,5-7,5	0,5-0,7
44 withworth thread in T.P.1	60-4	60-4
44 modular threads	0,25-3,75	0,25-3,75
44 pitch diametral thread	120-8	120-8
thread oflead screw	6	4h/1h"
SLIDE AND CARRIAGE		
cross slide travel	245	9 5/8"
tool post slide travel	120	4 3/4"
maximum tool dimensions	20*20	3/4"-3/4"
TAILSTOCK		
tailstock barrel diameter	58	2 9/32"
tailstock barrel travel	200	7 7/8"
tailstock taper	4	4
MOTORS		
main motor power in kW	4	4
pump motor power in kW	0,06	0,06
STEALDIES		
max~min capacity of fixed steady	10-130	3/8"-5"
max~min capacityof traveling steady	Oct-80	3/8"-3" 3/16"

Figure 3.4: Specifications of the centre lathe used in this research

3.4.2 Surface Profilometer or Surface Roughness Tester

A surface profilometer was used to measure surface roughness in this research. The details of the surface profilometer model are shown below:

Manufactured by: Mitutoyo
Model: SURFTEST SJ-210

The figure below show the surface profilometer used in this research.



Figure 3.5: Photograph of Mitutoyo SURFTEST SJ-210 Surface Profilometer

The specifications of the surface profilometer used in this study are given in the table below.

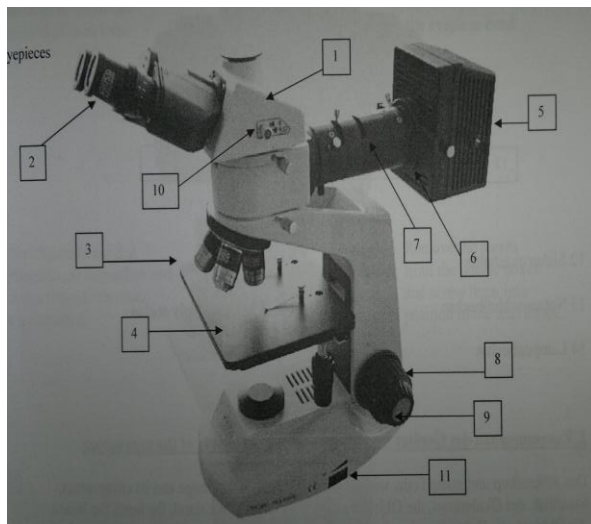
Table 3.2: Specifications of the surface profilometer used in this research

Drive unit type	Standard
Detector type	4mN measuring force, 5 μ m stylus tip radius
Standards met	JIS (1982, 1994, and 2001), ISO 1997, VDA, and ANSI
Measuring range	X-axis: .69 inches (17.5mm); Z-axis 14200 μ in (-7900 μ in ~+6300 μ in)/360 μ in / .08 μ in (25 μ m / 0.002 μ m)
Resolution	14170 μ in / .8 μ in (360 μ m / 0.02 μ m), 4000 μ in / .2 μ in (100 μ m / 0.006 μ m), 1000 μ in / .08 μ in (25 μ m / 0.002 μ m)
Assessed profile	Primary profile (P), roughness profile (R), DIN4776 [Primary profile (P), Roughness profile (R), MOTIF (R): M-type
Parameters	Rv, Rsk, Rku, Rc, RPc, RSm, Rmax, Rz1max, RzJIS, Rppi, R Δ a, R Δ q, Rlr, Rmr, R δ , ζ , HSC, Rpm, tp, Htp, Ra, Ry, Rz, Rq, S, Sm, Pc, R3z, mr ©, Rt, Rp, Rk, Rpk, Rvk, Mr1, Mr2, A1, A2, Vo (customizable)(R, AR, Rx: M-type)
Overall dimensions	52.1 x 65.8 x 160 mm / 2.05 x 2.6 x 6.3 inches (H x W x D)
Weight	1.1 lb (500g) including display unit, drive unit, and detector

3.4.3 Optical Microscope

To measure the tool wear and for capturing images of surfaces, optical microscope was used. The magnification used was 100X.

The model of the optical microscope used in this research is “METALLURGICAL MICROSCOPE MMB2300”. The figure below shows a labeled figure of the optical microscope.



1. Eyepiece head with photo/video connection
2. Eyepieces
3. Objective
4. Stage with clips
5. Illumination
6. Diaphragm
7. Color filters
8. Coarse adjustment knob
9. Fine adjustment knob
10. Change between eyepiece head and photo/video connection
11. On/off and brightness control

Figure 3.6: Photograph of labelled Metallurgical Microscope MMB2300

The specifications of the microscope are given in the table below:

Table 3.3: Specifications of Metallurgical Microscope MMB2300

Plano eyepieces	10X
Lenses	Plan achromatic 4X,10X,40X
Magnification	40 to 400
Filter	Blue
Power supply	90 to 240 VAC
Fuse	3.15 A
Illumination	Built in lamp 6V 30W, brightfield condenser
Stage moving range	132 x 140 mm
Photo-/video-mounting	Photoadapter with eyepiece Videoadapter with eyepiece
Weight	10kg net, 15kg cross

3.4.4 Thermometer

To take the temperature readings, a digital thermometer was used in this study. It was a **Model 305 Digital Thermometer**. It is a portable hand held and compact digital thermometer designed to use an external K type thermocouple as a temperature sensor. Temperature indication follows National Bureau of Standards and IEC 584 temperature/voltage tables for K type thermocouples. The thermocouple used was copper-constantan. Figure below shows the digital thermometer used in this study.



Figure 3.7: Photograph of Model 305 Digital Thermometer

The specifications of the digital thermometer are given in the table below:

Table 3.4: Specifications of Digital Thermometer Model 305

ELECTRICAL
Temperature Scale: Celsius or Fahrenheit, selected by user.
Measurement Range: -50°C to 1300°C (-58°F to 2000°F).
Resolution: 1°C or F, 0.1°C or 0.1°F.
Accuracy: Accuracy is specified for operating temperatures over the range of 18°C to 28°C (68°F to 82°F), for 1 year, not including thermocouple error. ((0.3% rdg +1 C) - 50°C to 1000°C. ((0.5% rdg +1 C) -1000°C to 1300°C. ((0.3% rdg +2 F) -58°F to 2000°F).
Temperature Coefficient: 0.1 times the applicable accuracy specifications per C from 0°C to 18°C and 28°C and 50°C (32°F to 64°F and 82°F to 122°F).
Input Protection: 60V dc or 24V rms ac maximum input voltage on any combination of input pins.
Reading Rate: 2.5 times per second.
Input Connector: Accepts standard miniature thermocouple connectors (flat blades spaced 7.9 mm, center to center).

ENVIRONMENTAL
Ambient Operating Range: 0°C to 50°C (32°F to 122°F).
Storage Temperature: -20°C to 60°C (-4°F to 140°F).
Relative Humidity: <ul style="list-style-type: none"> • 0% to 80% (0°C to 35°C) (32°F to 95°F). • 0% to 70% (35°C to 50°C) (95°F to 122°F).
GENERAL
Display: 3 1/2 digit liquid crystal display (LCD) with maximum reading of 1999.
Battery: Standard (9V battery (NEDA 1604, IEC 6F22)).
Battery Life: 200 hours typical with carbon zinc battery.
Dimensions: 147 mm (H), 70mm (W), 39mm (D).
Weight 7.4 Oz (210g).

3.4.5 Oscilloscope

A PC oscilloscope was used to calibrate the ultrasound creator and emitting device to ensure that the input signal gives accurate output signal frequency. It consists of a specialized signal acquisition board (which can be an external USB or parallel port device, or an internal add-on PCI or ISA card). The details of the oscilloscope are shown below:

Manufactured by: Picotech
Model: PicoScope 3204

The figure below shows the PC oscilloscope used in this study for calibration.



Figure 3.8: Photograph of PicoScope 3204

The specifications of the oscilloscope are given in the table below:

Table 3.5: Specifications of PC oscilloscope PicoScope 3204

Bandwidth	50 MHz
Sampling rate (single shot)	50 MS/s
Sampling rate (repetitive)	2.5 GS/s
Channels	2 + External trigger / Signal generator
Signal generator	1 kHz square wave
Oscilloscope timebases	5 ns/div to 50 s/div
Timebase accuracy	50 ppm
Spectrum ranges	DC to 25 MHz
Record length	256 k samples
Resolution/accuracy	8 bits / 3%
Ranges	± 100 mV to ± 20 V
PC connection	USB 2.0 (USB 1.1 compatible)

3.4.6 Ultrasound Frequency Generator Device

For this research, a unique ultrasound device was developed which is able to generate ultrasound frequency within a range of 1 kHz-65 kHz. The ultrasound generator device developed is able to apply ultrasonic sound waves on the cutting tool insert from both sides. The sound waves are applied with two piezo device. Signal generators are used in the device to generate sound signals which is then converted to ultrasound frequency by a piezo driver. The signals are controlled by a microcontroller. LCD controller and display are used which displays the values of the frequency used in each experiment for flexibility of control. The figure below shows the ultrasound generator device developed and used in this research.

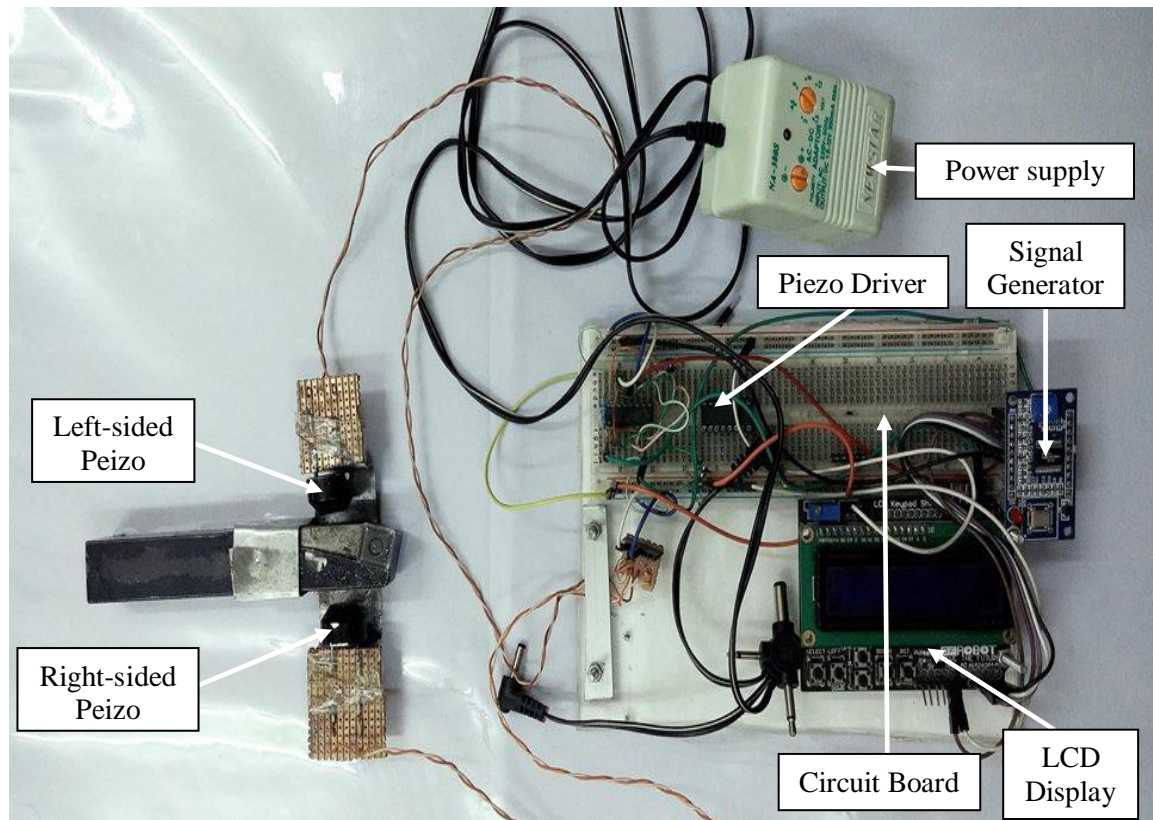


Figure 3.9: Photograph of labelled ultrasound generator device developed specifically for this research

The signal generator used to make the device was AD9850, CMOS, 125 MHz, Complete DDS Synthesizer. The AD9850 is a highly integrated device that uses advanced DDS technology coupled with an internal high speed, high performance D/A converter and comparator to form a complete, digitally programmable frequency synthesizer and clock generator function. When referenced to an accurate clock source, the AD9850 generates a spectrally pure, frequency/ phase programmable, analog output sine wave. This sine wave can be used directly as a frequency source. The figure below shows the functional block diagram of the signal generator.

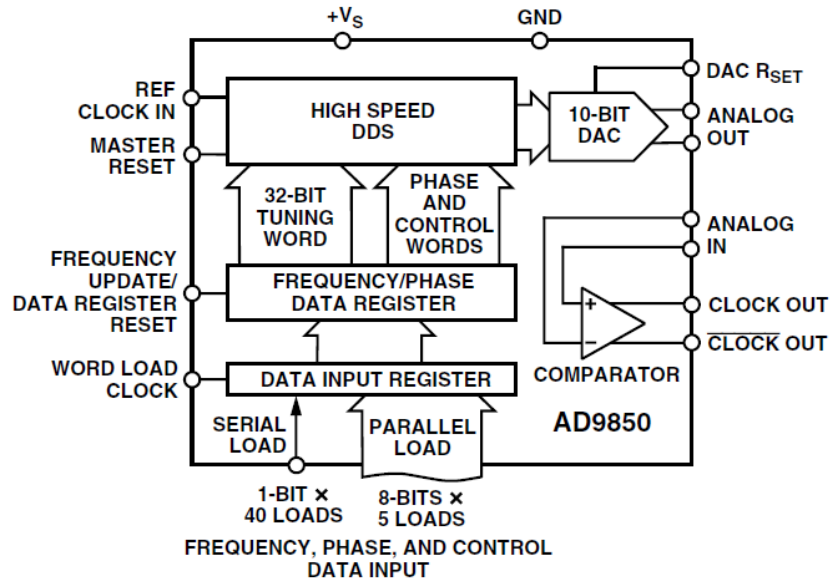


Figure 3.10: Functional block diagram of AD9850

The figure below shows the circuit diagram for the signal generator.

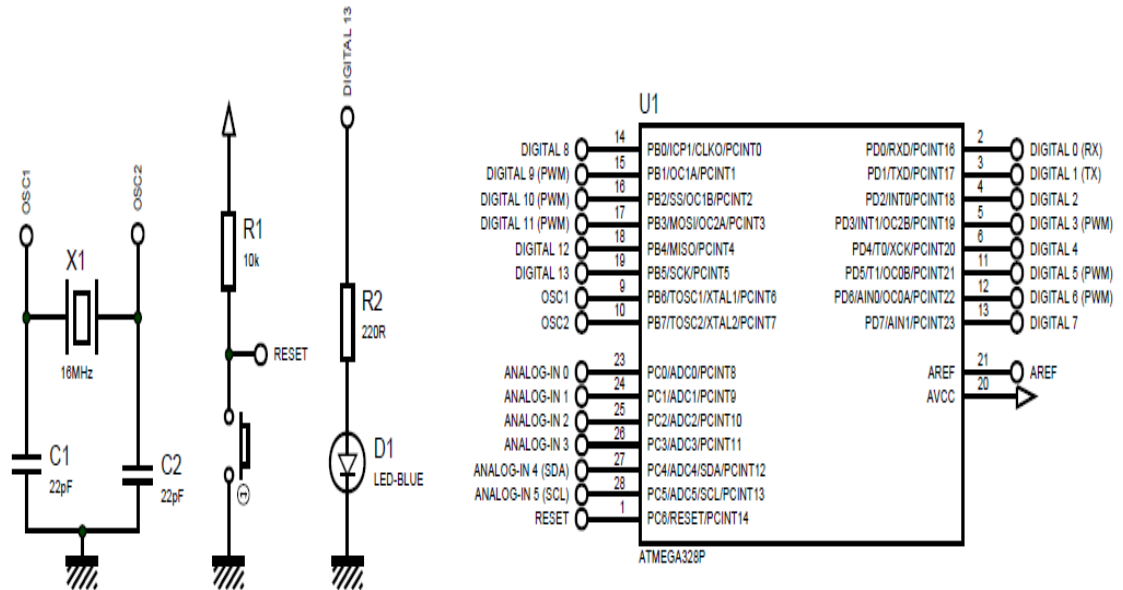


Figure 3.11: Circuit diagram of the signal generator

The signal from the signal generator is then sent to a piezo driver which converts the signal into frequency. The piezo driver used in the device is L293, L293D, Quadruple Half-H Drivers. The figure below shows the piezo driver used in the device,

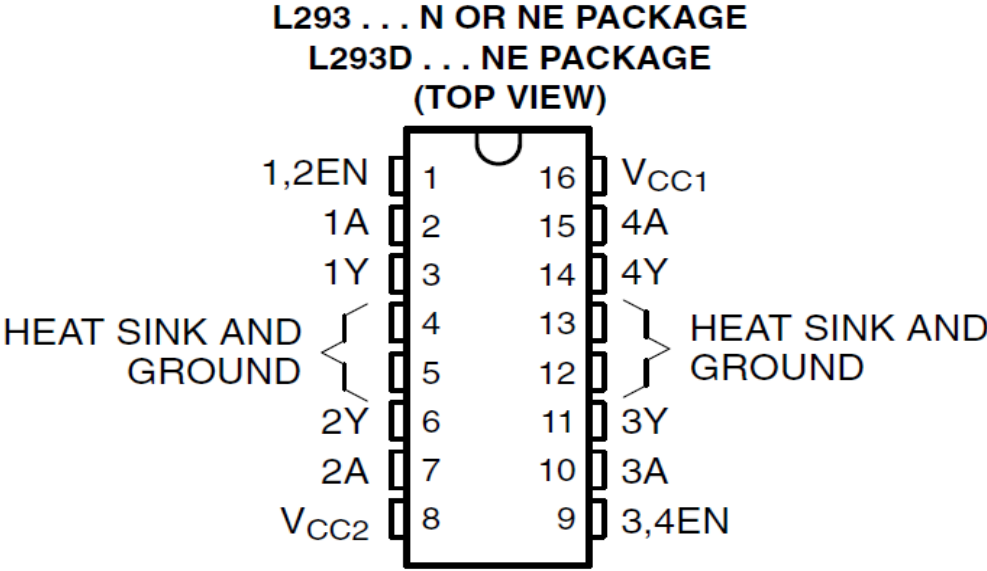


Figure 3.12: Piezo Driver

The figure below shows the circuit diagram for the piezo driver.

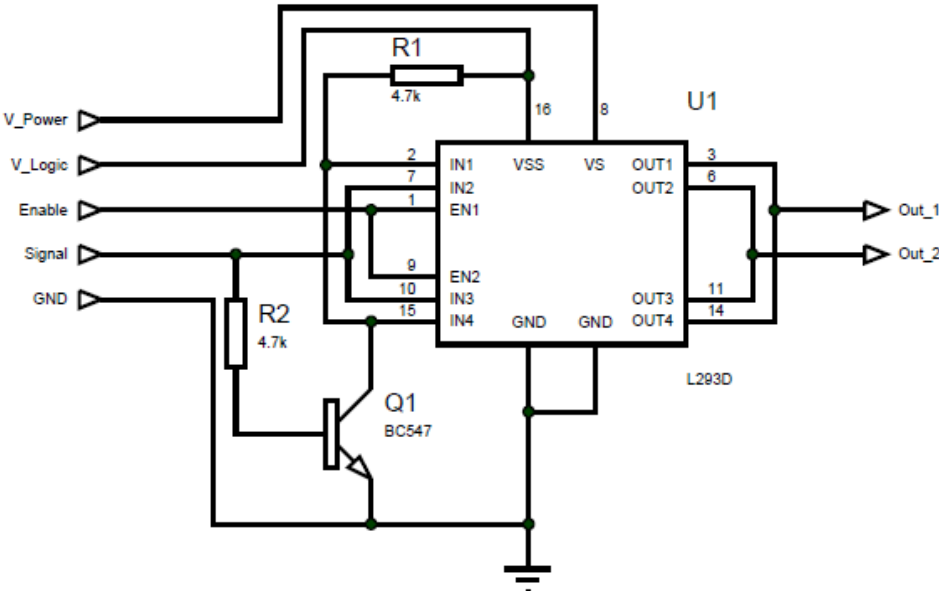


Figure 3.13: Circuit diagram of the Piezo Driver

The figure below shows the overall circuit diagram of the ultrasound generator device.

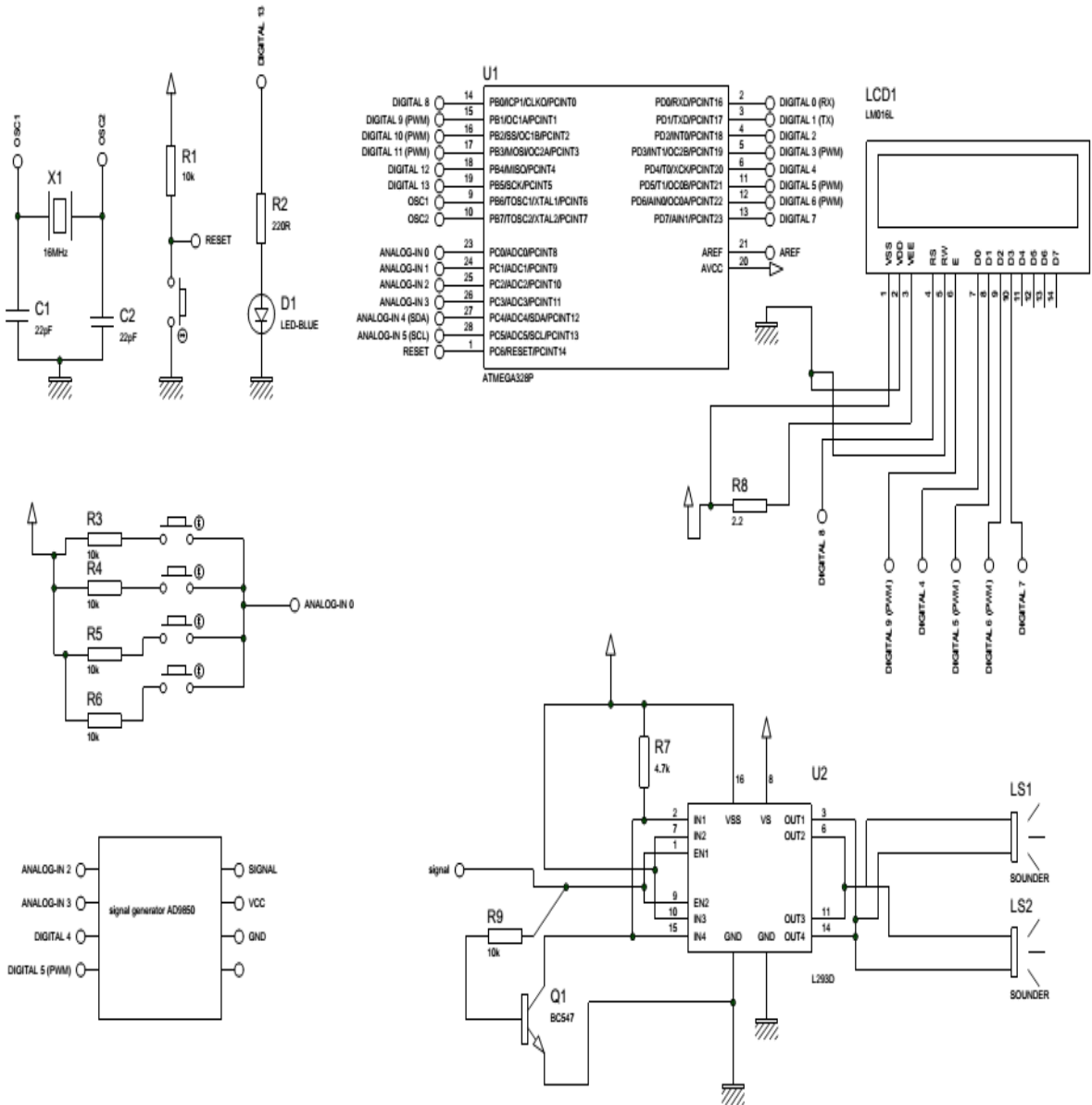


Figure 3.14: Complete circuit diagram of the ultrasound generator device

Calibration of the Device

The device developed was calibrated to ensure that the correct ultrasound frequency was obtained. Different ultrasound frequencies were checked with a picoscope to ensure that there were no error in the input signal and the out ultrasound frequency. The figure below shows the setup used for the calibration purpose.

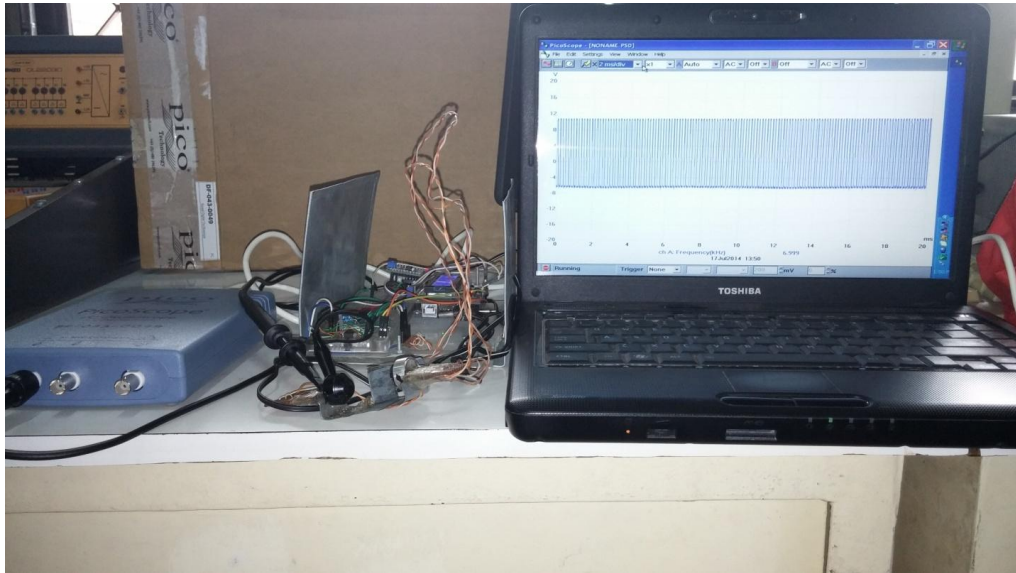


Figure 3.15: Photograph of the setup for calibrating the ultrasound generator device

The table below shows the results obtained with picoscope of the various ultrasound frequencies emitted by both the left-sided and right-sided piezo.

Table 3.6: Input and output data of ultrasound frequency measured for calibration purposes

Input Signal (kHz)	Output Ultrasound Frequency (kHz)	
	Left-sided Piezo	Right-sided Piezo
20	20	20
30	29.99	30
40	40	40
50	50	50
60	60.01	60

The figures below shows the graphs obtained with picoscope for the left-sided and right-sided piezo at 60 kHz. The rest of the graphs are given in Appendix B.

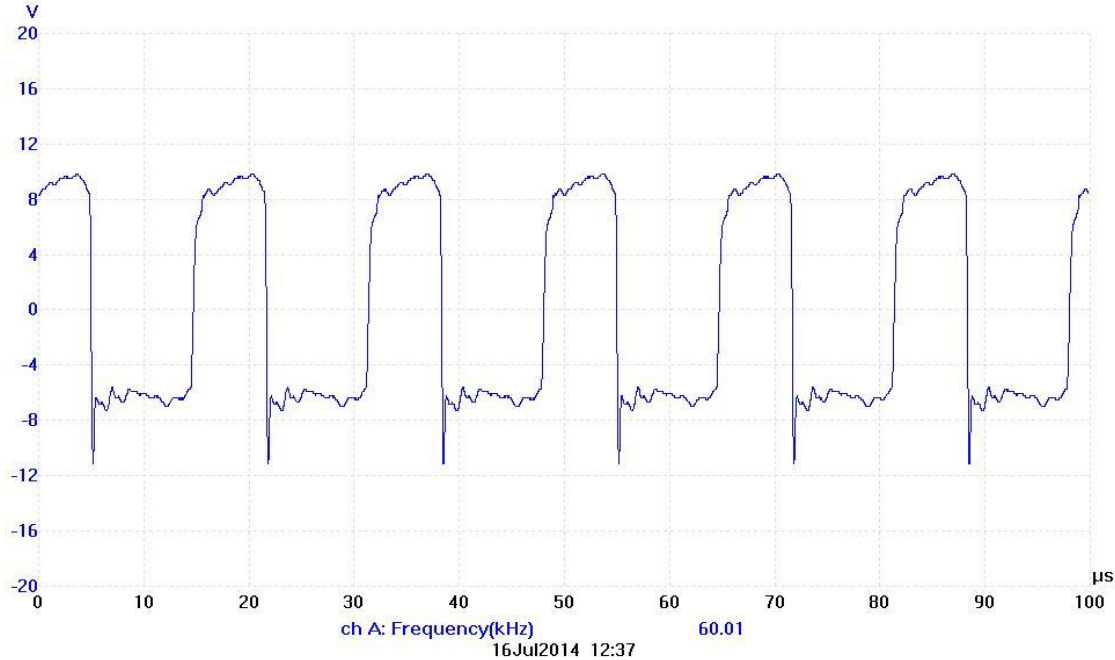


Figure 3.16: Ultrasound wave generated at 60 kHz obtained with a picoscope from the left-sided ultrasound emitter for calibration purposes

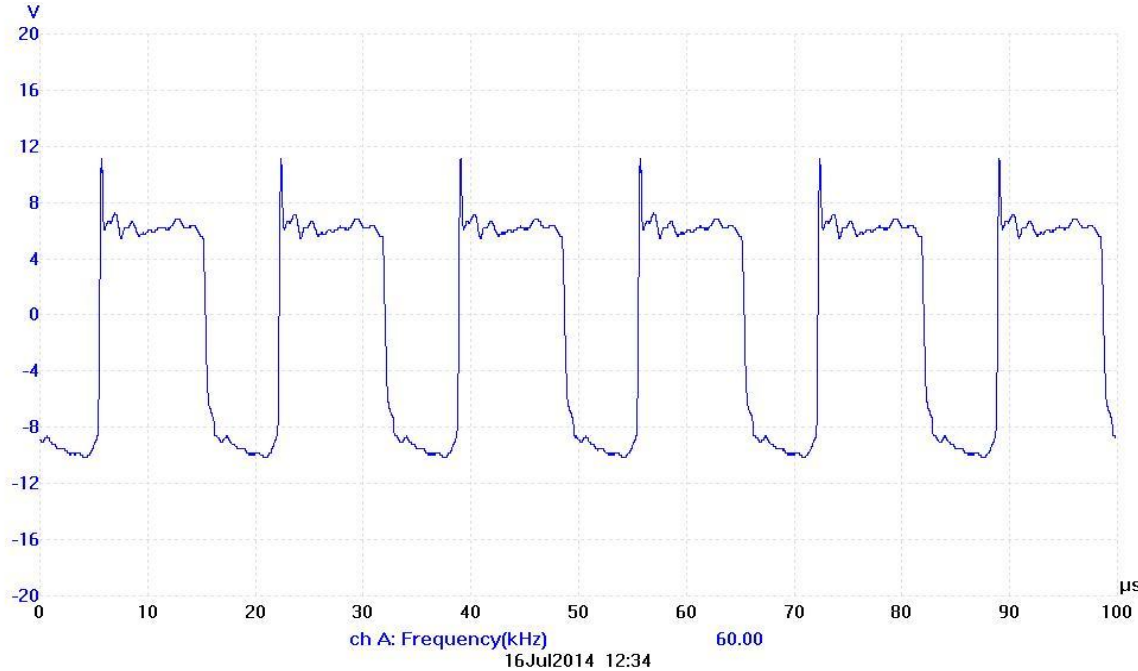


Figure 3.17: Ultrasound wave generated at 60 kHz obtained with a picoscope from the right-sided ultrasound emitter for calibration purposes

3.4.7 Accelerometer

To measure the vibration of the tool holder and the cutting tool, an accelerometer was used in this research. The model of the accelerometer is MPU-6050. It is a three-Axis MEMS Accelerometer with 16-bit ADCs and Signal Conditioning. The MPU-6050's 3-Axis accelerometer uses separate proof masses for each axis. Acceleration along a particular axis induces displacement on the corresponding proof mass, and capacitive sensors detect the displacement differentially. The MPU-6050's architecture reduces the accelerometers' susceptibility to fabrication variations as well as to thermal drift. When the device is placed on a flat surface, it will measure 0g on the X- and Y-axes and +1g on the Z-axis. The accelerometers' scale factor is calibrated at the factory and is nominally independent of supply voltage. Each sensor has a dedicated sigma-delta ADC for providing digital outputs. The full scale range of the digital output can be adjusted to $\pm 2g$, $\pm 4g$, $\pm 8g$, or $\pm 16g$. the figure below shows the accelerometer used.

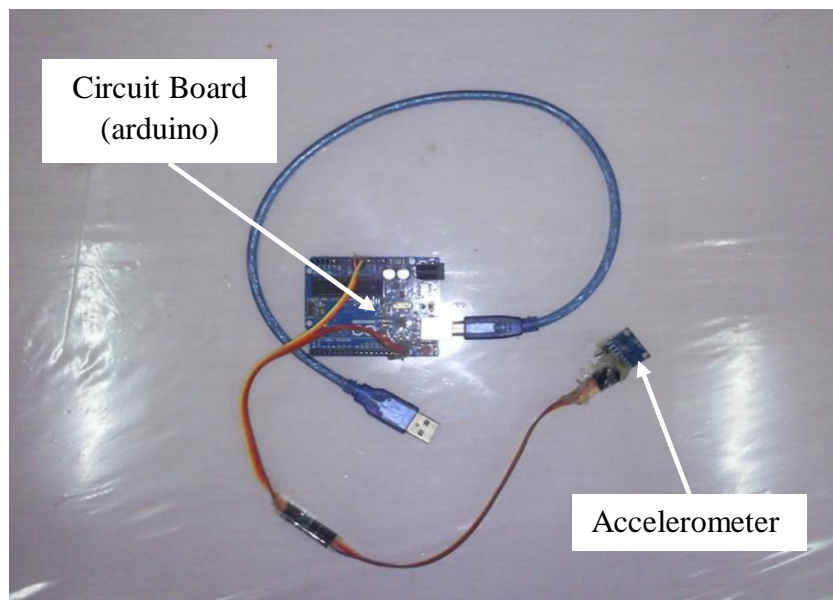


Figure 3.18: Photograph of three-Axis MEMS MPU-6050 Accelerometer

The figures below show the typical operating circuit and the block diagram of MPU-6050 accelerometer respectively.

3.4.8 Cutting Tool

Inserts were used in place of single point cutting tools in this research. The details of the inserts are:

Tool: Tungsten carbide coated insert

Model: TX 20

Dimension: 10mm × 10mm × 5mm

The figure below shows the insert used with dimensions.

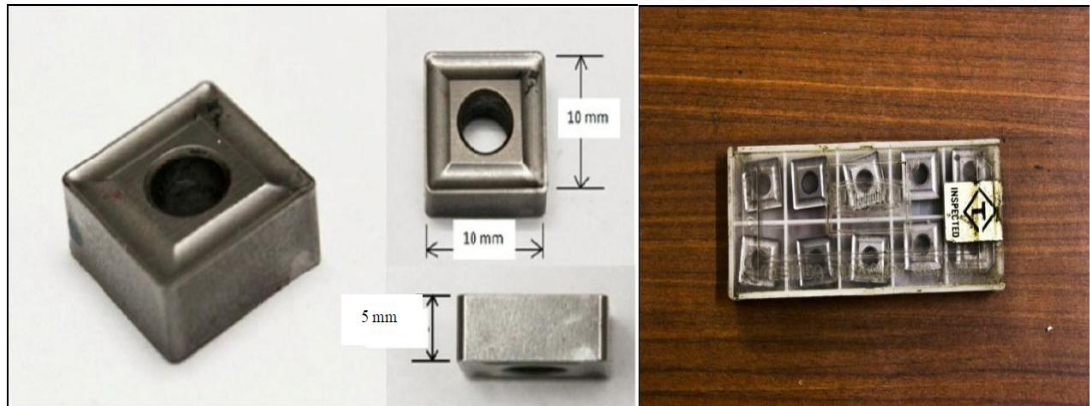


Figure 3.21: Photograph of insert with dimensions

3.4.9 Work piece

Mild steel shafts were used as the work piece material of the experiments. The initial diameter of the shaft was always same. However, lengths of the shafts were different for surface roughness and tool wear measurement experiments. The figure below shows the work piece used for experimentation.

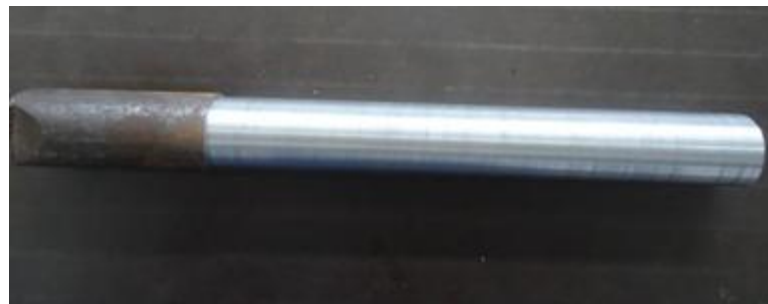


Figure 3.22: Photograph of Mild Steel work piece

For surface roughness, total shaft length was 200mm. Experimentation length was 150mm and 50mm was used for holding the work piece in the chuck. Each experiment was carried out over 50 mm length. Thus three experiments were done on each single work piece.

For tool wear, total shaft length was 250mm. Experimentation length was 200mm and 50mm was used for holding the work piece in the chuck. Total cutting length for each experiment was 1000mm. This was achieved by doing five cuts of length 200mm in each work piece. The details of the work piece are as follows:

Table 3.7: Work piece material and dimensions

	Surface Roughness Experiment	Tool Wear Experiment
Shaft material	Mild Steel	
Initial Shaft diameter	32mm	
Shaft Length	200mm	250mm
Cutting length	150mm (50mm for each experiment, total three experiment in each work piece)	200mm (five cuts in each work piece, total 1000mm for each experiment)

A sample of the work piece was tested in the laboratory to find out the chemical composition. The result is given in table 3.8. The base metal is iron (Fe).

Table 3.8: Chemical composition of the mild steel used in the experimentation

CONTENTS	PERCENTAGE
Carbon (C)	0.16
Silicon (Si)	0.35
Manganese (Mn)	1.65
Sulphur (S)	0.004
Phosphorus (P)	0.027

3.5 Measurement Technique

3.5.1 Measurement of Surface Roughness

Surface topographical measurements are very important in controlling the quality of finished products. As such, various sophisticated techniques and devices have been invented and implemented for the purposes of surface metrology. A surface roughness tester, most widely accepted, was used in this study to measure surface roughness of the work piece. It is also known as a profilometer, surfest, etc. It is a device used to inspect and measure surface roughness of flats, rounds, sloping planes, and recesses in machined, ground, or polished metal and non-metal surfaces. Surface roughness testing is a type of form measurement that identifies surface profiles such as grooves and recessions, commonly known as peaks and valleys, of a surface. A roughness tester traces a surface profile using a skid-type (contact-type) method with a tracer tip such as a diamond stylus and piezo-electric detection to calculate roughness. Common types of parameters include Ra (roughness average), Rv (maximum profile valley depth), and Rsk (skewness), and assessed profiles. Profiles can have valuations such as cutoff, sampling, traversing, and evaluation-types of lengths. A surface roughness tester can have analog or digital display. A surface roughness tester can be portable, handheld, or desktop-type.

The Mitutoyo SURFTEST SJ-210 is a contact profilometer. Here, a stylus is moved vertically in contact with a sample and then moved laterally across the sample for a specified distance and specified contact force. It can measure small surface variations in vertical stylus displacement as a function of position. The height position of the stylus generates an analog signal which is converted into a digital signal stored, analyzed and displayed. The radius of stylus ranges from 20 nanometres to 25 μm , and the horizontal resolution is controlled by the scan speed and data signal sampling rate. The stylus tracking force can range from less than 1 to 50 milligrams. Figure below is a picture of the setup of the profilometer used in this research.

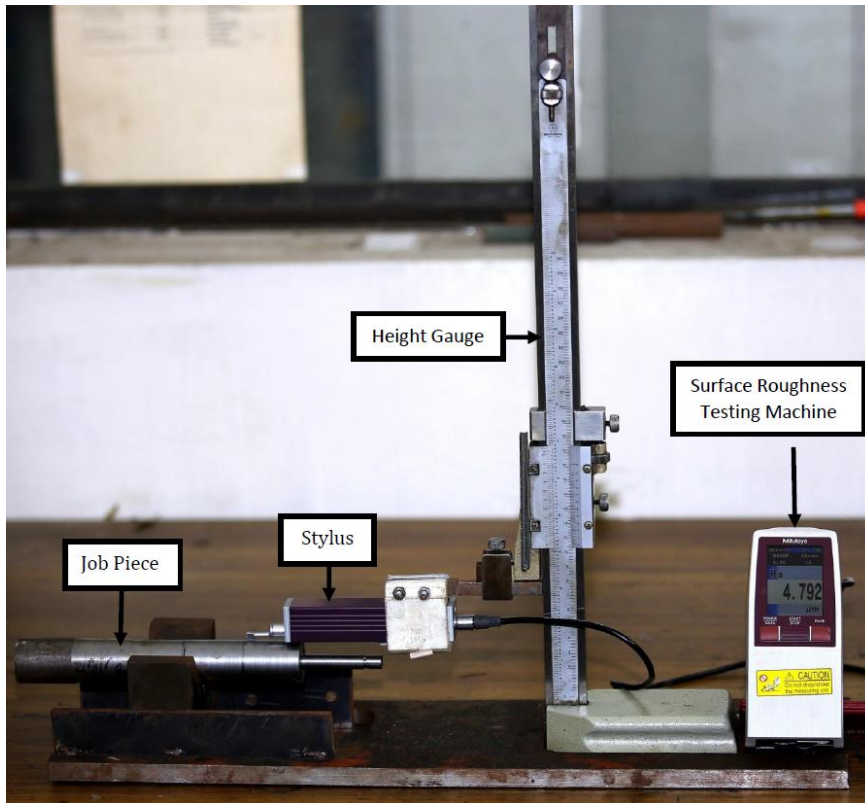


Figure 3.23: Photograph of the setup of the SURFTEST SJ-210 for measuring surface roughness

In this study, values of Ra, Rq, Rz, assessed surface roughness profiles and BAC and ADC curves were measured with the profilometer. The figure below shows a surface roughness result sample.

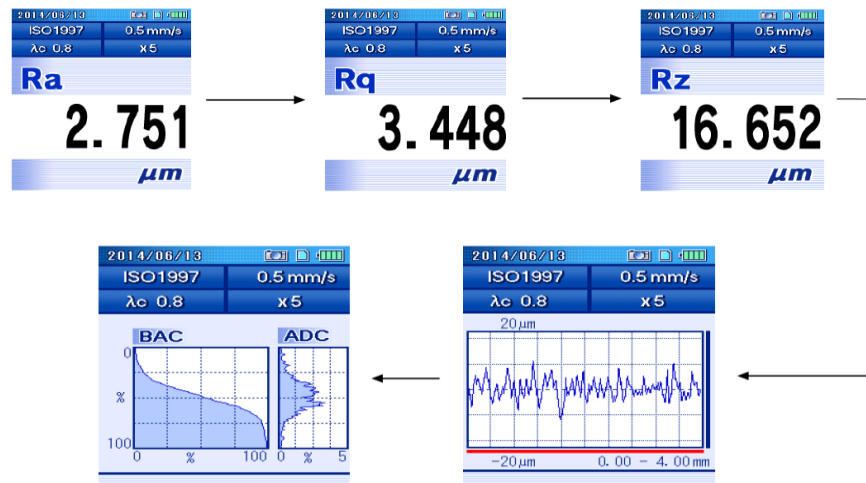


Figure 3.24: Surface roughness result sample measured by SURFTEST SJ-210

3.5.2 Measurement of Tool Wear

To measure tool wear, optical microscope and software named Scopetek was used. The measurement of tool wear using the optical microscope and the software is described below:

1. The image of the tool flank is captured with optical microscope.
2. The image of the tool wear that is to be measured is then opened with the software.
3. From the layout bar of the software, new layer is selected and layer name is given.
4. Then from annotation bar, any line drawing option is selected.
5. Now putting the cursor on the image will allow drawing lines. The line drawn upon the wear will give the measurement of the tool wear in pixel.
6. This value is then converted to mm using a standard converter.

The figure below shows a tool wear sample measured with scopetek.

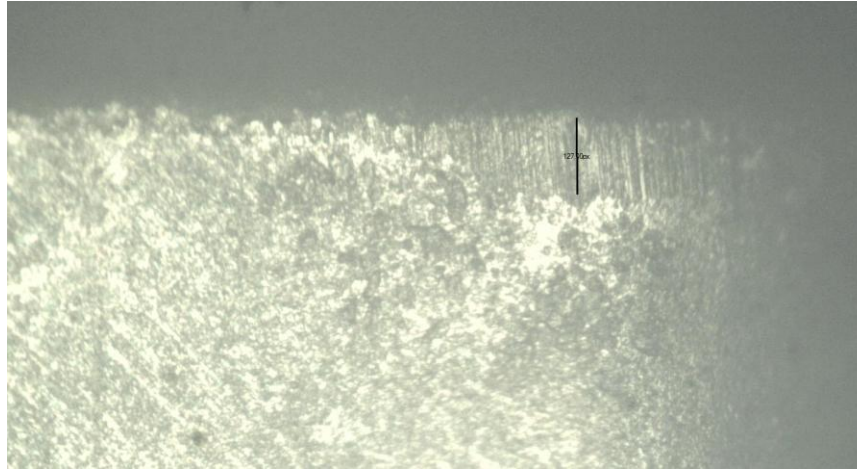


Figure 3.25: Tool wear measured with scopetek

3.5.3 Observation of Chip Behavior

The chips formed during turning were investigated and it has been observed that at some specific cutting conditions chip formation presents extreme cases of secondary and primary chip serration. To study the chip behavior the following steps were followed:

1. The chip at different cutting conditions were collected, labeled and kept accordingly.
2. Each chip was mounted using a mixture of resin and hardener. The mixture was stirred for about a minute and left to solidify. The solidified mixture is called mounting.
3. The mounted surface was then grinded in order to reveal the chip to the surface. Various grade of abrasive paper are used starting with grade 240 followed by 400, 800 and 1200.
4. In order to remove the scratches on the surfaces, the mounting was then polished using alumina solution starting from grain size 6.0 μ , followed by 1.0 μ , 0.3 μ and 0.01 μ . As a safety precaution, before polishing; the mounting was viewed under the microscope to ensure that the chip is visible on the surface.
5. Nital was then applied to the surface to reveal the grain boundaries of the ferrite and pearlite.
6. The mounting was then viewed under the microscope to capture the structure of the chip.

The figures below show the samples of the mounted chips and the instruments used for the chip analysis.



Figure 3.26: Samples of mounted chips

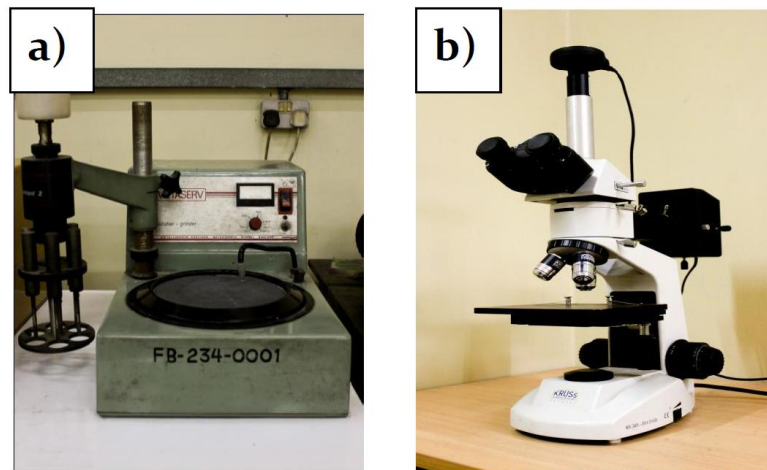


Figure 3.27: Instruments used for chip analysis (a) Polishing wheel (b) Optical microscope

3.5.4 Measurement of Temperature

Metal cutting generates a significant amount of heat and the temperature in the cutting zone can change with tool wear due to changes in the tool geometry and tool's capability to cut. Therefore, the temperature can be used to monitor the tool condition. The high temperatures around the cutting tool edges affects the rate and mode of cutting tool wear, the friction between chip and cutting tool, and also that between the cutting tool and the newly formed surface.

To measure the temperature of the tip of the insert a digital thermocouple was used. The hot end of the thermocouple was welded to the tip of the insert. Readings

were taken from the display of the thermocouple after cutting a total length of cut of 200mm. Temperature readings were taken at two conditions: without ultrasound and with 60 kHz ultrasound frequency. The depth of cut and spindle speed was 1mm and 530 RPM respectively for both conditions.

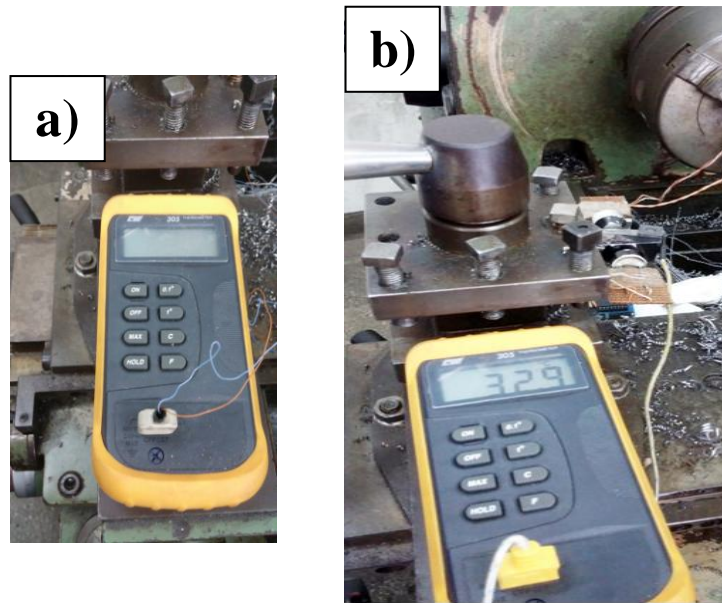


Figure 3.28: Photograph of arrangement for measuring cutting temperature
a) thermocouple b) thermocouple hot end attached with insert tip

3.5.5 Measurement of Vibration

The vibration of the tool holder and the cutting tool were measured by an accelerometer. Vibrations were measured for experiments without ultrasound and with 60 kHz ultrasound frequency at a depth of cut of 1 mm and spindle speed of 530 RPM. The data obtained from the accelerometer were then plotted by MATLAB for study and comparison. The graph obtained is a time-series graph where the X-axis shows time and the Y-axis shows amplitude in g.

The figure below shows the overall setup of the accelerometer for measuring the vibration of the tool holder and the cutting tool.



Figure 3.29: Photograph of the setup of the accelerometer for measuring the vibration of the tool holder and the cutting tool

CHAPTER 4

Results, Analysis and Discussions

4.1 Introduction

This research was entirely based on experimentations. Straight turning operation on specimens in various cutting environments involving various combinations of process control parameters like: spindle speed, depth of cut and ultrasonic frequency were done. Surface roughnesses of the work pieces from each and every experiment were measured and the data were analyzed to obtain the optimum conditions in terms of depth of cut, spindle speed and ultrasound frequency. Further experiments based on the attained optimum conditions were done to study the effect on tool wear, effect of input power variations on surface roughness and to determine the best orientation of the application of ultrasound.

4.2 Effect of Ultrasound Frequency on Surface Roughness

For surface roughness, total work piece length was 200mm. Experimentation length was 150mm and 50mm was used for holding the work piece in the chuck. Each experiment was carried out over 50 mm length. Thus three experiments were done on each single work piece. Apple to apple comparisons were done to rule out experimental errors. It was ensured that the overhang lengths of the work piece were same for each set of compared data's to avoid experimental errors. The surface roughness measurement technique is explained in section 3.5.1 of Chapter 3.

The different combination of the process variables are shown in table 3.1 [Chapter 3-Article 3.3]. The following graphs depict the results obtained from different combinations of experiments. The tables are given in the appendix.

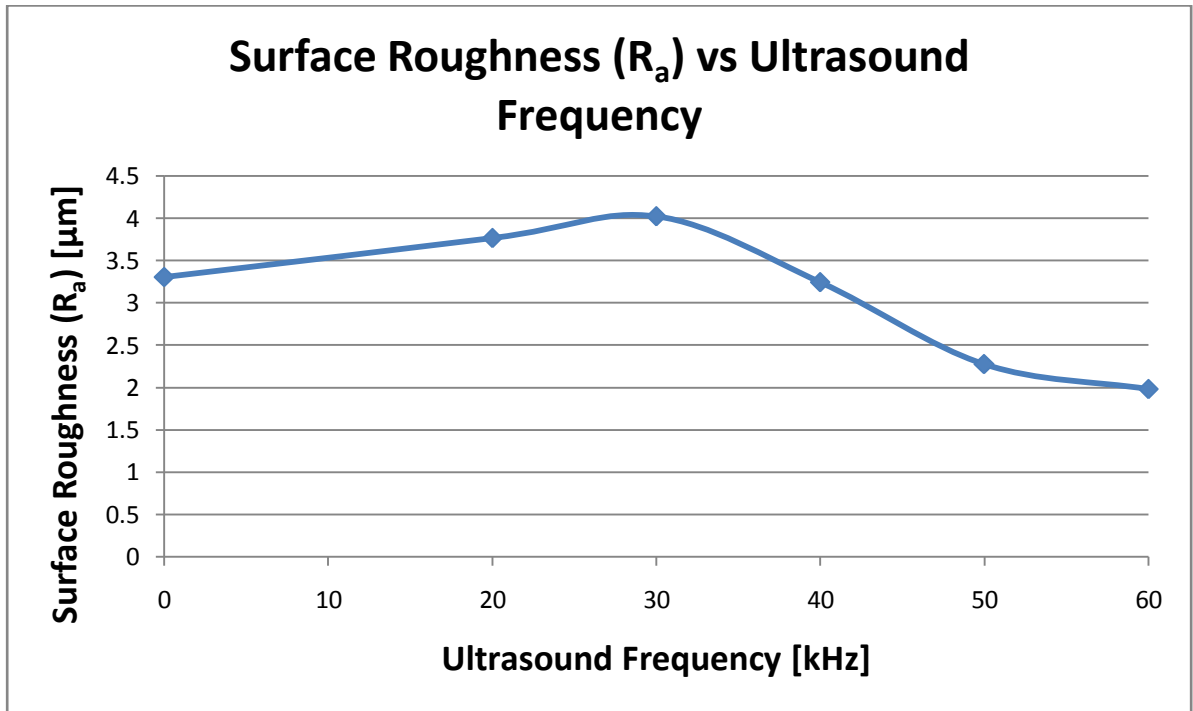


Figure 4.1: Surface Roughness (R_a) readings at 0.5 mm depth of cut, 360 RPM spindle speed and different ultrasound frequencies

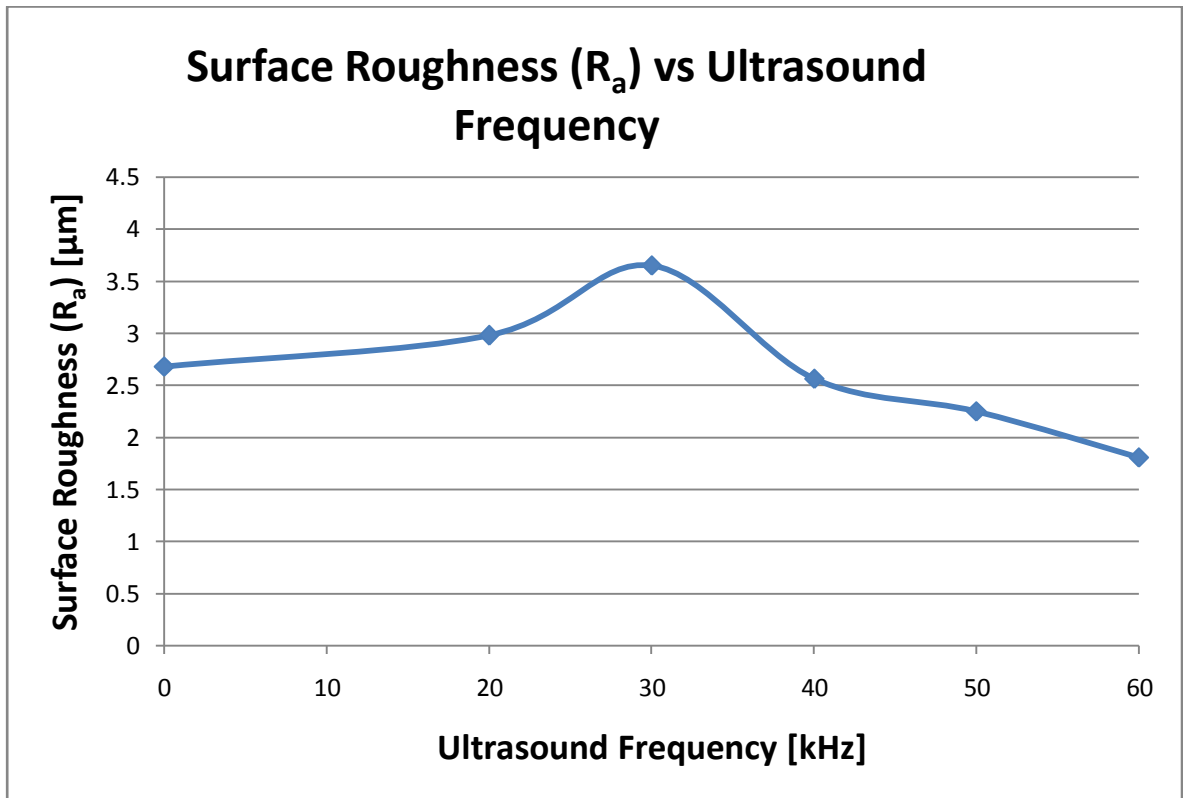


Figure 4.2: Surface Roughness (R_a) readings at 0.5 mm depth of cut, 530 RPM spindle speed and different ultrasound frequencies

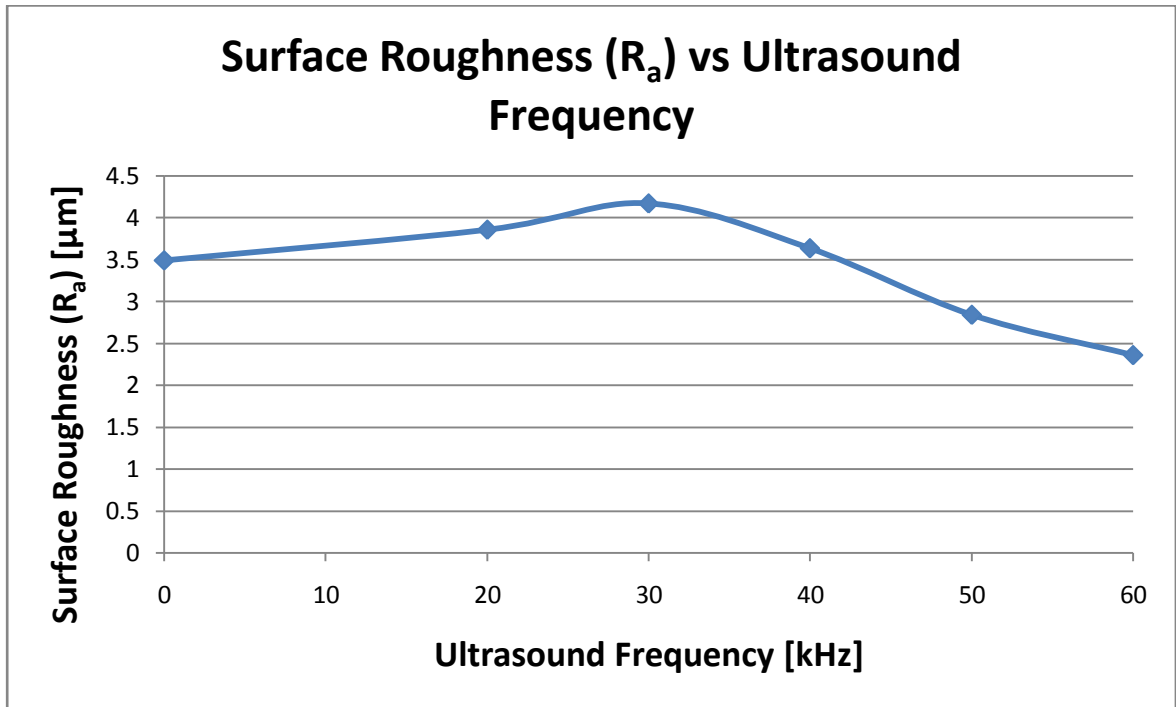


Figure 4.3: Surface Roughness (R_a) readings at 1mm depth of cut, 360 RPM spindle speed and different ultrasound frequencies

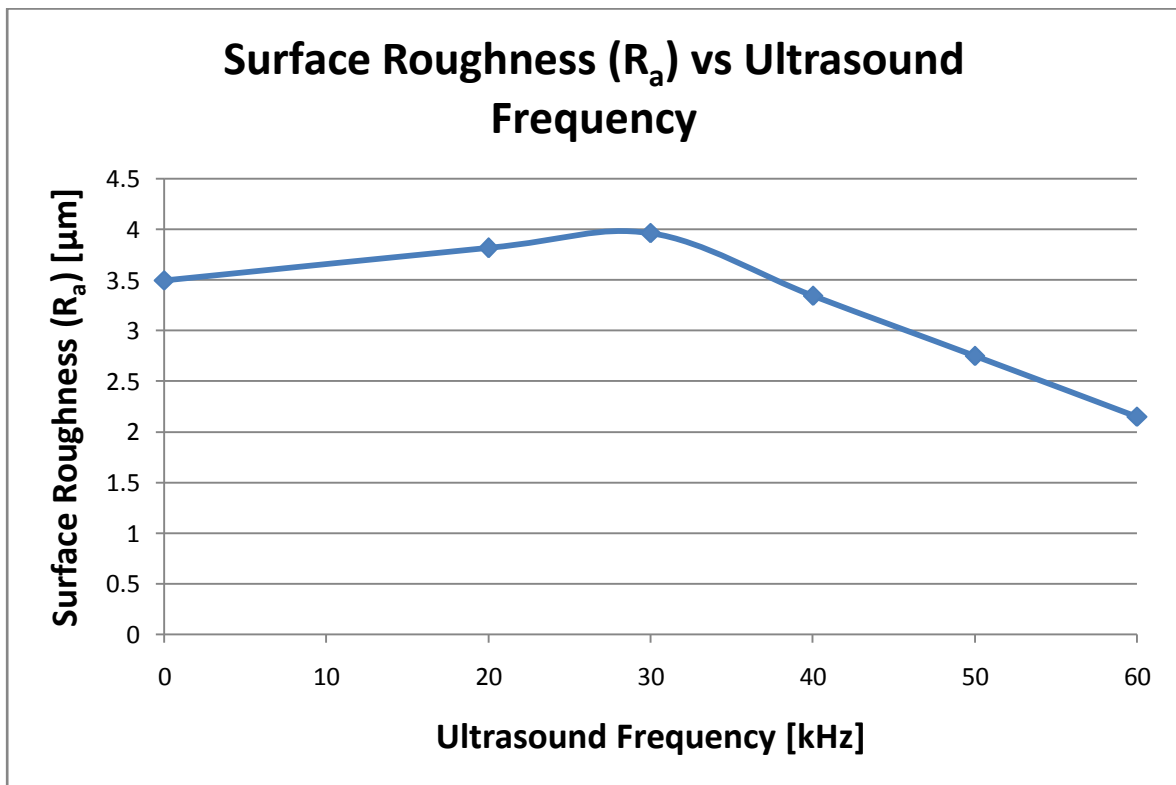


Figure 4.4: Surface Roughness (R_a) readings at 1mm depth of cut, 530 RPM spindle speed and different ultrasound frequencies

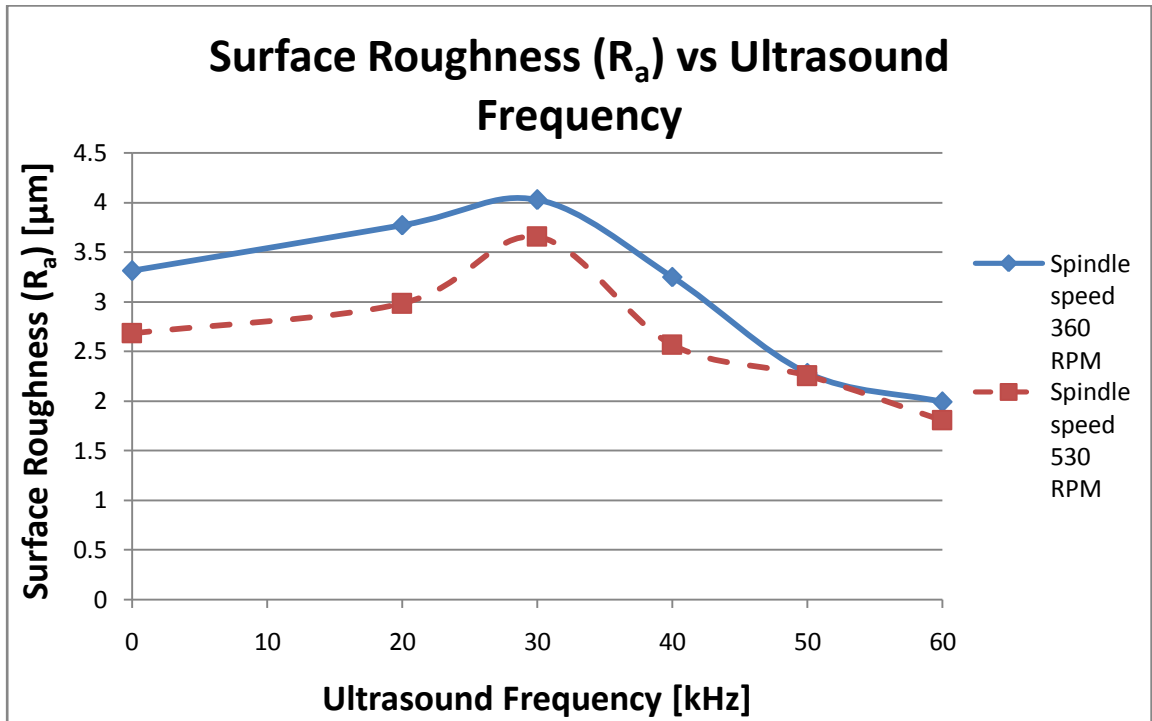


Figure 4.5: Comparison of Surface Roughness data at 0.5 mm depth of cut and different ultrasound frequencies for different spindle speeds

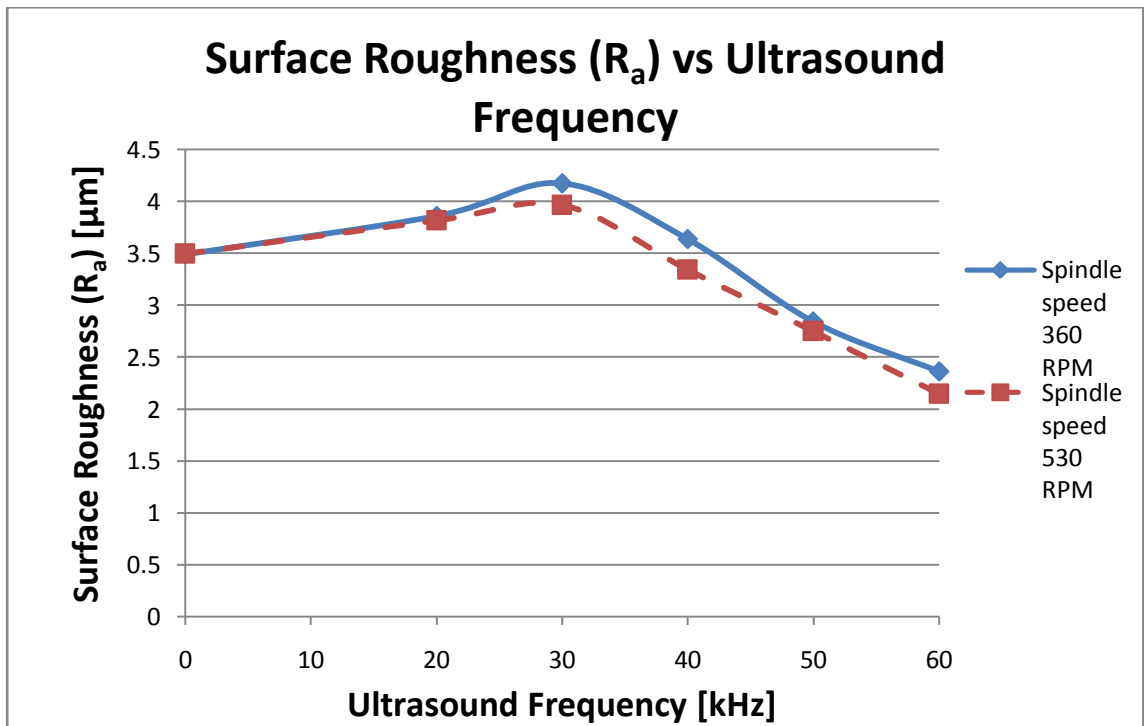


Figure 4.6: Comparison of Surface Roughness data at 1 mm depth of cut and different ultrasound frequencies for different spindle speeds

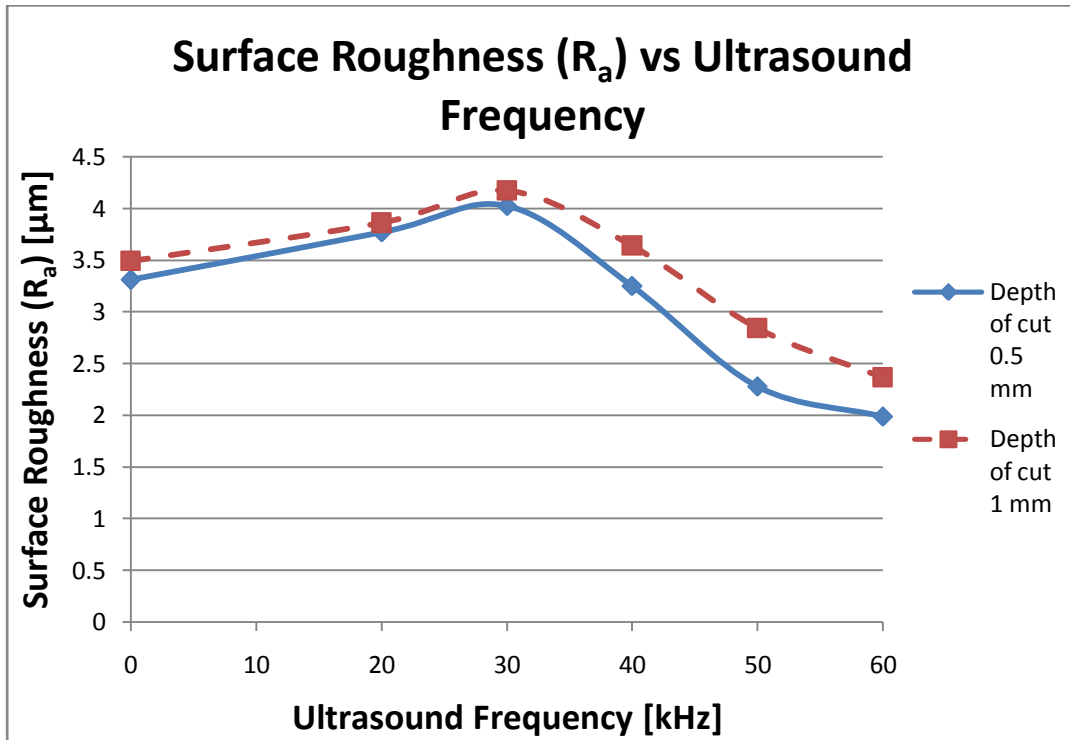


Figure 4.7: Comparison of Surface Roughness data at 360 RPM spindle speed and different ultrasound frequencies for different depth of cuts

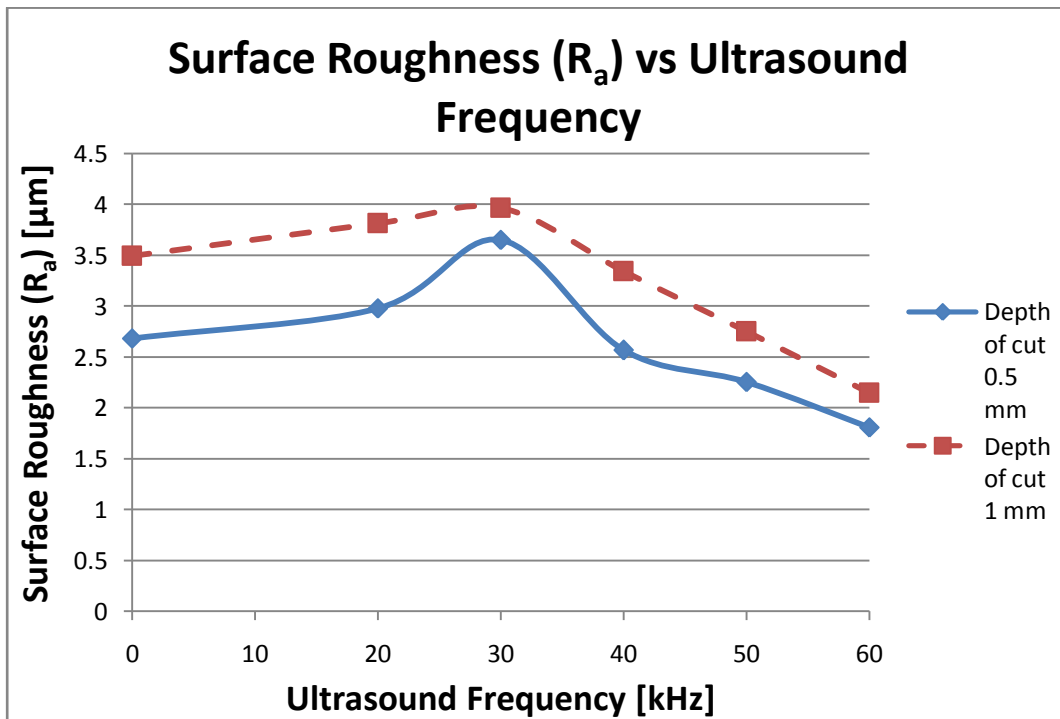


Figure 4.8: Comparison of Surface Roughness data at 530 RPM spindle speed and different ultrasound frequencies for different depth of cuts

From the graphs a comparative idea about surface roughness at each cutting conditions in different cutting environment can be obtained. From the graphs it can be seen that for 20 kHz and 30 kHz ultrasound frequency, the surface quality degrades a bit in comparison to the surface quality at normal cutting. From 40 kHz ultrasound frequency and onwards the surface quality improves and the surface roughness values are less than that obtained during normal machining.

This improvement in surface roughness can be explained in relation to chatter reduction. Chatter occurs due to resonance occurring at certain machining frequencies. Application of external ultrasound acts as an additional source to shift the resonance zone from the current trend. From the detailed study, it can be said that ultrasound of 40 kHz and upwards effectively shifts the resonance zone and consequently causes reduction in chatter resulting in better surface quality.

Almost all the graphs show a consistent trend, however some points have deviated from its expected position. This may occur due to any error during experimentation, and beside this the experiments are huge in number for which it is very difficult to maintain constant experimental condition every time the machining operation is performed. For example the depth of cut has been given by using a rotating wheel in the carriage. This may cause some variation in the depth of cut. However, repeated experiments were carried out and average values were taken to minimize the errors.

The best results are obtained at ultrasound frequency of 60 kHz. Considering the surface quality, material removal rate, spindle speed and rate of improvement from normal cutting, the best optimum condition was determined to be at depth of cut of 1 mm, spindle speed of 530 RPM and ultrasound frequency of 60 kHz. This particular condition gives the highest material removal rate, highest spindle speed and huge improvement in terms of surface quality compared to normal machining.

The table below shows the material removal rate for different combinations of depth of cut and spindle speed.

Table 4.1: Material removal rate at different depth of cuts and spindle speeds

Depth of Cut (mm)	Spindle Speed (RPM)	Material Removal Rate (mm ³ /min) [$\times 10^{-3}$]
0.5	360	28.7
0.5	530	43.1
1	360	114.8
1	530	172.33

The figure below show the surface roughness readings obtained by profilometer at a depth of cut of 1 mm, spindle speed of 530 RPM and ultrasound frequency of 60 kHz. The surface profile of the work piece after machining, BAC and ADC graphs are also shown.

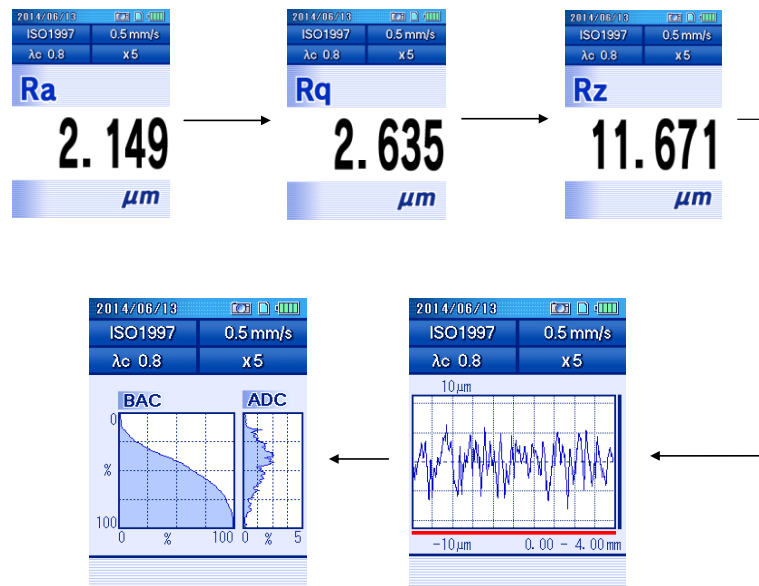
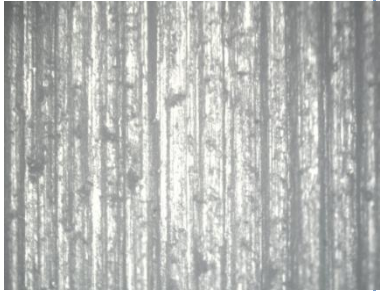




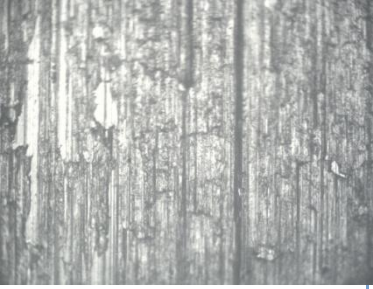


Figure 4.9: Surface roughness result measured by SURFTTEST SJ-210 at a depth of cut of 1 mm, spindle speed of 530 RPM and ultrasound frequency of 60 kHz

The table below shows the images obtained with optical microscope at depth of cut of 1mm, spindle speed of 530 RPM and at different ultrasound frequencies.

Table 4.2: Images of surfaces at 1 mm depth of cut, 530 RPM spindle speed and different ultrasound frequencies

<u>Images of surfaces after machining</u>		
		
Without Ultrasound	20 kHz	30 kHz
		
40 kHz	50 kHz	60 kHz

4.3 Effect of Ultrasound Frequency on Tool Wear

Tool wear was measured at normal cutting condition (without ultrasound frequency) and at the optimum condition as determined by the surface roughness results [discussed in detail in article 4.2]. The optimum conditions were: Depth of cut-1 mm, Spindle speed-530 RPM and Ultrasound frequency-60kHz. The two results were then compared to determine the effect of the application ultrasound frequency on tool wear. For measuring the tool wear, optical microscope and scopetek software was used. The measurement technique of tool wear is explained in section 3.5.2 of Chapter 3.

For tool wear, total shaft length was 250mm. Experimentation length was 200mm and 50mm was used for holding the work piece in the chuck. Total cutting length for each experiment was 1000 mm. This was achieved by doing five cuts of length 200mm in each work piece. The initial diameter of the work piece was 32 mm.

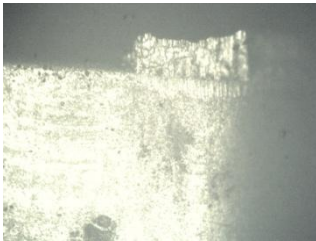
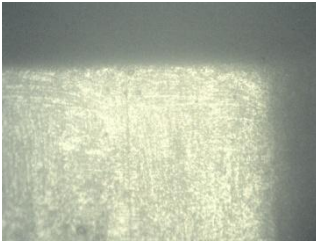
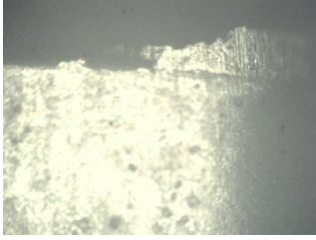
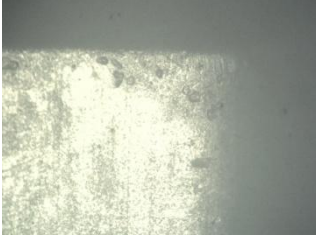

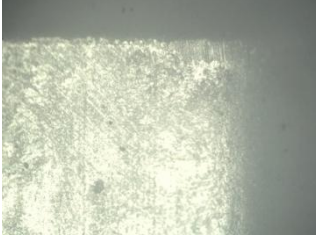

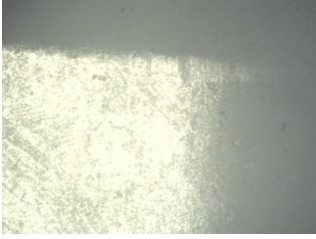
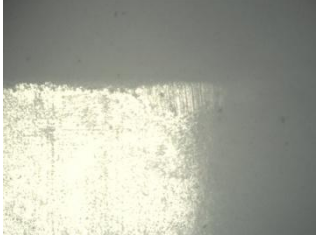
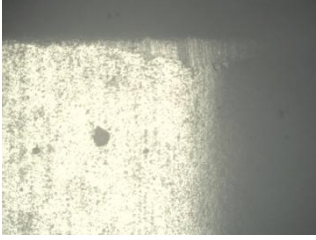
The table below show the results of tool wear obtained for normal machining and machining with ultrasound frequency of 60 kHz at depth of cut of 1 mm and spindle speed of 530 RPM.

Table 4.3: Tool wear values at depth of cut of 1 mm and spindle speed of 530 RPM

Without Ultrasound		Ultrasound Frequency 60 kHz	
Length of Cut (mm)	Tool Wear (mm)	Length of Cut (mm)	Tool Wear (mm)
0	0	0	0
200	0.31	200	0.09
400	0.37	400	0.25
600	0.44	600	0.34
800	0.48	800	0.40
1000	0.55	1000	0.46

The table below shows the images of the tool showing tool wear on the flank face of the tool taken by optical microscope.

Table 4.4: Images of tool wear for normal machining and machining with 60 kHz ultrasound frequency taken by optical microscope at depth of cut of 1 mm and spindle speed of 530 RPM

Length of cut	Without ultrasound	Ultrasound Frequency 60kHz
After cutting 200 mm		
After cutting 400 mm		
After cutting 600 mm		
After cutting 800 mm		
After cutting 1000 mm		

The graph below compares the tool wear obtained for normal machining and machining with 60 kHz ultrasound frequency at depth of cut of 1 mm and spindle speed of 530 RPM.

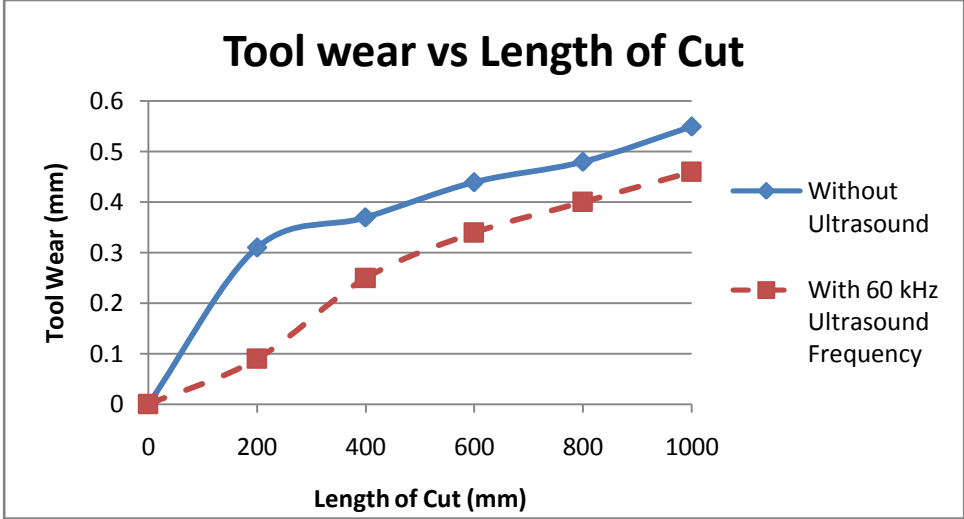


Figure 4.10: Comparison of tool wear at depth of cut of 1 mm and spindle speed of 530 RPM for cutting without ultrasound and with ultrasound frequency of 60 kHz

From the graph it can be seen that tool wear is reduced when external ultrasonic sound wave is applied during machining operation by a significant amount. Reduction in tool wear when ultrasound is applied is almost three times than that of normal machining. It is also observed that build up edges were formed in normal machining upto 800mm length of cut whereas with ultrasound of 60 kHz no build up edges were formed on the tool.

Slight errors might be there in measuring the tool wears as the accuracy of tool wear measurement depends on the quality of the captured image by the microscope. In some cases the built up edges formed created problems during measurement. As tool wear occurs on the edge of insert it was very difficult to focus at the exact point of the maximum flank wear. Because of these reasons slight errors may be there. To ensure better results, experiments were repeated several times and average values of tool wears were taken. Furthermore, apple to apple comparisons were done. Thus errors were minimized to a great extent and the errors had little effect on overall result.

4.4 Effect of Ultrasound Frequency on Vibration of Tool Holder and Cutting Tool

To support the theory suggested in this research that improvements in surface roughness and tool wear occurred due to reduction in vibration of the tool holder and the cutting tool, the vibration of the tool holder during non-cutting condition, during cutting without ultrasound and during cutting with 60 kHz ultrasound frequency were measured and studied. The cutting conditions were: Depth of cut of 1 mm and Spindle speed of 530 RPM. The vibration data were measured with an accelerometer and a time series graphs were plotted. The measurement technique of tool holder vibration is explained in section 3.5.5 of Chapter 3. The figures below shows the time series graphs obtained at different conditions.

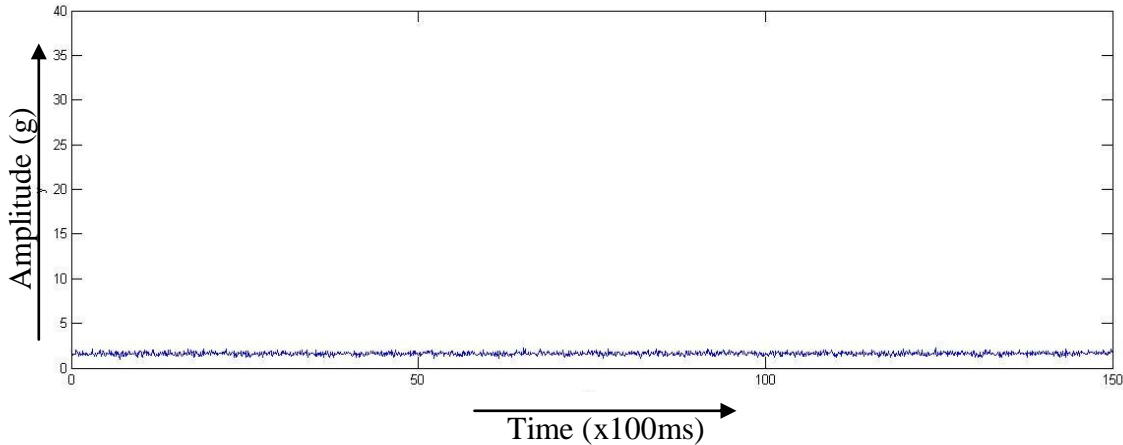


Figure 4.11: Tool holder vibration during non cutting condition at 530 RPM

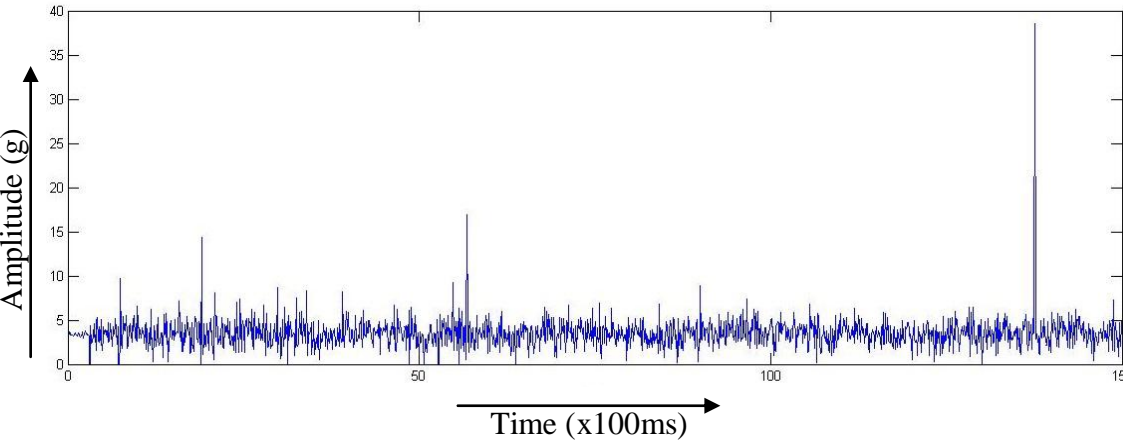


Figure 4.12: Tool holder vibration during cutting without ultrasound (Normal Cutting) at a depth of cut of 1 mm and spindle speed of 530 RPM

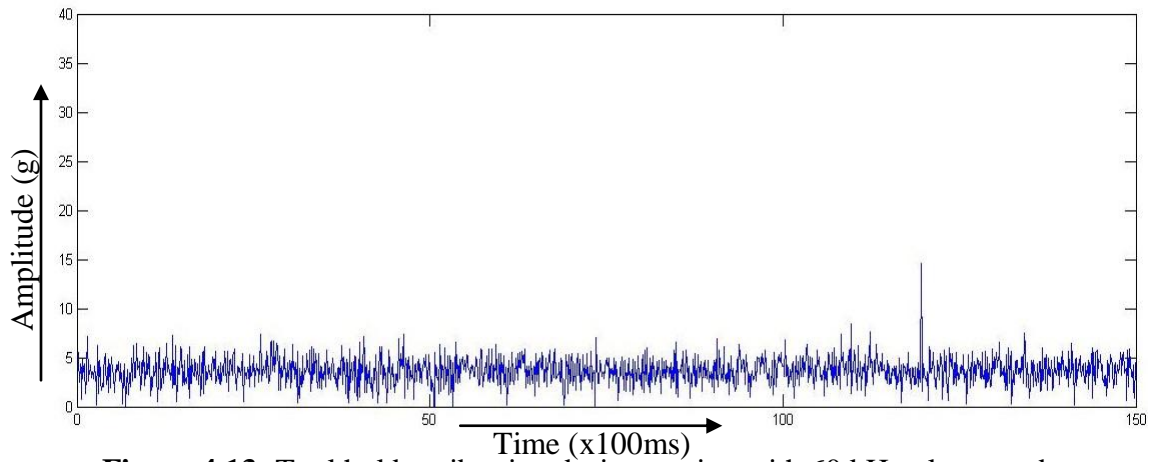


Figure 4.13: Tool holder vibration during cutting with 60 kHz ultrasound frequency at a depth of cut of 1 mm and spindle speed of 530 RPM

From the time series graph of non-cutting condition, it is clear that the system is stable during non-cutting condition at 530 rpm. After apple to apple comparison of the time series graph of cutting without ultrasound and cutting with 60 kHz ultrasound frequency, it is observed that that the vibration amplitudes in case of normal machining without ultrasound is comparatively higher than that of machining with 60 kHz ultrasound frequency. From the vibration analysis data it has been clearly observed that the system in normal cutting is little unstable compared to ultrasonic sound frequencies cutting which may affect the surface quality and tool life of the cutting tool.

4.5 Effect of Ultrasound Frequency on Cutting Temperature

The effect on ultrasound frequency on cutting temperature was also studied in this research. A copper-constantan thermocouple was used to measure the temperature. The temperature was measured after a length of cut of 200mm. Experiments were repeated and average values were taken. The table and chart below compares the cutting temperature obtained at depth of cut of 1 mm and spindle speed of 530 RPM for without ultrasound and with ultrasound frequency of 60 kHz. It has been observed that with the application ultrasound frequency temperature is slightly reduced.

Table 4.5: Cutting Temperature measured at depth of cut of 1 mm and spindle speed of 530 RPM for without ultrasound and with ultrasound frequency of 60 kHz

Length of cut (mm)	Temperature (°C)	
	Without Ultrasound	Ultrasound Frequency 60 kHz
200	127.5	119.3

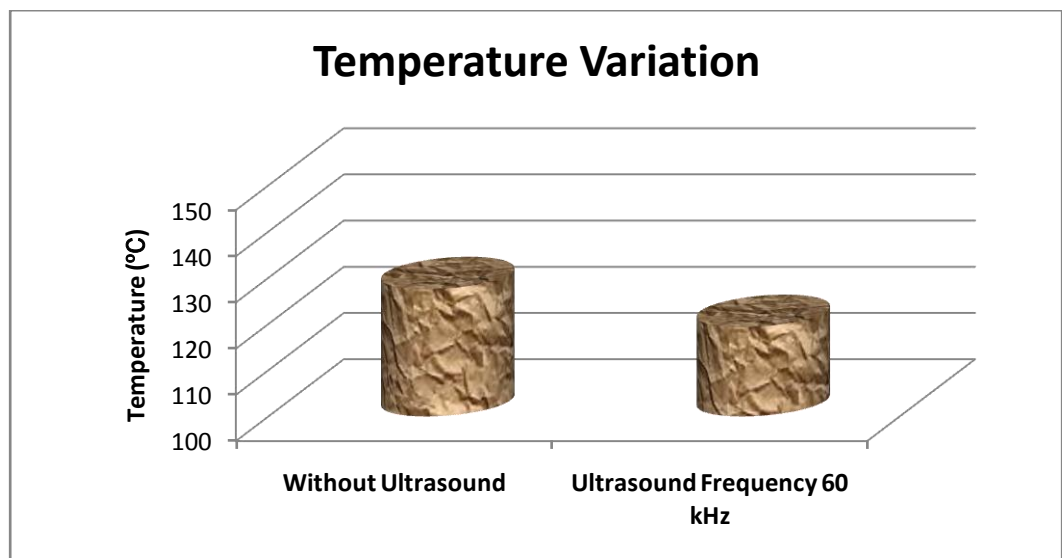


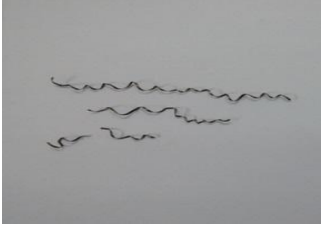

Figure 4.14: Comparison of cutting temperature at depth of cut of 1 mm and spindle speed of 530 RPM for cutting without ultrasound and with ultrasound frequency of 60 kHz

4.6 Effect of Ultrasound Frequency on Chip Behavior

While performing the experiments for tool wear, the chips produced for experiments with 60 kHz ultrasound and without ultrasound were collected for analysis. The characteristics of chip produced in non-ultrasonic and ultrasonic conditions were then compared to study chip behavior in each case. Mainly the continuity and primary and secondary tooth formation of chip were analyzed for comparison. The details of the technique of collecting and preparation of the chips are given in section 3.5.3 of Chapter 3.

The table below shows the chips collected at cutting conditions without ultrasound and with 60 kHz ultrasound frequency at a depth of cut of 1 mm and spindle speed of 530 RPM.

Table 4.6: Chip collected in each cutting environment showed different continuity

Without Ultrasound	Ultrasound Frequency 60kHz
	

After observing the chips, it is clear that the chips showed different continuity in each cutting environment. Chips produced in normal cutting condition without ultrasound were generally discontinuous and loosely packed whereas the chips produced in cutting with ultrasound frequency were continuous and very closely packed. The color variation of the chips was slight as temperature variation during normal cutting without ultrasound and cutting with ultrasound frequency was less.

Serrated chips show primary and secondary tooth formation. The chips formed are found to be mainly with primary serrated teeth appearing in the main body of the chip. Secondary serrated teeth also happen to appear at the free or constrained edge of the chip resulting from the coagulation of a certain number of primary serrated teeth especially when chatter occurs. The figure below shows the magnified view of the teeth of the chips. This illustrates the serration behavior of the chips. In this study, the length wise views of the chips were taken under optical microscope.

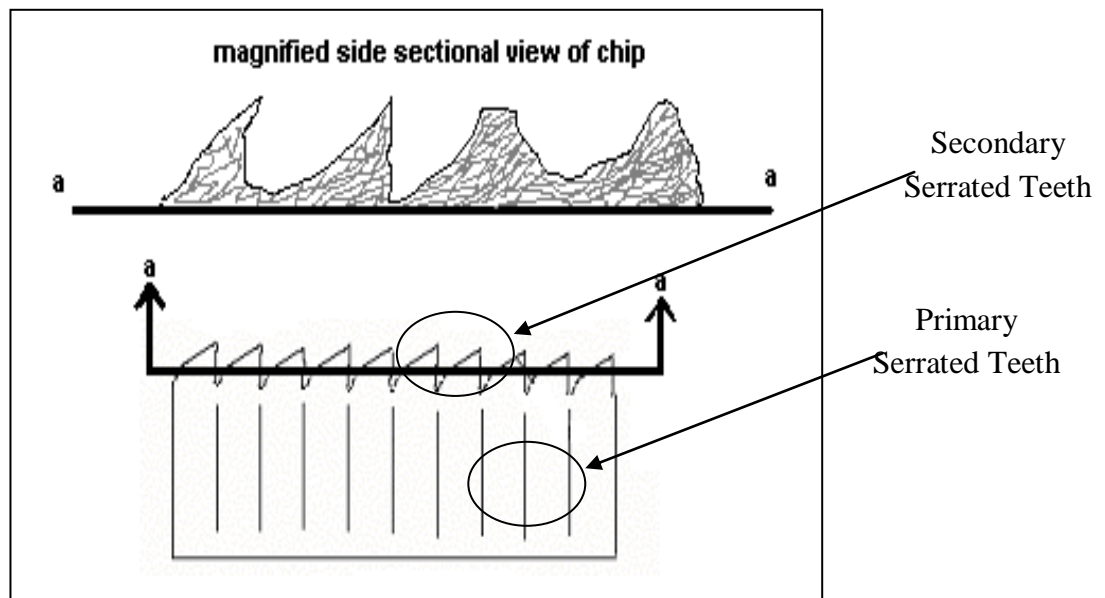

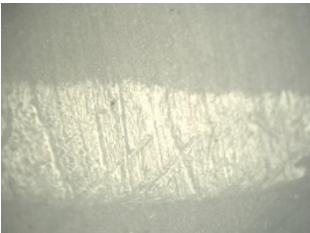


Figure 4.15: Schematic of chip showing sectioning for viewing side cross sectional view [Patwari et al., 2010]

The table below shows the images of the chips taken with an optical microscope for machining without ultrasound and with 60 kHz ultrasound at 1 mm depth of cut and 530 RPM spindle speed. The chips are shown side by side for easiness of apple to apple comparisons.

Table 4.7: Images of chips for normal machining and machining with 60 kHz ultrasound frequency taken by optical microscope at depth of cut of 1 mm and spindle speed of 530 RPM

Without Ultrasound	Ultrasound Frequency 60 kHz
	

From comparison, it is clearly visible that the tooth of serrated chip is larger in case of machining without ultrasound. It is also observed that the number of secondary

serrated teeth is less with ultrasonic machining. This phenomenon is a clear indication of change in vibration characteristic of the system in different conditions and is a proof of reduction of chatter in addition to surface roughness and tool wear reduction.

4.7 Effect of Orientation of the Application of Ultrasound

Frequency

To study the effect of orientation of the application of ultrasound frequency on the surface quality, experiments were carried out at depth of cut of 1mm and spindle speed of 530 RPM with two orientations: Horizontal and Vertical. Surface roughness readings were taken and compared to determine the best orientation of the application of ultrasound frequency. The figure below shows the setup used for horizontal and vertical orientation experimentation.

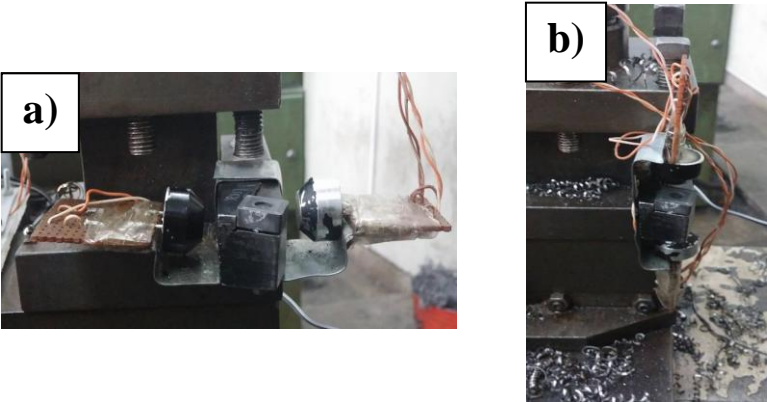


Figure 4.16: Experimental setup for (a) Horizontal orientation
(b) Vertical orientation

The table and graph below shows the surface roughness results and compares the data for the two orientations.

Table 4.8: Surface roughness data measured at depth of cut of 1 mm and spindle speed of 530 RPM for horizontal and vertical orientation

Ultrasound Frequency (kHz)	Surface Roughness (μm)					
	Horizontal Orientation			Vertical Orientation		
	R_a	R_q	R_z	R_a	R_q	R_z
Without ultrasound	3.496	4.353	20.393	3.496	4.353	20.393
20	3.817	4.669	21.163	4.826	6.001	26.508
30	3.964	5.283	22.046	4.121	5.066	21.068
40	3.343	4.104	18.716	3.219	4.065	19.571
50	2.751	3.448	16.652	2.854	3.459	14.971
60	2.149	2.635	11.671	2.562	3.144	15.362

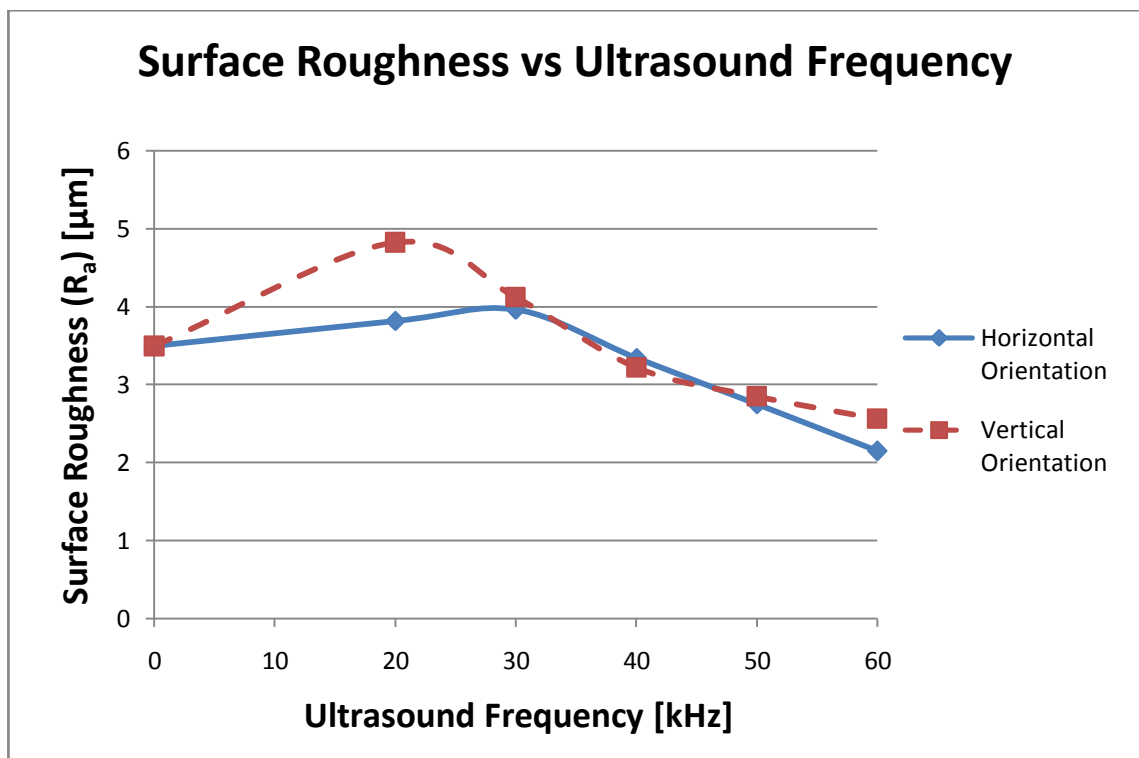

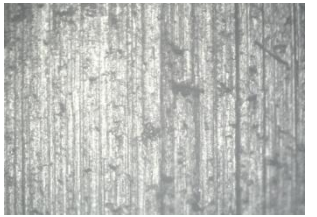

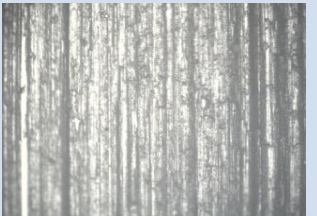


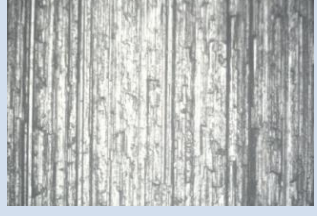





Figure 4.17: Comparison of surface roughness at depth of cut of 1 mm and spindle speed of 530 RPM for horizontal and vertical orientation

The table below shows the images obtained with optical microscope at depth of cut of 1mm, spindle speed of 530 RPM and at different ultrasound frequencies for both horizontal and vertical orientation.

Table 4.9: Images of surfaces at 1 mm depth of cut, 530 RPM spindle speed and different ultrasound frequencies for horizontal and vertical orientation

Ultrasound Frequency (kHz)	Orientation	
	Horizontal	Vertical
20		
30		
40		
50		
60		

From the above graphs and figures it is clear that horizontal orientation gives better surface roughness compared to vertical orientation of the application of the ultrasound waves. This indicates that horizontal orientation is more effective in reducing the vibration of the tool holder and the cutting tool.

4.8 Effect of Input Power Variation

To study the effect of input power variation of the ultrasound wave on the surface quality, experiments were carried out at the optimum conditions of depth of cut of 1mm, spindle speed of 530 RPM and 60 kHz ultrasound frequency with three levels of voltages: 6V, 9V and 12V. It may be mentioned here that all previous experiments were done with 12V input power to the ultrasound wave generator. Surface roughness readings were taken and studied. The table and graph below shows the surface roughness results and compares the data obtained for different input voltages.

Table 4.10: Surface Roughness data at 1 mm depth of cut, 530 RPM spindle speed and 60 kHz ultrasound frequency for different input voltages

<u>Input Voltage (V)</u>	<u>Surface Roughness (μm)</u>		
	<u>R_a</u>	<u>R_q</u>	<u>R_z</u>
6	3.661	4.663	20.537
9	3.018	3.763	22.323
12	2.149	2.635	11.671

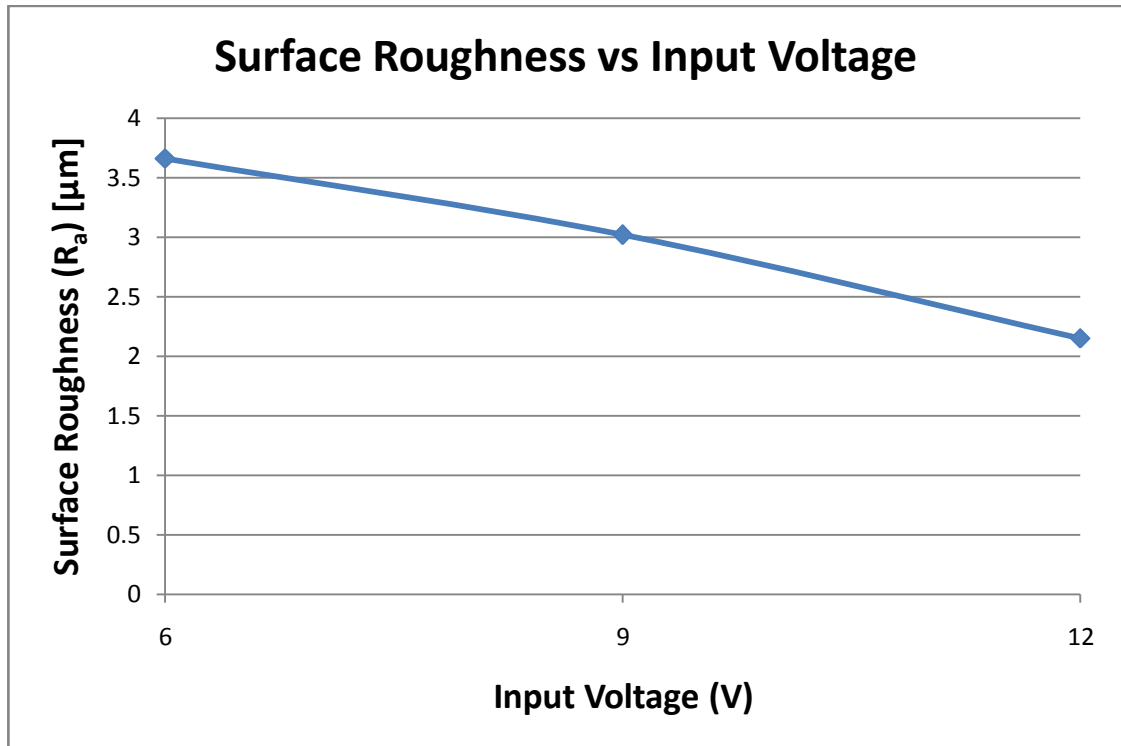


Figure 4.18: Effect of input voltage of the ultrasound wave generator on surface roughness

The table below shows the images obtained with optical microscope at different input voltages of the ultrasound generator.

Table 4.11: Images of surfaces at 1 mm depth of cut, 530 RPM spindle speed and 60 kHz ultrasound frequency for different input voltages

	Input Voltage		
	6V	9V	12V
Images of surfaces			

The graphs below show the voltage against time graphs obtained at different input voltages of the ultrasound generator with a picoscope.

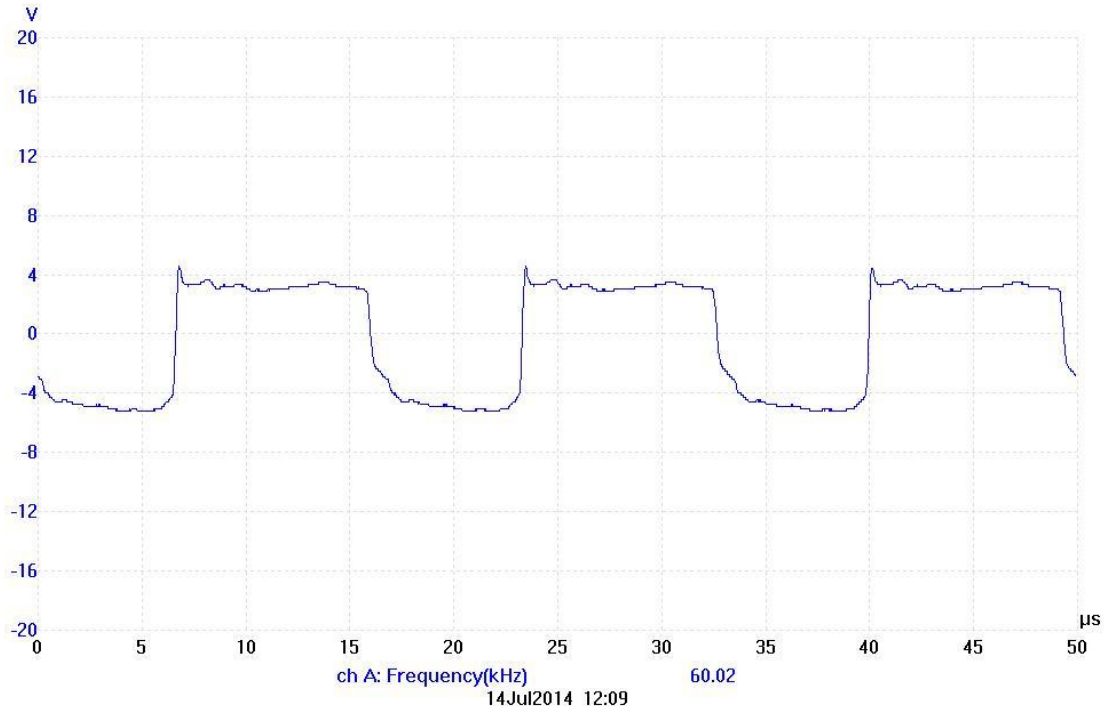


Figure 4.19: Ultrasound wave generated at input voltage of 6V

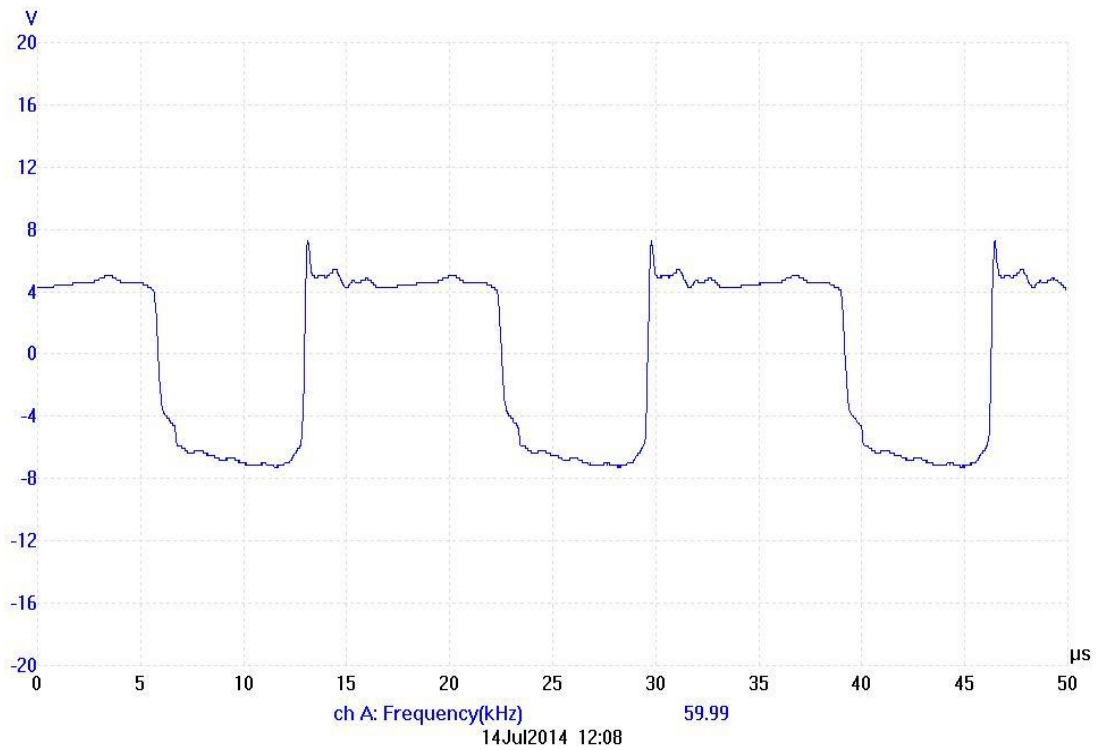


Figure 4.20: Ultrasound wave generated at input voltage of 9V

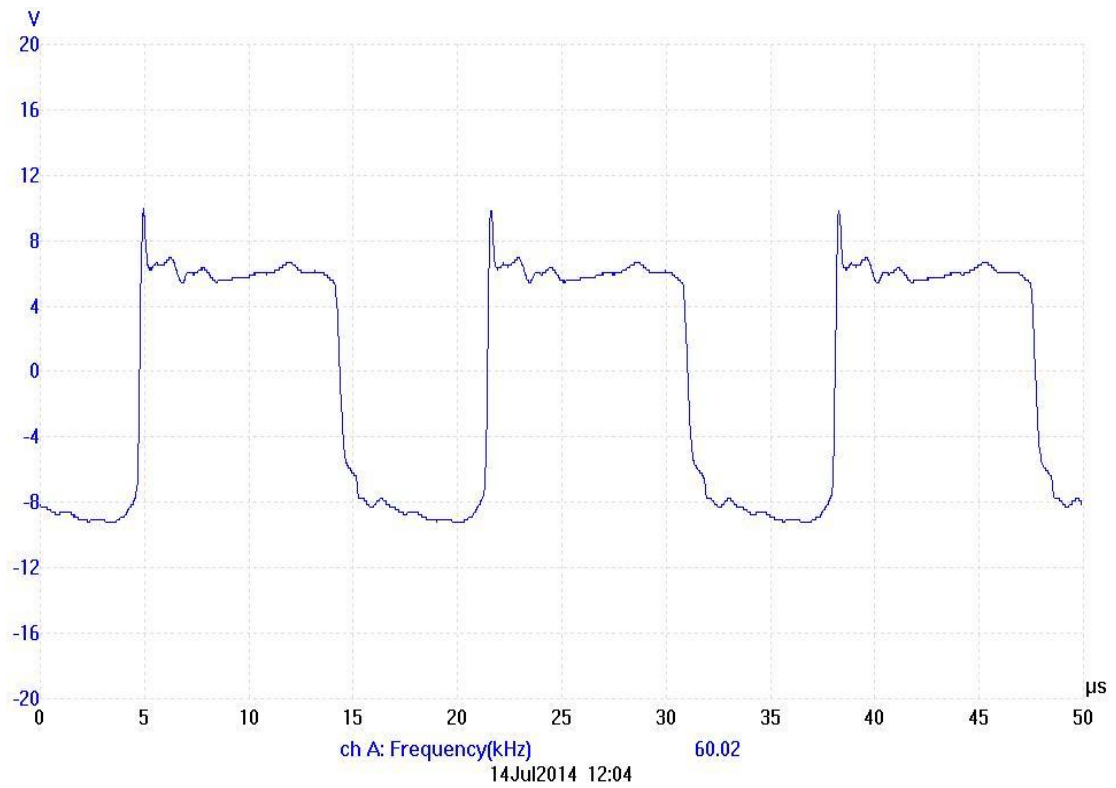


Figure 4.21: Ultrasound wave generated at input voltage of 12V

From the above graphs it is clear that with decrease in voltage, the amplitude of the ultrasound waves decreases. The surface roughness trend shows that with increase in voltage surface roughness decreases which indicates that higher amplitude gives lesser surface roughness and vice versa.

CHAPTER 5

Conclusions and Recommendations

5.1 Conclusions

From this study the following conclusions may be drawn:

1. It is observed that the application of external ultrasound has significant effect in improving the surface roughness in dry turning operation of mild steel. This can be explained by the reduction of the vibration of tool and work piece system in case of ultrasonic sound wave. It was found that ultrasound frequency of 40 kHz or above gives better surface roughness in comparison to dry turning operation without ultrasound at different combinations of cutting parameters. The best results are obtained at ultrasound frequency of 60 kHz.
2. Tool life of WC Coated carbide insert used in turning is improved with the application of external ultrasound. It was found that tool flank wear at 60 kHz ultrasound frequency was less in comparison with wear at normal turning. There was an improvement of almost three times.
3. The accelerometer data shows that vibration of tool holder and the cutting tool is reduced with the application of ultrasound. This compliments the reduction in surface roughness and tool wear and supports the theory that the application of external ultrasound in turning process reduces chatter.
4. With the application of external ultrasound at 60 kHz a slight reduction of temperature was observed.
5. Chips produced during cutting with ultrasound frequency were observed to be continuous and closely packed whereas the chips produced during normal cutting were discontinuous and loosely packed. Color variation of the chips was slightly changed. In case of machining with ultrasound, the tooth of secondary serrated chips is larger and the number of secondary serrated teeth is less with ultrasonic machining. This phenomenon is a clear indication of change in vibration characteristic of the system.
6. Horizontal orientation of the application of ultrasound gives better surface roughness results than the vertical orientation. This indicates that chatter is more effectively reduced with horizontal orientation.

7. With the input power variation of the ultrasound waves, the amplitude of the waves decreases. Results show that higher amplitude of the ultrasound waves gives lesser surface roughness and vice versa.

5.2 Recommendations

Considering the limitations of the current research, the following recommendations are made which can further improve on this research.

1. The experiment conducted in this project used only mild steel, a ferrous and conducting material. Experiments using other materials that is conducting and nonferrous, or non-conducting and ferrous, can be done to gain further understanding in the mechanism behind the reduction of tool wear and surface roughness by the application of external ultrasound.
2. In this research maximum ultrasound frequency of 60 kHz was used due to device limitations. Experiments may be done with higher ultrasound frequency range to determine whether frequencies above 60 kHz show greater improvement in surface roughness and tool wear or not.
3. Since the application of external ultrasound is capable of improving surface roughness and tool life, there is great potential in using it to reduce costs for the manufacturing industry. Add-ons can be designed to provide external ultrasound on currently existing machining equipments. New machinery can also be designed to be fitted with ultrasound emitting devices to apply an external ultrasound on the work piece and/or tool to achieve better machining output. However, having an additional ultrasound device would subsequently increase energy usage. Thus, it should be evaluated first if the improvements in tool life and surface roughness of the product can justify the increase in operating costs.
4. Feed is an important machining parameter. Due to the limitation of the machine feed was kept constant in this study. But the effect of change of feed with different ultrasonic frequencies can also be observed by carrying out similar experiments at different feed.

5. Based on this study, a mathematical model can be generated to predict the tool wear and surface roughness at different ultrasonic frequencies. To increase the accuracy of the model new sets of experiments can be introduced. An optimization model will provide the best machining parameters for obtaining any desired result.

BIBLIOGRAPHY

- [1] Johnson, K. L., “Contact Mechanics”, *Cambridge University Press*, ISBN 0-521-34796-3, pp. 407, (1985).
- [2] Stachowiak, G. W. and Batchelor, A. W., “Engineering tribology”, *Boston: Butterworth-Heinemann*, ISBN 0-7506-7304-4, pp. 450, (2001).
- [3] Kalpakjian, S., and Schmid, S.R., “Manufacturing Processes for Engineering Materials”, 5th ed., *India: Dorling Kindersley Pvt. Ltd.* (under license from Pearson Education in South Asia), pp. 440-447, (2009).
- [4] Silberschmidta, V.V, Mahdyb, S.M.A., Goudab, M.A., Naseera, A., Agostino Maurotto, A. and Roya, A., “Surface-roughness improvement in ultrasonically assisted turning”, *2nd CIRP Conference on Surface Integrity (CSI)*, Procedia CIRP, Volume 13, pp. 49 – 54, (2014).
- [5] Mahdy, S.M.A., Gouda, M.A. and Silberschmidt, V.V., “Study of ultrasonically assisted turning of stainless steel and brass alloys”, *Journal of Physics: Conference Series 451*, paper 012037, (2013).
- [6] Muhammad, R., Maurotto, A., Roy, A. and Silberschmidt, V.V., “Ultrasonically assisted turning of Ti-6Al-2Sn-4Zr-6Mo”, *Journal of Physics: Conference Series 382*, paper 012016, (2012).
- [7] Rimkevičienė, J., Ostaševičius, V., Jūrėnas, V. and Gaidys, R., “Experiments and simulations of ultrasonically assisted turning tool”, *MECHANIKA*, ISSN 1392 – 1207, Volume 1, Issue 75, (2009).
- [8] Maurotto, A., Muhammad, R., Roy, A. and Silberschmidt, V.V., “Enhanced ultrasonically assisted turning of a β -titanium alloy”, *Ultrasonics 53*, pp. 1242, (2013).
- [9] Patil, S., Joshi, S., Tewari, A. and Joshi, S.S., “Modelling and simulation of effect of ultrasonic vibrations on machining of Ti6Al4V”, *Ultrasonics*, Volume 54, Issue 2, pp. 694–705, (2014).
- [10] Sahoo, A.K. and Sahoo, B., “Experimental investigation on flank wear and tool life, cost analysis and mathematical model in turning hardened steel using coated carbide inserts”, *International Journal of Industrial Engineering Computations*, Issue 4, pp. 571–578, (2013).
- [11] Das, S.R., Nayak, R.P. and Dhupal, D., “Optimization of Cutting Parameters on Tool Wear and Work piece Surface Temperature In Turning of AISI D2 Steel”, *International journal of Lean Thinking*, Volume 3, Issue 2, (2012).
- [12] Zhou, Q., Hong, G. S. and Rahman, M., “A New Tool Life Criterion For Tool Condition Monitoring Using a Neural Network”, *Engineering Application Artificial Intelligence*, Volume 8, Number 5, pp. 579-588, (1995).
- [13] Braghini, A. Jr., and Coelho, R.T., “An Investigation of the Wear Mechanisms of Polycrystalline Cubic Boron Nitride (PCBN) Tools When End Milling Hardened Steels At Low/Medium Cutting Speeds”, *International Journal on Advanced Manufacturing Technology*, Volume 17, pp. 244-257, (2001).

- [14] Chien, W.T. and Tsai, C.S., “The investigation on the prediction of tool wear and the determination of optimum cutting conditions in machining 17-4PH stainless steel”, *Journal of Materials Processing Technology*, Volume 140, pp. 340–345, (2003).
- [15] Ghani, J.A., Choudhury, I.A. and Hassan, H.H., “Application of taguchi method in the optimization of end milling parameters,” *Journal of Materials Processing Technology*, Volume 145, pp. 84-92, (2004).
- [16] Özel, T. and Karpat, Y., “Predictive modeling of surface roughness and tool wear in hard turning using regression and neural networks”, *International Journal of Machine Tools and Manufacture*, Volume 45, pp. 467–479, (2005).
- [17] Kumar, S., Durai, A.R. and Sornakumar, A., “The Effect of Tool Wear on Tool Life Of Alumina-Based Ceramic Cutting Tools While Machining Hardened Martensitic Stainless Steel,” *Journal of Materials Processing Technology*, Volume 173, pp. 151-156, (2006).
- [18] Amin, A. K. M. N., Hafiz, A. M. K., Lajis, M. A. and Patwari, A. U., “Prediction of tool life and experimental investigation during hot milling of AISI H13 tool steel,” *Advanced Materials Research*, Volume 83-86, pp. 190-197, (2010).
- [19] Mahmoud, E. A. E. and Abdelkarim, H. A., “Optimum Cutting Parameters in Turning Operations using HSS Cutting Tool with 45⁰ Approach Angle”, *Sudan Engineering Society Journal*, Volume 53, Number 48, pp. 25-30, (2006).
- [20] Takeyama, H. and Murata, R., “Basic Investigation of Tool Wear,” *Trans. ASME, J. Eng. Ind.*, Volume 85, pp. 33–38, (1963).
- [21] Al-Ahmari, A. M. A., “Predictive machinability models for a selected hard material in turning operations”, *Journal of Materials Processing Technology*, Volume 190, pp. 305–311, (2007).
- [22] Oxley, P.L.B., “The Mechanics of Machining: An Analytical Approach to Assessing Machinability”, *Ellis Horwood, Chichester*, (1989).
- [23] Trent, E.M. and Wright, P.K., “Metal Cutting”, *4th Edition, Butterworth-Heinemann, Boston*, (2000).
- [24] Natarajan, U., Arun, P. and Periasamy, V. M., “On-line Tool Wear Monitoring in Turning by Hidden Markov Model (HMM)”, *Institution of Engineers (India) Journal (PR)*, Volume 87, pp. 31-35, (2007).
- [25] Özel, T., Karpat, Y., Figueira, L. and Davim, J. P., “Modeling of surface finish and tool flank wear in turning of AISI D2 steel with ceramic wiper inserts”, *Journal of Materials Processing Technology*, Volume 189, pp.192–198, (2007).
- [26] Lan, T.S., Lo, C. Y., Wang M.Y. and Yen, A.Y., “Multi Quality Prediction Model of CNC Turning Using Back Propagation Network”, *Information Technology Journal*, Volume 7, Number 6, pp. 911-917, (2008).
- [27] Fnides, B., Aouici, H. and Yallese, M.A., “Cutting forces and surface roughness in hard turning of hot work steel X38CrMoV5-1 using mixed ceramic”, *Mechanika*, Volume 2, Number 70, pp. 73-78, (2008).
- [28] Biswas, C. K., Chawla, B. S., Das, N.S. and Srinivas, E.R.K.N.K., “Tool Wear Prediction using Neuro-Fuzzy System”, *Institution of Engineers (India) Journal (PR)*, Volume 89, pp. 42-46, (2008).

- [29] Fu, P. and Hope, A.D, “A Hybrid Pattern Recognition Architecture for Cutting Tool Condition Monitoring”, *Technology and Applications*, Volume 24, Number 4, pp. 548-558, (2008).
- [30] Wang, M.Y. and Lan, T.S, “Parametric Optimization on Multi-Objective Precision Turning Using Grey Relational Analysis”, *Information Technology Journal*, Volume 7, pp.1072-1076, (2008).
- [31] Kitagawa, T., Maekawa, K., Shirakashi, T. and Usui, E., “Analytical prediction of flank wear of carbide tools in turning plain carbon steels (part 1),” *Japanese Society of Precision Engineering*, Volume 22, Issue 4, pp. 263–269, (1988).
- [32] Iwata, K., Ashara, J. and Okushima, K., “On the mechanism of built-up edge formation in cutting,” *Annals of the CIRP*, Volume 19, Issue 2, pp. 323–330, (1971).
- [33] Lin, W.S., Lee, B.Y. and Wu, C.L., “Modeling the surface roughness and cutting force for turning”, *Journal of Materials Processing Technology*, Volume 108, pp. 286-293, (2001).
- [34] Feng, C.X. and Wang, X., “Development of Empirical Models for Surface Roughness Prediction in Finish Turning”, *International Journal of Advanced Manufacturing Technology*, Volume 20, pp. 348–356, (2002).
- [35] Suresh, P.V.S., Rao, P.V. and Deshmukh, S.G, “A genetic algorithmic approach for optimization of surface roughness prediction model”, *International Journal of Machine Tools and Manufacture*, Volume 42, pp. 675–680, (2002).
- [36] Lee, S.S. and Chen, J.C, “Online surface roughness recognition system using artificial neural networks system in turning operations”, *International Journal of Advanced Manufacturing Technology*, Volume 22, pp. 498–509, (2003).
- [37] Choudhury, S. K. and Bartarya, G., “Role of temperature and surface finish in predicting tool wear using neural network and design of experiments”, *International Journal of Machine Tools and Manufacture*, Volume 43, pp. 747– 753, (2003).
- [38] Kirby, E.D., Zhang, Z. and Chen, J.C., “Development of An Accelerometer based surface roughness Prediction System in Turning Operation Using Multiple Regression Techniques”, *Journal of Industrial Technology*, Volume 20, Number 4, pp. 1-8, (2004).
- [39] Eze, S.C., Izelu, C.O., Oreko, B.U. and Edward, B.A., “Experimental Study of Induced Vibration and Work Surface Roughness in the Turning of 41Cr4 Alloy Steel using Response Surface Methodology”, *International Journal of Innovative Research in Science, Engineering and Technology*, ISSN: 2319-8753, Volume 2, Issue 12, (2013).
- [40] Kumar, K.A., Ratnam, C., Murthy, B.S.N., Ben, B.S. and Reddy, K.R.R.M., “Optimization of Surface Roughness in Face Turning Operation in Machining Of En-8”, *International Journal of Engineering Science & Advanced Technology*, ISSN: 2250–3676, Volume 2, Issue 4, pp. 807 – 812, (2012).
- [41] Basha, N.Z. and Vivek, S., “Optimization of CNC Turning Process Parameters on Aluminium 6061 Using Response Surface Methodology”, *Engineering Science and Technology: An International Journal (ESTIJ)*, Volume XXX, No. XXX, (2013).
- [42] Raghunandan, B.V., Bhandarkar, S.L. and Pankaj, K.S., “An Experimental Mathematical Modelling of Surface Roughness in Turning Operation of En19 with Carbide Tool”, *International Journal of Mechanical Engineering and Research*, ISSN No. 2249-0019, Volume 3, Number 5, pp. 495-502, (2013),

- [43] Rodrigues, L.L.R., Kantharaj, A.N., Kantharaj, B., Freitas, W.R.C. and Murthy, B.R.N., "Effect of Cutting Parameters on Surface Roughness and Cutting Force in Turning Mild Steel", *Research Journal of Recent Sciences*, ISSN 2277-2502, Volume , Issue 10, pp. 19-26, (2012).
- [44] Kohli, A. and Dixit, U.S., "A neural-network-based methodology for the prediction of surface roughness in a turning process", *International Journal of Advanced Manufacturing Technology*, Volume 25, pp.118–129, (2005).
- [45] Pal, S.K. and Chakraborty, D., "Surface roughness prediction in turning using artificial neural network", *Neural Computing and Application*, Volume 14, pp. 319–324, (2005).
- [46] Singh, H. and Kumar, P., "Optimizing Feed Force for Turned Parts through the Taguchi Technique", *Sadhana*, Volume 31, Number 6, pp. 671–681, (2006).
- [47] Ahmed, S.G., "Development of a Prediction Model for Surface Roughness in Finish Turning of Aluminium", *Sudan Engineering Society Journal*, Volume 52, Number 45, pp. 1-5, (2006).
- [48] Abburi, N.R. and Dixit, U.S., "A knowledge-based system for the prediction of surface roughness in turning process", *Robotics and Computer- Integrated Manufacturing*, Volume 22, pp. 363–372, (2006).
- [49] Zhong, Z.W., Khoo, L.P. and Han, S.T., "Prediction of surface roughness of turned surfaces using neural networks", *International Journal of Advance Manufacturing Technology*, Volume 28, pp. 688–693, (2006).
- [50] Kumanan, S., Saheb, S.K.N. and Jesuthanam, C.P., "Prediction of Machining Forces using Neural Networks Trained by a Genetic Algorithm", *Institution of Engineers (India) Journal*, Volume 87, pp. 11-15, (2006).
- [51] Doniavi, A., Eskanderzade, M. and Tahmasebian, M., "Empirical Modeling of Surface Roughness in Turning Process of 1060 steel using Factorial Design Methodology", *Journal of Applied Sciences*, Volume 7, Number 17, pp. 2509-2513, (2007).
- [52] Kassab, S.Y. and Khoshnaw, Y.K., "The Effect of Cutting Tool Vibration on Surface Roughness of Work piece in Dry Turning Operation", *Engineering and Technology*, Volume 25, Number 7, pp. 879-889, (2007).
- [53] Thamizhmanii, S., Saparudin, S. and Hasan, S., "Analysis of Surface Roughness by Using Taguchi Method", *Achievements in Materials and Manufacturing Engineering*, Volume 20, Issue 1-2, pp. 503-505, (2007).
- [54] Srikanth, T. and Kamala, V., "A Real Coded Genetic Algorithm for Optimization of Cutting Parameters in Turning IJCSNS", *International Journal of Computer Science and Network Security*, Volume 8, Number 6, pp. 189-193, (2008).
- [55] Arif, M.D., Patwari, A.U. and Chowdhury, N.A., "Surface roughness characterization using digital image processing technique", *Proceedings of the 13th Annual Paper Meet (APM), Mechanical Engineering Division, The Institution of Engineers, Bangladesh*, Volume 13, pp. 29-35, (2010).
- [56] Patwari, A.U., Arif, M.D., Chowdhury, N.A. and Chowdhury, S. I., "3-D Contour generation and determination of surface roughness of shaped and horizontally milled

plates using digital image processing,” *International Journal of Engineering, Annals of Faculty of Engineering, Hunedoara*, Issue: 3, Issn: 1584-2673, (2011).

[57] Sahoo, P., Barman, T.K. and Routara, B.C., “Taguchi based practical dimension modeling and optimization in CNC turning”, *Advance in Production Engineering and Management*, Volume 3, Number 4, pp. 205-217, (2008).

[58] Reddy, B.S., Padmanabhan, G. and Reddy, K.V.K., “Surface Roughness Prediction Techniques for CNC turning”, *Asian Journal of Scientific Research*, Volume 1, Number 3, pp. 256-264, (2008).

[59] Wannas, A.A, “RBFNN Model for Prediction Recognition of Tool Wear in Hard Turning”, *Journal of Engineering and Applies Science*, Volume 3, Number 10, pp. 780-785, (2008).

[60] Lan, T.S., Lo, C.Y., Wang M.Y. and Yen, A.Y., “Multi Quality Prediction Model of CNC Turning Using Back Propagation Network”, *Information Technology Journal*, Volume 7, Number 6, pp. 911-917, (2008).

[61] Thamma, R., “Comparison between Multiple Regression Models to Study Effect of Turning Parameters on the Surface Roughness”, *Proceedings of the 2008 IAJC-IJME International Conference, ISBN 978-1-60643-379-9*, Paper 133, ENG 103, pp. 1-12, (2008).

[62] Shetty, R., Pai, R., Kamath, V. and Rao, S.S, “Study on Surface Roughness Minimization in Turning of DRACs using Surface Roughness Methodology and Taguchi under Pressured Steam Jet Approach”, *ARPJ Journal of Engineering and Applied Sciences*, Volume 3, Number 1, pp. 59-6, (2008).

[63] Sahu, M. and Sahu, K., “Optimization of Cutting Parameters on Tool Wear, Work piece Surface Temperature and Material Removal Rate in Turning of AISI D2 Steel”, *International Journal of Advanced Mechanical Engineering*, ISSN 2250-3234, Volume 4, Number 3, pp. 291-298, (2014).

[64] Lan, T.S., “Fuzzy Deduction Material Removal Rate Optimization for Computer Numerical Control Turning”, *American Journal of Applied Sciences*, ISSN 1546-9239, Volume 7, Issue 7, pp. 1026-1031, (2010).

[65] Shivakoti, I., Diyaley, S., Kibria, G. and Pradhan, B.B., “Analysis of Material Removal Rate using Genetic Algorithm Approach”, *International Journal of Scientific & Engineering Research*, ISSN 2229-5518, Volume 3, Issue 5, (2012).

[66] Zeqiri, H., Salihu, A., Bunjaku, A., Osmani, H., Qehaja, N., and Zeqiri, F., “Chip deformation and its morphology in orthogonal cutting of hardened steel 42CrMo4”, *14th International Research/Expert Conference on Trends in the Development of Machinery and Associated Technology*, (2010).

[67] Sima, M. and Ozel, T., “Modified material constitutive models for serrated chip formation simulations and experimental validation in machining of titanium alloy Ti–6Al–4V”, *International Journal of Machine Tools & Manufacture*, Volume 50, Issue 11, pp. 943-960, (2010).

[68] Deshayes, L., Mabrouki, T., Ivester, R. and Rigal, J.F., “Serrated Chip Morphology And Comparison With Finite Element Simulations”, *Proceedings of IMECE04 2004 ASME International Mechanical Engineering Congress and Exposition, IMECE2004-60717*, (2004).

- [69] Morehead, M.D., Huang, Y. and Luo, J., “Chip morphology characterization and modeling in machining hardened 52100 steels”, *Machining Science and Technology*, ISSN: 1091-0344, Volume 11, pp. 335-354, (2007).
- [70] Patwari, A.U., Amin, A.K. M. N. and Faris, W., “Identification of instabilities of chip formation by image processing techniques,” *Proceedings of ICME*, ICME09-RT-21, Bangladesh, (2009).
- [71] Chen, G.J., Kong, L.G., Gao, Q. and Liu, X.L., “Chip Morphology in High Speed Precision Turning Process of Hardened Steel GCr15”, *Key Engineering Materials*, Volumes 579 – 580, pp. 12-15, (2014).
- [72] Mhamdi, M.B., Salem, S.B., Boujelbene, M. and Bayraktar, M., “Experimental study of the chip morphology in turning hardened AISI D2 steel”, *Journal of Mechanical Science and Technology*, Volume 27, Issue 11, pp. 3451-3461, (2013).
- [73] Shankar, M.C.G., Shivaprakash, Y.M., Jayashree, P.K. and Sharma, S.S., “Study on Chip-morphology in Turning of Ti-6Al-4V Alloy under High Pressure Neat oil and Soluble oil”, *International Journal of Earth Sciences and Engineering*, ISSN 0974-5904, Volume 6, Issue 4, pp. 832-837, (2013).
- [74] Salem, S.B., Bayraktar, E., Boujelbene, M. and Katundi, D., “Effect of cutting parameters on chip formation in orthogonal cutting”, *Journal of Achievements in Materials and Manufacturing Engineering*, Volume 50, Issue 1, pp. 7-17, (2012).

APPENDIX A: DATA TABLES

Table A1: Surface Roughness data at 0.5 mm depth of cut, 360 RPM spindle speed and different ultrasound frequencies

<u>Experiment No.</u>	<u>Ultrasound Frequency (kHz)</u>	<u>Depth of Cut (mm)</u>	<u>Spindle Speed (RPM)</u>	<u>Surface Roughness (μm)</u>		
				<u>R_a</u>	<u>R_q</u>	<u>R_z</u>
Exp 1	Without Ultrasound	0.5	360	3.31	3.998	19.028
Exp 2	20 kHz	0.5	360	3.769	4.586	19.327
Exp 3	30 kHz	0.5	360	4.025	5.030	20.596
Exp 4	40 kHz	0.5	360	3.250	3.910	17.218
Exp 5	50 kHz	0.5	360	2.281	2.839	13.701
Exp 6	60 kHz	0.5	360	1.988	2.435	12.153

Table A2: Surface Roughness data at 0.5 mm depth of cut, 530 RPM spindle speed and different ultrasound frequencies

<u>Experiment No.</u>	<u>Ultrasound Frequency (kHz)</u>	<u>Depth of Cut (mm)</u>	<u>Spindle Speed (RPM)</u>	<u>Surface Roughness (μm)</u>		
				<u>R_a</u>	<u>R_q</u>	<u>R_z</u>
Exp 1	Without Ultrasound	0.5	530	2.682	3.212	13.133
Exp 2	20 kHz	0.5	530	2.981	3.672	16.314
Exp 3	30 kHz	0.5	530	3.652	4.436	19.367
Exp 4	40 kHz	0.5	530	2.566	3.168	13.938
Exp 5	50 kHz	0.5	530	2.253	2.780	13.156
Exp 6	60 kHz	0.5	530	1.807	2.305	11.443

Table A3: Surface Roughness data at 1 mm depth of cut, 360 RPM spindle speed and different ultrasound frequencies

<u>Experiment No.</u>	<u>Ultrasound Frequency (kHz)</u>	<u>Depth of Cut (mm)</u>	<u>Spindle Speed (RPM)</u>	<u>Surface Roughness (μm)</u>		
				<u>R_a</u>	<u>R_q</u>	<u>R_z</u>
Exp 1	Without Ultrasound	1	360	3.491	4.268	22.392
Exp 2	20 kHz	1	360	3.861	4.747	21.479
Exp 3	30 kHz	1	360	4.175	5.271	22.232
Exp 4	40 kHz	1	360	3.641	4.555	20.052
Exp 5	50 kHz	1	360	2.845	3.389	14.577
Exp 6	60 kHz	1	360	2.365	2.879	13.534

Table A4: Surface Roughness data at 1 mm depth of cut, 530 RPM spindle speed and different ultrasound frequencies

<u>Experiment No.</u>	<u>Ultrasound Frequency (kHz)</u>	<u>Depth of Cut (mm)</u>	<u>Spindle Speed (RPM)</u>	<u>Surface Roughness (μm)</u>		
				<u>R_a</u>	<u>R_q</u>	<u>R_z</u>
Exp 1	Without Ultrasound	1	530	3.496	4.353	20.393
Exp 2	20 kHz	1	530	3.817	4.669	21.163
Exp 3	30 kHz	1	530	3.964	5.283	22.046
Exp 4	40 kHz	1	530	3.343	4.104	18.716
Exp 5	50 kHz	1	530	2.751	3.448	16.652
Exp 6	60 kHz	1	530	2.149	2.635	11.671

Table A5: Comparison of Surface Roughness data at 0.5 mm depth of cut and different ultrasound frequencies for different spindle speeds

<u>Ultrasound Frequency</u> <u>(kHz)</u>	<u>Depth of Cut</u> <u>(mm)</u>	<u>Surface Roughness (R_a)</u> <u>(μm)</u>	
		<u>Spindle Speed</u> <u>360 RPM</u>	<u>Spindle Speed</u> <u>530 RPM</u>
Without Ultrasound	0.5	3.31	2.682
20 kHz	0.5	3.769	2.981
30 kHz	0.5	4.025	3.652
40 kHz	0.5	3.250	2.566
50 kHz	0.5	2.281	2.253
60 kHz	0.5	1.988	1.807

Table A6: Comparison of Surface Roughness data at 1 mm depth of cut and different ultrasound frequencies for different spindle speeds

<u>Ultrasound Frequency</u> <u>(kHz)</u>	<u>Depth of Cut</u> <u>(mm)</u>	<u>Surface Roughness (R_a)</u> <u>(μm)</u>	
		<u>Spindle Speed</u> <u>360 RPM</u>	<u>Spindle Speed</u> <u>530 RPM</u>
Without Ultrasound	1	3.491	3.496
20 kHz	1	3.861	3.817
30 kHz	1	4.175	3.964
40 kHz	1	3.641	3.343
50 kHz	1	2.845	2.751
60 kHz	1	2.365	2.149

Table A7: Comparison of Surface Roughness data at 360 RPM spindle speed and different ultrasound frequencies for different depth of cuts

<u>Ultrasound Frequency</u> <u>(kHz)</u>	<u>Spindle Speed</u> <u>(RPM)</u>	<u>Surface Roughness (R_a)</u> <u>(μm)</u>	
		<u>Depth of Cut</u> <u>0.5 mm</u>	<u>Depth of Cut</u> <u>1 mm</u>
Without Ultrasound	360	3.31	3.491
20 kHz	360	3.769	3.861
30 kHz	360	4.025	4.175
40 kHz	360	3.250	3.641
50 kHz	360	2.281	2.845
60 kHz	360	1.988	2.365

Table A8: Comparison of Surface Roughness data at 530 RPM spindle speed and different ultrasound frequencies for different depth of cuts

<u>Ultrasound Frequency</u> <u>(kHz)</u>	<u>Spindle Speed</u> <u>(RPM)</u>	<u>Surface Roughness (R_a)</u> <u>(μm)</u>	
		<u>Depth of Cut</u> <u>0.5 mm</u>	<u>Depth of Cut</u> <u>1 mm</u>
Without Ultrasound	530	2.682	3.496
20 kHz	530	2.981	3.817
30 kHz	530	3.652	3.964
40 kHz	530	2.566	3.343
50 kHz	530	2.253	2.751
60 kHz	530	1.807	2.149

APPENDIX B: PICOSCOPE GRAPHS

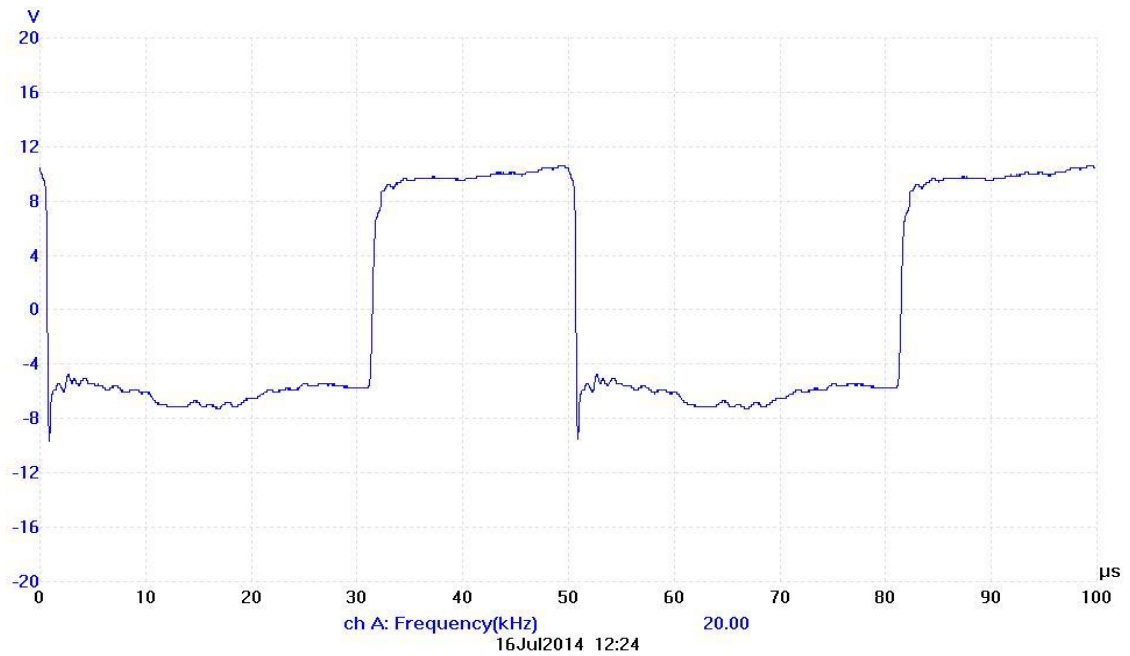


Figure A1: Ultrasound wave generated at 20 kHz obtained with a picoscope from the left-sided ultrasound emitter for calibration purposes

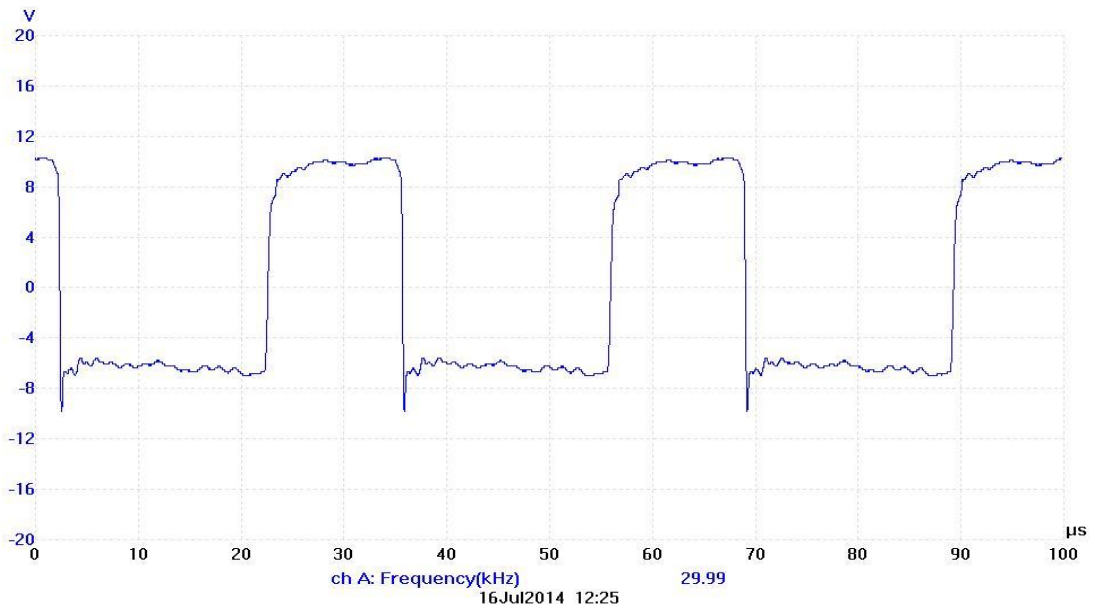


Figure A2: Ultrasound wave generated at 30 kHz obtained with a picoscope from the left-sided ultrasound emitter for calibration purposes

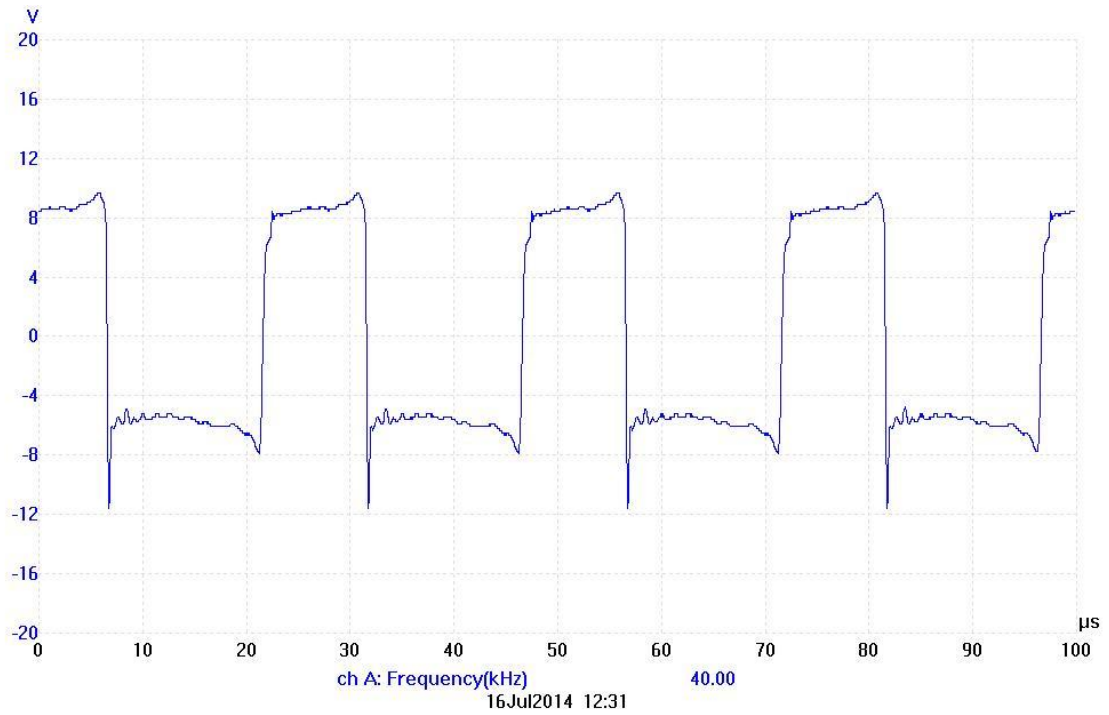


Figure A3: Ultrasound wave generated at 40 kHz obtained with a picoscope from the left-sided ultrasound emitter for calibration purposes

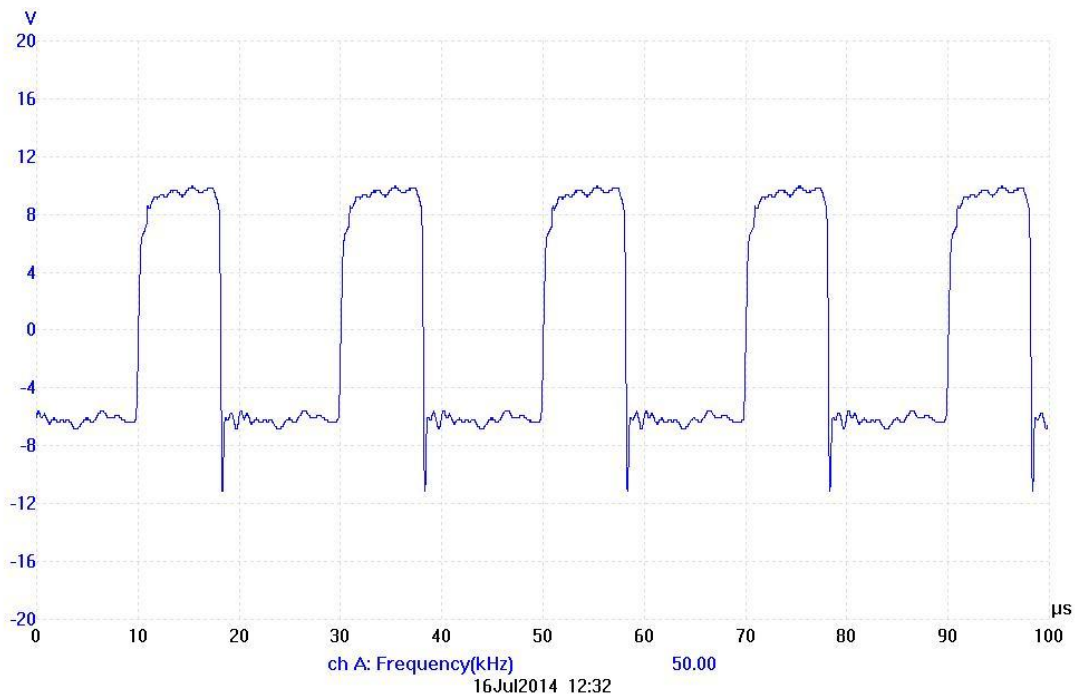


Figure A4: Ultrasound wave generated at 50 kHz obtained with a picoscope from the left-sided ultrasound emitter for calibration purposes

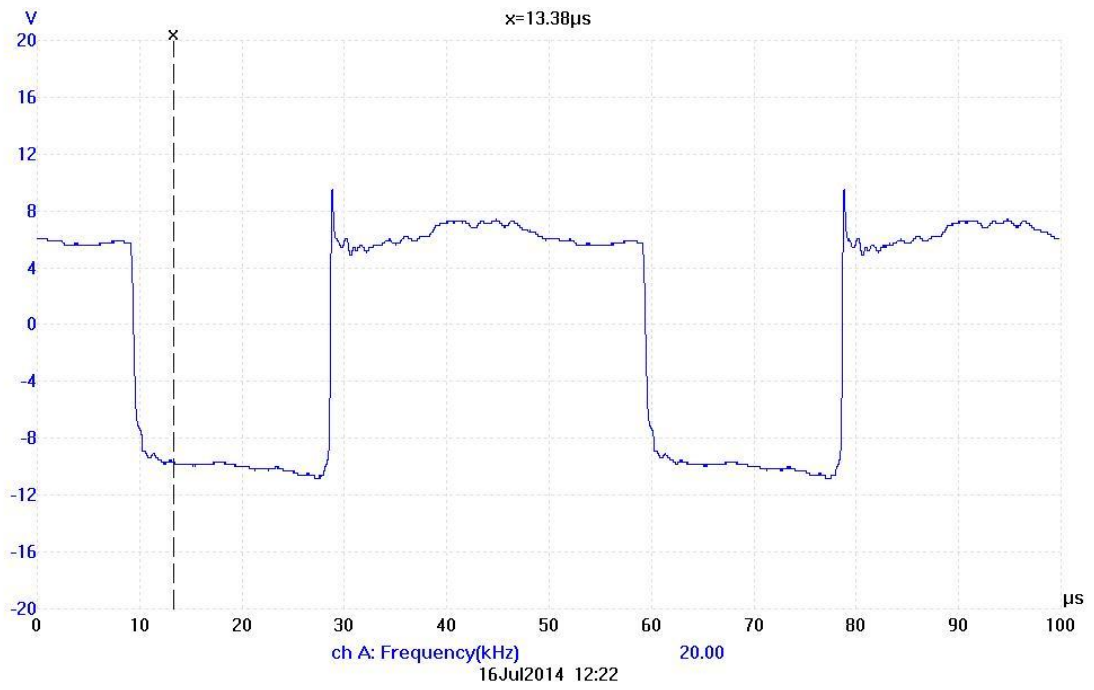


Figure A5: Ultrasound wave generated at 20 kHz obtained with a picoscope from the right-sided ultrasound emitter for calibration purposes

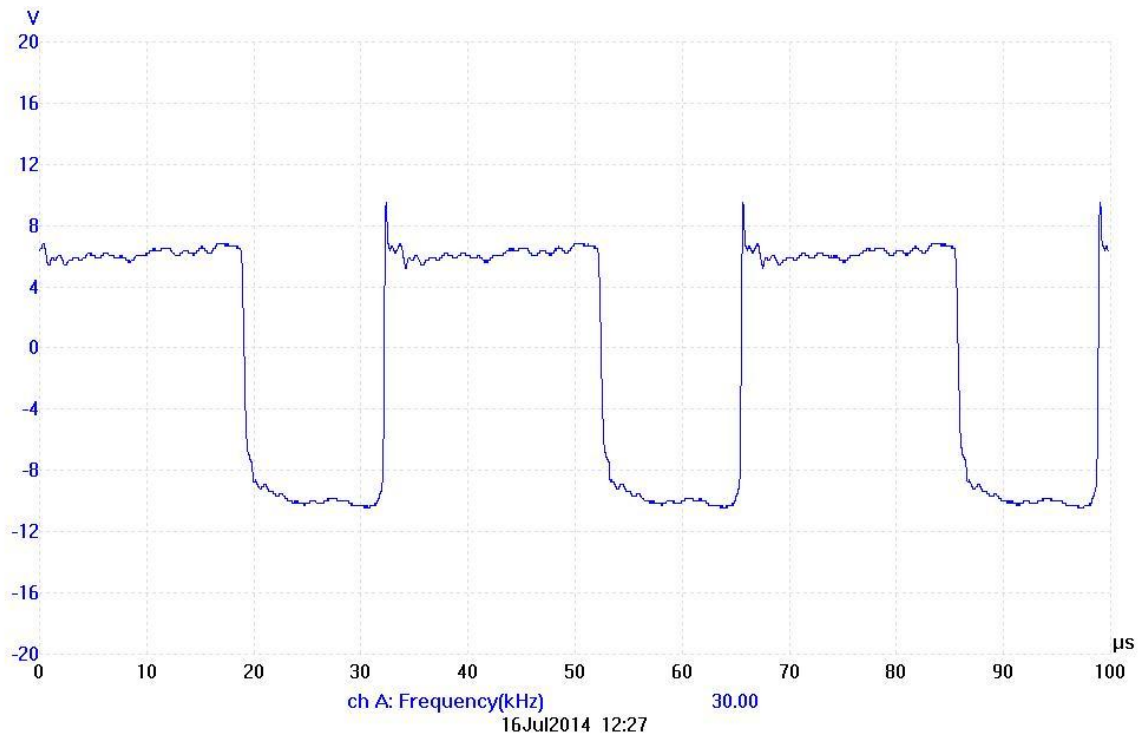


Figure A6: Ultrasound wave generated at 30 kHz obtained with a picoscope from the right-sided ultrasound emitter for calibration purposes

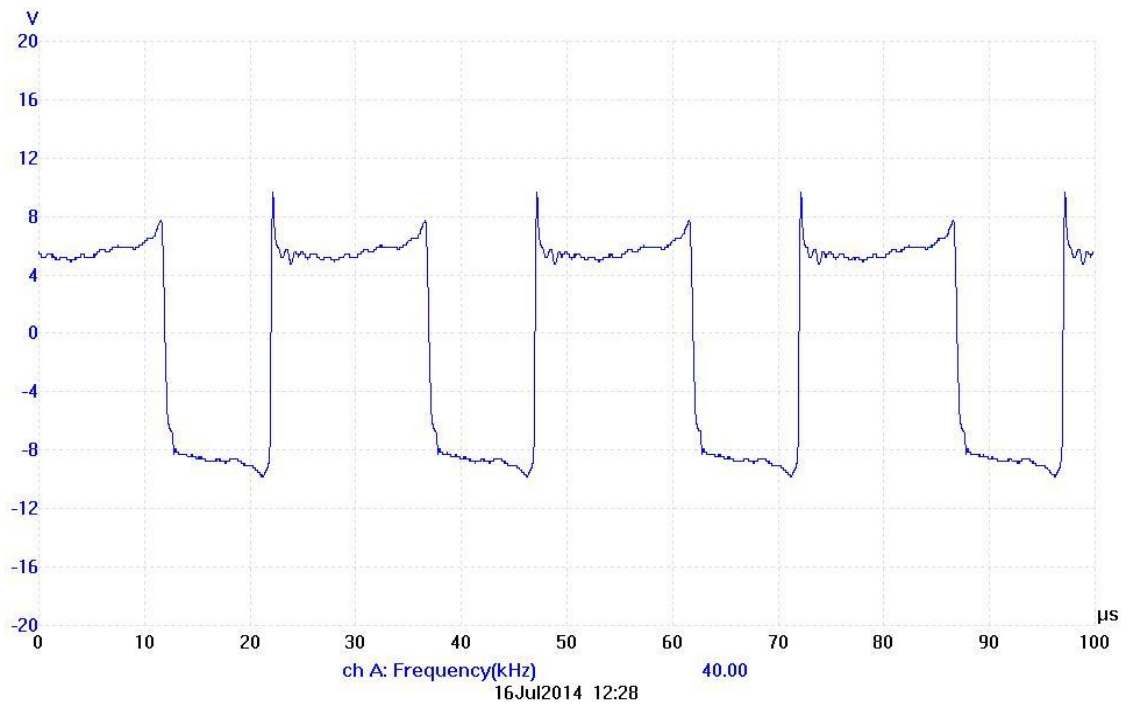


Figure A7: Ultrasound wave generated at 40 kHz obtained with a picoscope from the right-sided ultrasound emitter for calibration purposes

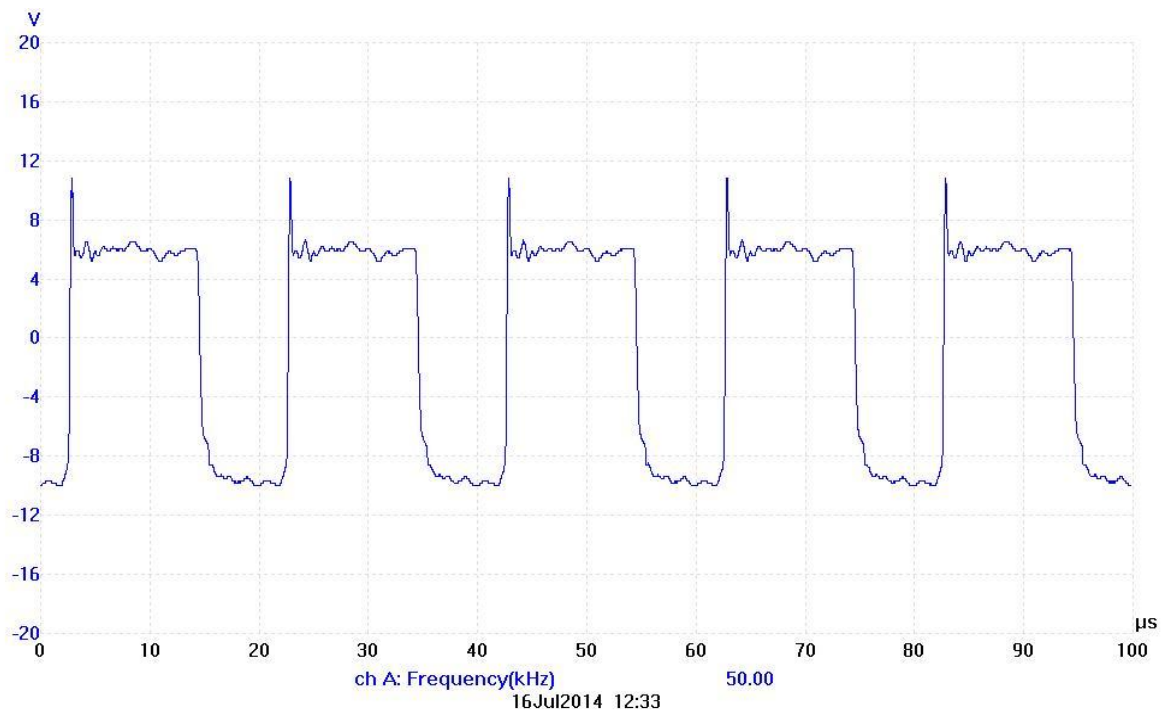


Figure A8: Ultrasound wave generated at 50 kHz obtained with a picoscope from the right-sided ultrasound emitter for calibration purposes